GENETIC AND BIOCHEMICAL ANALYSIS OF THE INTERACTION BETWEEN THE YEAST FATTY ACID SYNTHESIS ENZYME YBR159W AND THE TRANSLATION INITIATION COMPLEX eIF2B

By

Christopher Michael Browne

Dissertation

Submitted to the Faculty of the

Graduate School of Vanderbilt University

In partial fulfillment of the requirements

For the degree of

DOCTOR OF PHILOSOPHY

In

Biochemistry

August, 2013

Nashville, Tennessee

Approved:

Professor Andrew J. Link

Professor Kevin L. Schey

Professor Claus Schneider

Professor P. Anthony Weil

Professor Nicholas J. Reiter

This dissertation focuses on the biochemical and genetic characterization of the protein-protein interaction in the budding yeast *Saccharomyces cerevisiae* between the cytosolic translation initiation guanine nucleotide exchange factor eIF2B and the endoplasmic reticulum (ER) membrane-embedded very-long-chain fatty acid (VLCFA) synthesis beta-keto-reductase enzyme YBR159W (*IFA38*). The dissertation is divided between the physical characterization of the interaction and examination of the functional consequences the *ybr159wΔ* deletion has on the yeast cell's physiology. I first look at how the interaction is occurring in yeast. I utilize yeast 2-hybrid analysis to show that eIF2B subunits *GCD6* and *GCD7* interact with YBR159W. My experiments show that eIF2B does not interact with other VLCFA synthesis enzymes and that YBR159W does not interact directly with the other canonical components of the eIF2B complex. Compared to a wild type strain, a *ybr159wΔ* null yeast strain has a reduced growth rate and the hallmarks of a reduced translation activity including reduced ^{35}S-methionine incorporation and low levels of polyribosomes. It is unknown if the reduced translation rate is a direct or indirect consequence of the *ybr159wΔ* mutation. The total cellular abundance of eIF2B complex is reduced in a *ybr159wΔ* null strain but the stoichiometry of the eIF2B complex and its enzymatic activity appears equivalent to wild-type. Deletion of YBR159W or other VLCFA synthesis enzymes significantly alters sphingolipid production in yeast. Deletion of the eIF2B subunit *GCN3* does not cause a significant change in sphingolipid production in yeast. In the second section, I examine what effect YBR159W has on the localization of the cytoplasmic eIF2B complex. In yeast, eIF2B forms one or two large foci known as eIF2B bodies. I discover that YBR159W is important for either the formation or maintenance of the eIF2B body. In *ybr159wΔ* null yeast, eIF2B forms many smaller foci throughout the cell. Other VLCFA synthesis enzyme mutants display this same phenotype. I also find that a fraction of the eIF2B complex associates with lipid membranes. This lipid association is not dependent on the presence of YBR159W and is not mediated by rough ER bound ribosomes. Further experiments are required to determine the mechanistic and functional role of YBR159W interacting with eIF2B.

ACKNOWLEDGEMENT

I would like to thank everyone who has helped me get this doctorate. It was a long and hard journey but it is almost over. I hope each and every person that has helped me during this process the absolute best of luck in the future. I want to let them know how important they have been in my life.

First, I would like to thank my advisor Dr. Andy Link. Andy gave me a lab to call home. He gave me every freedom necessary to conduct the work I needed and was always open to new ideas and approaches. I always knew I could come to him with any questions or concerns. Advice and critiques were always forthcoming and helped me shape my actions and attitude to better reflect a doctoral candidate. Thank you Andy for the huge amount of support you have provided me.

I would like to thank the members of my doctoral committee Drs. Tony Weil, Kevin Schey, Claus Schneider and Nicholas Reiter. Your presence made committee meetings a joy to be a part of. Your comments and advice were extremely useful and helped focus my efforts when I would inevitably start veering in the wrong direction. I would also like to thank the former members of my committee Drs. Susan Wente and Zu-Wen Sun. I'm extremely grateful for your help during the early period of my graduate career.

I would also like to thank Dr. Robert Matusik. Your willingness to help me as an undergraduate sight unseen has made my career in science possible. I learned a great deal in your laboratory and I'm sure your recommendation got me a long way toward getting accepted into graduate school. I thank you from the bottom of my heart for this opportunity you gave me.

I would like to thank the Department of Biochemistry. I could never have navigated the twists and turns of graduate school without the support and guidance of my department every step of the way. I would like to especially thank Marlene Jayne for being the kindest and most supporting department administrator I know. I would also like to thank the Department of Microbiology and Immunology for providing me with the means to support my research. I thank the IGP. Without the IGP my first year of graduate school would have been a rough transition.

Thank you Parimal for lending me your considerable expertise in mass spectrometry so I could finish my doctorate and graduate. The fact you are a great friend and someone who also had a pair of "devil

horns" only made things better. I also want to thank Vince and Adam, my predecessors and mentors in the Link lab. You were both hugely influential on my decision to join the lab and I'm very glad I got to work with you both.

Andrew and Tanya, thank you for being my friends. My nights and weekends spent with you have been the most enjoyable moments of my life. Andrew, I never would have guessed that the annoying kid that always joked about me not finishing my math homework before class would become my lifelong friend. Tanya, I can still remember Andrew telling me about this girl from a Habitat for Humanity meeting that had messaged him on Facebook. Now that I've said that, I'm not totally sure that was you, but it could have been and that's all that matters. I'm glad things have worked out for you two and I hope you both have the best, most happy lives together.

To Huey and Malcolm: Meow meow meow meow meow, meow meow.

Lastly, I would like to thank my parents: Mom and Dad. You have given me an amazing 29 years of support and I can't possibly thank you enough for that. You taught me next to everything I know about how to live. You gave me a place to call home this last year when things got a bit uncertain. You put up with me when I was being an annoying monster, both as a child and a 29 year old. You have always supported every decision I made. No matter how things have been going in my life I have always known I have a family that loves me. You have made me the man I am today. I am eternally grateful for everything you have done for me.

TABLE OF CONTENTS

LIST OF TABLES

LIST OF FIGURES

CHAPTER I

INTRODUCTION

Abstract

Advances in our understanding of protein synthesis have revealed a wide array of factors necessary for the regulation of translation in the cell. Mass spectrometry techniques have led to the identification of new factors associated with translation. I hypothesize that as yet uncharacterized regulatory mechanisms exist for the synthesis of proteins. My laboratory discovered a novel protein-protein interaction in yeast between the eukaryotic translation initiation factor eIF2B and the ketoacyl-reductase involved in very-long-chain fatty acid synthesis YBR159W. I hypothesize that YBR159W serves as a novel regulator of eIF2B and translation initiation. If so, it stands to reason that a *ybr159wΔ* yeast strain would show changes in eIF2B activity and protein synthesis. In the past, translation has often taken a backseat to transcription in models of the regulation of gene expression. As new techniques are developed, I expect more and more factors will be found that aid in the regulation of gene expression through regulation of translation.

Background

An Understanding of the Mechanisms of Protein Translation

Translation is the fundamental biological process of turning genomic information on messenger RNA (mRNA) into polypeptides, or proteins. Translation is carried out by the ribosome, an organelle composed of multiple ribosomal RNAs (rRNA) and proteins (Klinge et al. 2012; Wilson and Doudna Cate 2012). In eukaryotes, the ribosome is composed of the large 60S ribosomal subunit and the small 40S ribosomal subunit, each named for its sedimentation coefficient (Claude 1937; Claude 1938; Claude 1940; Palade 1955). The 60S ribosomal subunit contains the 5S, 5.8S, and 28S/25S rRNA molecules and 46

ribosomal proteins (Gongadze 2011; Nazar 1984; Noller 1991; Poll et al. 2009). The largest rRNA molecule in humans is 28S while it is only 25S in yeast. The 40S ribosomal subunit is made up of the 18S rRNA and 33 proteins (Gerbasi et al. 2004; Karbstein 2011). The 40S and 60S ribosomal subunits bind together when active to form the 80S ribosome. Aminoacyl transfer RNA (tRNA) is a short segment of RNA bound with a specific charged amino acid (Ibba and Soll 2000; Sonenberg 2000). The tRNA contains a three nucleotide anti-codon loop that base-pairs with a codon on mRNA in the 80S ribosome. The ribosome then catalyzes the formation of a peptide bond between the charged amino acid and the growing polypeptide chain. For most mRNAs, the start codon that signals the beginning point for translation is the codon sequence AUG (Hinnebusch 2011). The AUG start codon encodes the amino acid methionine and base pairs with a special tRNA bound with methionine, the initiator tRNA (met_i-tRNA) (Kolitz and Lorsch 2010). Finally, translation is regulated by a number of proteins called translation factors that interact with the ribosome, RNAs, and each other (Sonenberg 2000; Warner 1999).

Translation is divided into three steps; initiation, elongation, and termination (Sonenberg 2000). Translation initiation is the primary mechanism of regulating protein synthesis (Pestova et al. 2001; Preiss and M 2003). The scanning model, as proposed by Marilyn Kozak details our current understanding of translation initiation in eukaryotes (Kozak 1987; Kozak and Shatkin 1978). The model details how a large group of translation initiation factors (eIFs) work in concert to position the ribosome and initiator tRNA on the AUG start codon of mRNA (Kozak 1980). The mechanism of translation initiation will be discussed in detail in the proceeding section.

After the initiation phase the elongation phase begins, elongation requires eukaryotic elongation factor 1 (eEF1) to catalyze the delivery of charged amino acid-tRNAs to the ribosome. Elongation factor eEF2 is a translocase that moves the ribosome along the mRNA one codon at a time (Sasikumar et al. 2012). In bacteria, the homologues of eEF1 are two factors, EF-Tu and EF-T. The bacterial homologue of eEF2 is EF-G (Agirrezabala and Frank 2009). These factors: eEF1/EF-Tu, EF-T and eEF2/EF-G help the ribosome elongate the growing polypeptide until a stop codon is reached; at which point the termination phase is triggered and release factors interact to promote polypeptide release and ribosome dissociation. Fungi are unique among eukaryotes for possessing a third elongation factor, EF-3. EF-3 is necessary for

stimulating the binding of eEF1, GTP, and charged amino acid-tRNA with the ribosome (Belfield and Tuite 1993).

For termination of translation, the three stop codons UAA, UAG, and UGA are recognized by release factors or RFs. In eukaryotes, eRF1 recognizes all three stop codons. eRF1 interacts with the A-site of the ribosome where it releases the polypeptide from the ribosome. eRF3 interacts with eRF1 and helps facilitate peptide release. Following peptide release, the ribosomal subunits dissociate from the mRNA (Jackson et al. 2012). In prokaryotes, RF1 and RF2 are homologues of eRF1 and each recognize different stop codons (Scolnick et al. 1968). Depending on the stop codon, one of the RFs will interact with the A-site and facilitate polypeptide release. Release factor RF3 then removes the bond RF from the A-site. Ribosome recycling factors (RRFs) and elongation factor eEF-G then dissociate the ribosomal subunits from the mRNA (Petry et al. 2008). Neither the elongation nor the termination phases of translation are strongly regulated, it is at the initiation phase where protein synthesis is controlled.

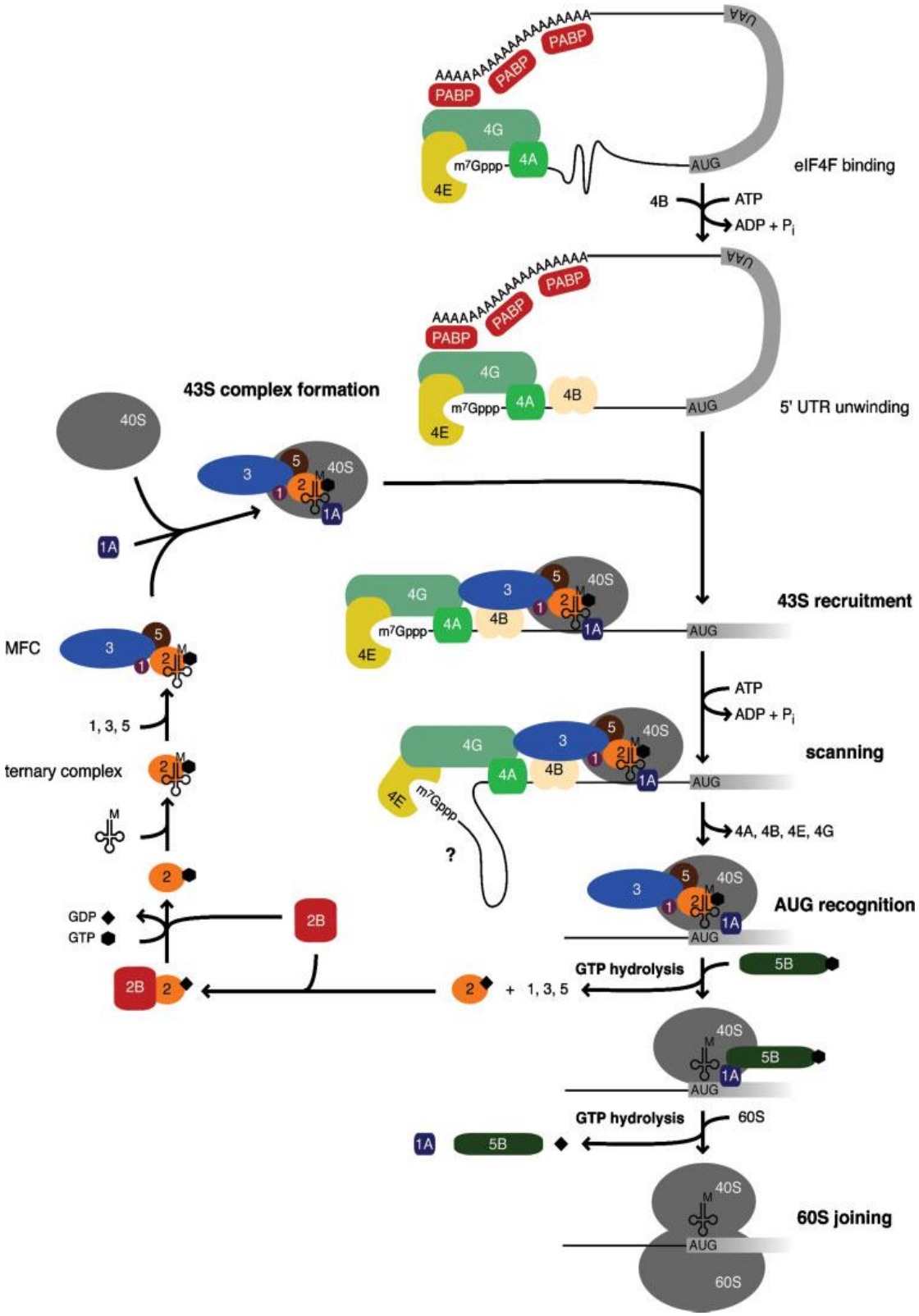

Figure 1-1 Eukaryotic translation initiation. Image taken from Preiss and Hertz. Bioessays. 2003, 25(12): 1201-1211.

Translation Initiation is the Fundamental Regulatory Step in Protein Synthesis

Eukaryotic translation initiation is a complex process requiring a large number of different factors. Figure 1-1 diagrams the major steps in translation initiation (Fig. 1-1) (Preiss and M 2003). Initial steps in the process include the activation of the mRNA and formation of the 43S preinitiation complex. Activation of mRNA involves the eIF4F complex situated at the 5' end of the mRNA binding with poly(A)-binding protein (PABP) situated at the 3' end of the mRNA to form a closed-loop structure (Sachs and Varani 2000). The eIF4F complex is composed of the cap-binding protein eIF4E, the scaffold protein eIF4G, and the RNA-helicase eIF4A (Gingras et al. 1999; McKendrick et al. 1999). eIF4G interacts with PABP, eIF4E, eIF4A, eIF4B, and eventually eIF3 (Keiper et al. 1999). The 43S preinitiation complex is composed of eIF1, eIF1A, eIF5, eIF3, and the 40S ribosomal subunit (Asano et al. 2001; Hinnebusch 2006; Merrick W. C.). The ternary complex composed of eIF2 bound with GTP and the initiator tRNA also binds to the 43S preinitiation complex (Kimball 1999). The activated mRNA and 43S preinitiation complex join together via interactions between eIF4G and eIF3 (Lamphear et al. 1995). Additional interactions between eIF5 and eIF4G and between eIF4B and eIF3 may also play an important role in mRNA and preinitiation complex binding (Asano et al. 2001; Methot et al. 1996; Vries et al. 1997). eIF4A then unwinds the 5' end of the mRNA to facilitate the 40S subunit to scan along the mRNA in search of the AUG start codon (Rogers et al. 2002). The translation start site is recognized by the complementary base-pairing of the anti-codon loop of the initiator tRNA with the start codon, eIF1 ensures the proper sequence and context of the start codon (Hinnebusch 2011). Upon start codon recognition, several events occur. Initially, eIF1 is displaced by the codon-anticodon base-pairing and dissociates from the initiation complex (Mitchell and Lorsch 2008). eIF1 acts as an inhibitor of the GTPase-activating protein (GAP) eIF5. Now uninhibited, eIF5 induces eIF2 to hydrolyze the GTP bound to itself, this causes eIF2 to dissociate from the initiation complex (Das and Maitra 2001). Next, eIF5B bound with GTP binds to the initiation complex (Dever et al. 2001). eIF5B mediates the dissociation of eIF1A and eIF3 from the initiation complex. The 60S ribosome can then join with the initiation complex. After GTP hydrolysis, eIF5B also dissociates from the now complete translation complex (Dever et al. 2001). The ribosome is now poised and ready to begin elongating the polypeptide chain.

Translation initiation in prokaryotes is considerably different from eukaryotes. In prokaryotes, the positioning of the ribosome for elongation is primarily mediated by an RNA-RNA interaction between the 16s rRNA of the small subunit and a 5-16 base RNA element localized just upstream of the start codon. There appears to be no small subunit scanning along the 5'-UTR to locate the start codon like is postulated in the Kozak model for translation initiation. There are only three initiation factors: IF1, IF2, and IF3. IF3 is responsible for binding to the small, 30S subunit and keeping it separated from the large, 50S subunit and localizing to the start codon. IF1, IF2, initiator tRNA, and the mRNA bind to the 30S subunit and IF3 to form the 30S initiation complex. IF1 and IF2 along with the prokaryote-only Shine-Delgarno sequence on the 5' Untranslated Region (UTR) of the mRNA facilitate recognition of the AUG start codon. IF3 then dissociates from the initiation complex and allows the 50S ribosome to join. IF1 and IF2 then dissociate from the ribosome and elongation can begin (Simonetti et al. 2009).

Internal Ribosome Entry Sites: Alternative Methods of Translation Initiation

The eukaryotic initiation pathway described above is termed cap-dependent initiation because it relies on the 5' cap structure on the mRNA acting as an anchor point for many of the initiation factors to bind. The cap structure is composed of eIF4E bound to modified guanine residues at the 5' end of the mRNA. An alternative method has been discovered that does not require a 5' mRNA cap. A class of mRNA contains what is known as an Internal Ribosome Entry Site (IRES) that initiates independent of the 5' end of the mRNA. An IRES is located in the 5' UTR of the mRNA and was first discovered in viral transcripts (Jang et al. 1988; Pelletier and Sonenberg 1988). A circular mRNA construct confirmed that no cap structure is needed for translation from an IRES (Chen and Sarnow 1995). While most IRESs are viral in nature, IRESs have also been shown to be purposefully translated by eukaryotic cells under certain stress conditions when cap-dependent translation is downregulated. The sequence of an IRES is highly variable and the mode of ribosome recruitment varies considerably as well. Translation initiation factors are still needed for many IRESs but the exact set of factors varies and no single initiation factor is required for all IRESs. For those IRESs that require initiation factors; eIF2, eIF3, and eIF4G are the most common constituents. Some IRESs do not require any initiation factors at all for translation (Pisarev et al. 2005). A special class of factors called IRES Transacting Factors (ITAF) help facilitate translation of some IRESs

(Thompson 2012). ITAFs are distinguished from initiation factors because they are not thought to be involved in canonical, cap-dependent translation initiation. Following cap-independent initiation, the elongation and termination phases occur normally. Though IRES translated genes have proven to play a significant role in the cell, the vast majority of proteins are translated by the cap-dependent mechanism. The efficiency of translation of an IRES is highly variable. Viral IRESs tend to be very efficiently translated, certain ones being more efficiently expressed than from cap-dependent translation. Under normal conditions, cellular IRESs tend to be less efficient than cap-dependent translation. During stress, cellular IRESs translation rate can often be higher than cap-dependent mechanisms because cap-dependent translation is often specifically downregulated during stress (Komar and Hatzoglou 2011).

The Role of eIF2B in Translation Initiation

The binding of GTP- and initiator tRNA-bound eIF2 to the 43S preinitiation complex is one of the key steps in cap-dependent translation initiation. The *S. cerevisiae* eIF2 is composed of three subunits: *SUI2* (α), *SUI3* (β), and *GCD11* (γ). The α subunit is the target of a number of kinases that regulate protein translation. The β subunit is thought to be important for initiator tRNA binding and the γ subunit is responsible for binding GDP/GTP for the complex (Schmitt et al. 2010). After start codon recognition, the GAP eIF5 induces the hydrolysis of the GTP bound to eIF2 to GDP. eIF2 then dissociates from the translation complex. To undergo another round of translation initiation, eIF2 must be recharged. eIF2 is unable to efficiently displace the GDP it has bound. This displacement is the job of initiation factor eIF2B.

Initiation factor eIF2B is the guanine-nucleotide exchange factor (GEF) for eIF2 (Preiss and M 2003). This GTP exchange event is one of the key steps in regulating translation initiation (Kimball 1999; Merrick W. C.). Though called GTP exchange, the catalytic activity of eIF2B is primarily to displace GDP from eIF2; eIF2B does not necessarily facilitate the rebinding of GTP on eIF2, which is something eIF2 can do on its own due to the much higher concentration of GTP in the cell versus GDP (Mohammad-Qureshi et al. 2008; Pilz et al. 1997). eIF2 is the only known target for the GEF exchange function of eIF2B (Pavitt 2005). eIF2B is unique among other GEFs in being composed of multiple subunits. There are 5 subunits of eIF2B in eukaryotes named α-ε. In yeast, the 5 subunits are *GCN3* (α), *GCD7* (β), *GCD1* (γ), *GCD2* (δ), and *GCD6* (ε) (Bushman et al. 1993; Cigan et al. 1993). Table 1-1 illustrates the different

nomenclature in humans and yeast for each eIF2B subunit as well as their sequence identity and functions (Table 1-1). The eIF2B complex is a large complex (almost 300 kD in yeast) (Pavitt 2005). Unlike many other translation complexes, no structure for the entire complex has been determined. The α subunit and the catalytic domains of the ε subunits of yeast and human eIF2B have crystal structures determined (Boesen et al. 2004; Hiyama et al. 2009; Wei et al. 2010).

In yeast, the first eIF2B subunit to be characterized was *GCD1* (originally called *TRA3*) in a screen of genes affecting amino acid biosynthesis (Wolfner et al. 1975). Other members of the eIF2B complex were also determined to affect amino acid biosynthesis in a similar fashion. The gene names of the subunits all derive from this connection to the amino acid general control pathway. The four GCD genes stand for General Control Derepressible, indicating mutation of them leads to constitutively upregulated amino acid biosynthesis. The single GCN gene, *GCN3*, stands for General Control Non-derepressible and indicates that amino acid biosynthesis cannot be induced in a $Gcn3^-$ mutant. From here it was eventually determined that *GCD1* played a role in protein synthesis itself (Hill and Struhl 1988). The various eIF2B genes weren't identified as being part of the GEF for eIF2 until later (Cigan et al. 1993).

Table 1-1 Nomenclature, Sequence Similarity, and Function of eIF2B Subunit Genes. Sequence identity is between each yeast and human subunit. In the function column; Y = Yeast, M = Mammalian, D = Drosophila. Adapted from Pavitt. Biochem Soc Trans. 2005 Dec (Pt 6): 1487-1492.

	Gene			
Subunit	Yeast	Human	Sequence Identity (%)	Function
eIF2Bα	GCN3	eIF2B1	42	Regulation of eIF2α phosphorylation (Y, M)
eIF2Bβ	GCD7	eIF2B2	36	Regulation of eIF2α phosphorylation (Y)
eIF2Bδ	GCD2	eIF2B4	36	Regulation of eIF2α phosphorylation (Y, M)
eIF2Bγ	GCD1	eIF2B3	25	Part of catalytic subcomplex; fusel alcohol regulation (Y)
eIF2Bε	GCD6	eIF2B5	30	Catalytic subunit (Y, D, M); regulated by phosphorylation (M, D)

In yeast, all subunits except the α subunit *GCN3* are essential (Giaever et al. 2002). In humans, all subunits are essential. *GCN3* is known to be an important regulator of stress responses (Hannig and Hinnebusch 1988). The *GCN3* subunit is similar in sequence to the δ and β subunits *GCD2* and *GCD7* (Paddon et al. 1989; Pavitt et al. 1997). *GCD2* and *GCD7* are thought to form a subcomplex with *GCN3* important for the regulatory function of *GCN3* (Yang and Hinnebusch 1996). The eIF2B ε subunit *GCD6* performs the enzymatic functions of eIF2B, binding to eIF2γ to exchange GDP with GTP. *GCD6* is capable of performing GEF exchange on its own, albeit at a slower rate than the holoenzyme. *GCD1* increases the efficiency of eIF2B GEF exchange. In fact, the subcomplex formed by *GCD1* and *GCD6* actually has an *in vitro* GEF exchange rate higher than that of the eIF2B holoenzyme (Pavitt et al. 1998).

The C-terminal domain of the eIF2B catalytic subunit *GCD6* contains a minimal enzymatic domain capable of binding eIF2 and displacing GDP (Gomez et al. 2002). This region is rich in aromatic and acidic residues and is similar in sequence to the C-terminal domain of the GAP eIF5. eIF5 is responsible for the hydrolysis of GTP bound to eIF2 during translation initiation. Mutations in the shared C-terminal domain of eIF2Bε or eIF5 reduce their affinities for eIF2. This domain has shown to bind to eIF2 via the N-terminal domain of the β subunit of eIF2. Mutations in this region of eIF2β reduce the affinity of eIF2 for not only eIF2B and eIF5 but also eIF3 (Asano et al. 1999). The N-terminal domain of eIF2β forms lysine rich blocks thought important for its interactions with these initiation factors (Asano et al. 1999). Residues Thr552 and Ser576 on eIF2Bε were determined to play an important role in guanine nucleotide exchange. A mutation in Glu569 is lethal and *in vitro* assays show eIF2Bε with this mutation is unable to perform enzymatic activity (Boesen et al. 2004). The atomic structure of eIF2Bε reveals the catalytic domain of the protein forms four stacked pairs of α-helixes similar to HEAT repeat domains. The residues Thr552, Ser576, and Glu569 are clustered at the surface of one end of the structure (Boesen et al. 2004). The surface is extensively charged and thought to be important for binding to eIF2β. The binding to eIF2β then puts the eIF2Bε active site in close proximity to eIF2γ for GTP exchange (Pavitt 2005). The eIF2B complex itself does not appear to actually bind guanine nucleotide as part of its exchange activity (Reid et al. 2012).

The eIF2B regulatory subunit *GCN3* functions via interactions with the phosphorylated form of the α subunit of eIF2. eIF2α is phosphorylated at serine 51 by a number of protein kinases during cellular

stresses. In yeast, the best characterized eIF2α ser51 kinase is *GCN2*, which is activated during amino acid starvation. Higher eukaryotic eIF2α ser51 is phosphorylated by *GCN2* as well as Protein Kinase R (PKR), PKR-like Endoplasmic Reticulum Kinase (PERK), and Heme-Regulated Inhibitor of translation (HRI) (Pavitt 2005). PKR is associated with the cell antiviral response and is activated by double-stranded RNA (Schneider and Mohr 2003). PERK is an ER membrane protein that responds to unfolded protein in the ER lumen to activate the unfolded protein response (Shi et al. 1998). HRI senses the availability of heme in cells and is activated in its absence. Homologues of HRI, *HRI1* and *HRI2*, have been described to regulate eIF2α phosphorylation in *Schizosaccharomyces pombe* during oxidative stress (Zhan et al. 2004; Zhan et al. 2002). Phosphorylated eIF2α binds to eIF2Bα, this binding event inactivates the eIF2B complex (Rowlands et al. 1988). In yeast, while eIF2Bα/*GCN3* is thought to be the primary interactor with phosphorylated eIF2α, it appears the interaction takes place on the eIF2B subcomplex composed of *GCN3*, *GCD2*, and *GCD7* at a separate location from the enzyme activity of eIF2B (Vazquez de Aldana et al. 1993; Yang and Hinnebusch 1996). Point mutations in *GCD2* and *GCD7* can rescue the translation inhibiting effects of phospho-eIF2α in a similar manner to mutations in *GCN3* (Pavitt et al. 1998; Yang and Hinnebusch 1996). The effects of the inhibition of eIF2B activity by binding to phosphorylated eIF2α is to downregulate translation of most cellular mRNAs and upregulate translation of stress response mRNAs. In yeast, upregulation is carried out by translation of the stress response transcription factor *GCN4*. In mammals, the gene Activating Transcription Factor 4 (*ATF4*) is upregulated in a similar manner to *GCN4* in yeast (Vattem and Wek 2004). Figure 1-2 illustrates yeast and human interactions with eIF2B (Fig. 1-2) (Pavitt 2005).

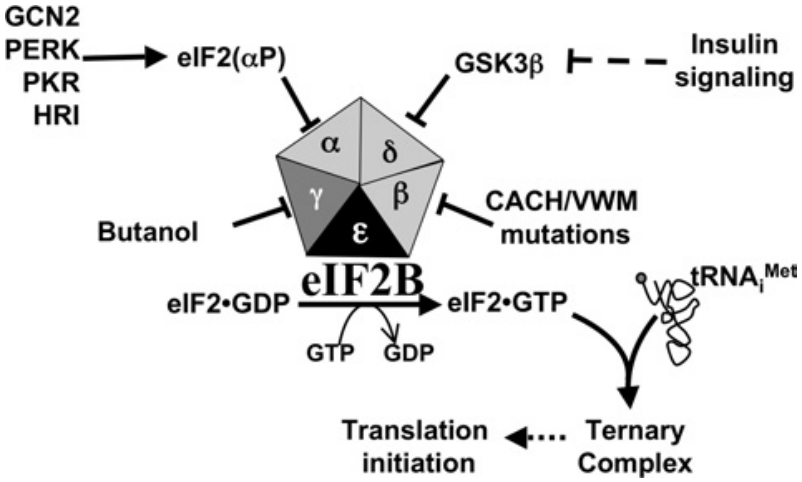

Figure 1-2 Interaction and regulation of eIF2B subunits in yeast and humans. Image taken from Pavitt. Biochem Soc Trans. 2005 Dec (Pt 6): 1487-1492.

In mammals, direct phosphorylation of eIF2Bε is also utilized to regulate translation initiation. Several protein kinases have been shown to carry out the phosphorylation including casein kinases 1 and 2 (CK1 and CK2), duel-specificity tyrosine phosphorylated and regulated kinase (DYRK), and glycogen synthase kinase 3 (GSK3) (Wang et al. 2001; Woods et al. 2001). GSK3 is thought to have the largest role in eIF2B regulation and is insulin regulated (Kim and Kimmel 2000). An additional phosphorylation site on eIF2Bε has been shown to regulate translation during amino acid starvation in humans. This regulation is independent of the classical amino acid starvation pathway via the eIF2α kinase *GCN2* (Wang and Proud 2008). eIF2Bε phosphorylation is downregulated during resistance exercise in humans (Glover et al. 2008). In yeast, eIF2B is directly regulated by fusel alcohols. Fusel alcohols are breakdown products of amino acid catabolism and are thought to signal nitrogen scarcity (Ashe et al. 2001; Taylor et al. 2010). Fusel alcohols bind to eIF2B and inhibit its activity.

In humans, eIF2B is linked with a number of diseases. One of the first to be characterized was Leukoencephalopathy with vanishing white matter (VWM) (Bugiani et al. 2010; van der Knaap et al. 1997). The cause of the disease is mutations in any of the 5 subunits of eIF2B. Over one hundred mutations that cause the disease have been identified in the 5 eIF2B subunits (Richardson et al. 2004). Figure 1-3 summarizes a number of these mutation sites on eIF2B subunits (Fig. 1-3).

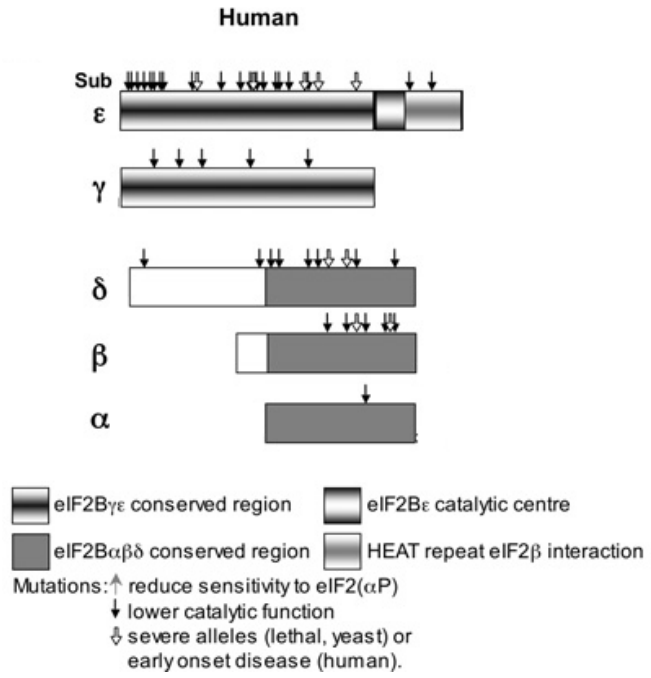

Figure 1-3 Sites of Mutations Linked to VWM. Closed down arrows represent mutations found in patients with VWM. Open down arrows represent mutations found in patients with severe, early-onset VWM. Image taken from Pavitt. Biochem Soc Trans. 2005 Dec (Pt 6): 1487-1492.

The disease is characterized by disruption of two brain cell types, oligodendrocytes and astrocytes (van der Knaap et al. 2006). There is a great reduction of myelin in the white matter regions of the brain (Pavitt and Proud 2009). The primary symptom of VWM is cerebellar ataxia (loss of motor control); under normal conditions the disease progresses slowly and is eventually fatal. During stress events such as infection or head trauma the progressive loss of motor function speeds up rapidly. Lymphoblasts and fibroblasts derived from affected patients show that the mutations in eIF2B typically reduce its activity from 20% to 70% (Horzinski et al. 2010; Li et al. 2004; van Kollenburg et al. 2006). There appears to be some correlation between the severity of the disease and the level of eIF2B inactivation, though this is rather inconsistent (Liu et al. 2011; van der Lei et al. 2010). Overall protein synthesis levels in affected cells are not reduced, leading to the hypothesis that it is not lower protein levels that are causing the disease but inability to adequately respond to cellular stresses (van Kollenburg et al. 2006). For example, during heat stress (as can occur as a response to infection) the cell's response is to reduce protein translation, this is partially done through the regulation of eIF2B activity (Clemens 2001). The eIF2B mutations in the disease could be affecting the cell's ability to respond to stress. Evidence shows upregulation of the unfolded protein response (UPR) in eIF2B mutant cells (Horzinski et al. 2010). The UPR is a cellular pathway that responds to unfolded proteins in the endoplasmic reticulum (ER) (Welihinda et al. 1999). Unfolded protein in the ER would indicate an inability to slow down protein translation in response to a cellular stress.

Localization of eIF2B in Yeast: the eIF2B Body

It has been found that a portion of eIF2B in yeast resides in distinct punctate structures or foci termed eIF2B bodies (Fig. 1-4) (Campbell et al. 2005). The eIF2B bodies appear as 1 to 2 bright areas per cell under a fluorescent microscope. The bodies can be single points or thin lines about a third the diameter of the cell. These foci contain both eIF2B and eIF2. During logarithmic growth, as much as 50% of total eIF2B and eIF2 reside in the foci; the rest of eIF2B and eIF2 are diffusely localized to the cytoplasm. Using Fluorescence Recovery After Photobleaching (FRAP), it was found that the presence of eIF2B in the bodies is relatively stable with little movement between the bodies and the cytoplasm but that eIF2 cycles in and out of the bodies fairly rapidly. It was shown that the rate of cycling of eIF2 in the bodies remains high during logarithmic growth and decreases during several different stresses that decrease the GEF

activity of eIF2B. This has led to the conclusion that eIF2B bodies are sites for eIF2B GEF exchange and that eIF2 cycles into the body to exchange its GDP with GTP (Campbell and Ashe 2006; Campbell et al. 2005). Fusel alcohols, an endpoint metabolite of amino acid catabolism, have been shown to inhibit translation initiation via interactions with eIF2B (Ashe et al. 2001). It has been found that treatment of cells with fusel alcohol causes eIF2B bodies to become immobile in the cell (Taylor et al. 2010). Under normal conditions eIF2B bodies are fairly mobile and can be seen to lightly vibrate and migrate throughout the cell; fusel alcohol treatment decreases the frequency of motion of the bodies and their subsequent movement throughout the cell is cut in half. It is not known what mechanism causes the body's loss of movement. One possibility is that they become tethered to some cellular structure and lose their freedom of motion. The fact that fusel alcohol also decreases the GEF activity of eIF2B lends itself to the theory that the free movement of the bodies is important for translation initiation (Taylor et al. 2010). So far, eIF2B bodies have not been found in any other organism besides *Saccharomyces cerevisiae*.

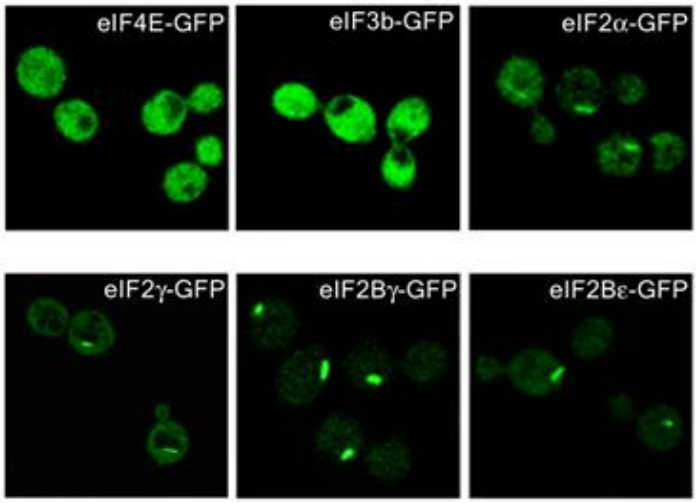

Figure 1-4 Live cell fluorescence microscopy of yeast eIF2B bodies. All strains are genomically tagged with GFP. The α and γ subunits of eIF2 as well as γ and ε subunits of eIF2B are found to localize to punctate foci in the cell. These foci have been named eIF2B bodies. eIF4E and eIF3b are included as cytoplasmic controls. In addition, eIF4E is a component of stress induced P-bodies. This shows that eIF2B bodies are distinct from P-bodies. eIF2B bodies contain subunits of both eIF2 and eIF2B. Images were taken during logarithmic growth. Image taken from Campbell et al. J Cell Biol. 2005 Sep 12;170(6):925-34.

The General Control Pathway: Sensing Amino Acid Availability in Yeast

In yeast, regulation of eIF2B activity via eIF2α phosphorylation activates the primary stress response pathway known as the general control pathway (Hinnebusch 1994). This pathway is activated during a number of cellular stresses including amino acid starvation, membrane stress, heat stress, oxidative stress, and heat shock. The pathway was first described for amino acid starvation and it is the best characterized method of translation control (Hinnebusch and Fink 1983). The pathway begins with activation of the protein kinase *GCN2* by uncharged tRNAs (de Haro et al. 1996). In the cell, tRNA exists predominately in its amino acid charged form and a very small change in the concentration of charged to uncharged tRNA can activate *GCN2* (Qiu et al. 2001). The only kinase target of *GCN2* is the previously described serine 51 on eIF2α (de Haro et al. 1996). Phosphorylated eIF2 then binds to *GCN3* on eIF2B at a site separate from GEF exchange and is thought to inhibit eIF2B GEF activity by sequestration (Hinnebusch 1993; Sarre 1989). Cells express an excess of eIF2 in comparison to eIF2B and phosphorylation of a small percentage of eIF2 can sequester a much larger percentage of total eIF2B and have a significant effect on the number of active eIF2B complexes. The reduction in GEF exchange reduces the rate of formation of ternary complex, composed of eIF2 bound with GTP and initiator tRNA. This reduction in ternary complex formation has a unique effect on the translation of the stress response transcription factor *GCN4*. The *GCN4* gene is unusual in that protein expression is completely controlled at the level of translation. *GCN4* mRNA is present in cells under all conditions and does not seem to be precisely regulated (Mueller and Hinnebusch 1986). Upstream of the *GCN4*open reading frame (ORF) are 4 smaller upstream ORFs (uORF), each only encoding a 3-5 amino acid product (Mueller and Hinnebusch 1986). Though there are 4 of these uORFs the first and last ones are sufficient for full wild-type regulation of *GCN4* protein translation(Mueller and Hinnebusch 1986). Translation initiation and elongation occur at the first uORF in a cap-dependent manner (Hinnebusch et al. 1988). Sequences surrounding the first uORF prevent normal dissociation of the ribosome after termination (Grant and Hinnebusch 1994). Instead, a special form of cap-independent translation called translation reinitiation allows the 40S subunit to stay associated with the mRNA and continue scanning (Powell 2010). The scanning 40S ribosome lacks ternary complex and must rebind it to detect an AUG start codon. The 40S ribosome will pause and initiate translation at the first AUG start codon it encounters after rebinding ternary complex (Hinnebusch 2005).

Under normal growth conditions the ribosome rebinds ternary complex quickly and the first AUG codon encountered is the fourth uORF before the actual *GCN4* ORF. The fourth uORF does not promote translation reinitiation and *GCN4* protein is not made (Grant and Hinnebusch 1994). During amino acid starvation, the reduction in ternary complex formation delays its rejoining with the scanning 40S ribosome. This delay is enough that the 40S ribosome can bypass the fourth uORF and reinitiation translation at the *GCN4* ORF and allow for *GCN4* protein to be synthesized. Expression of *GCN4* protein is sensitive enough to perturbations in ternary complex formation that it has become an important readout to detect changes in activity of a variety of translation initiation factors, including eIF2B (Hinnebusch 2005).

An Overview of Fatty Acid Synthesis

Lipids are an essential class of biological molecule in cells. They form the basis of cellular membranes and thus enable the compartmentalization that allows cells to maintain homeostasis in a changing environment. Lipids serve as important signaling molecules both intra- and inter-cellularly (English 1996; Hannun and Bell 1989; Mineo and Shaul 2012; van Meer 1993). Excluding sterols, the fundamental building block of a lipid is the fatty acid. A fatty acid is comprised of an acyl chain of hydrocarbons with a carboxyl head group. The carboxyl group reacts with other molecules to form the more complex lipid species such as phospholipids, triglycerides and sphingolipids. Cells can gain new fatty acids from their environment, such as lipid particles in the blood stream, or can synthesize them from precursors.

The fundamentals of lipid synthesis were discovered by Earl Stadtman and Horace Barker in the late 1940's (Barker et al. 1945; Stadtman and Barker 1949; Stadtman and Barker 1949; Stadtman and Barker 1949; Stadtman and Barker 1949; Stadtman and Barker 1950). Lipid synthesis in cells begins with an acetyl group conjugated to coenzyme A (CoA) being carboxylated to malonyl-CoA by the enzyme acetyl-CoA carboxylase. Malonyl-CoA is activated for further reactions by exchanging the CoA group with acyl carrier protein (ACP). This reaction is carried out by malonyl-CoA:ACP transacylase. Malonyl-ACP is condensed with acetyl-ACP by 3-ketoacyl synthetase. Acetyl-ACP is generated from acetyl-CoA by acetyl-CoA:ACP transacylase. The 3-keto group on the newly elongated acyl chain is reduced to 3-hydroxyacyl-ACP by 3-ketoacyl reductase using NADPH as a

cofactor. The hydroxyl group in the 3 position is then dehydrated to produce enoyl-ACP by 3-hydroxyacyl dehydratase. The double bond in enoyl-ACP is then reduced to form acyl-ACP by enoyl reductase. The acyl-ACP is analogous to acetyl-ACP in the original reaction and can now undergo a new round of elongation with another molecule of malonyl-ACP. The elongation, reduction, dehydration, and reduction reactions are usually grouped as a 4 step cycle in fatty acid synthesis. Two carbons are added to the chain length of a growing fatty acid with each cycle of elongation. Figure 1-6 displays the pathway and intermediates in fatty acid synthesis (Fig. 1-6). The enzyme thio esterase releases a fully elongated fatty acid from ACP (Wakil et al. 1983).

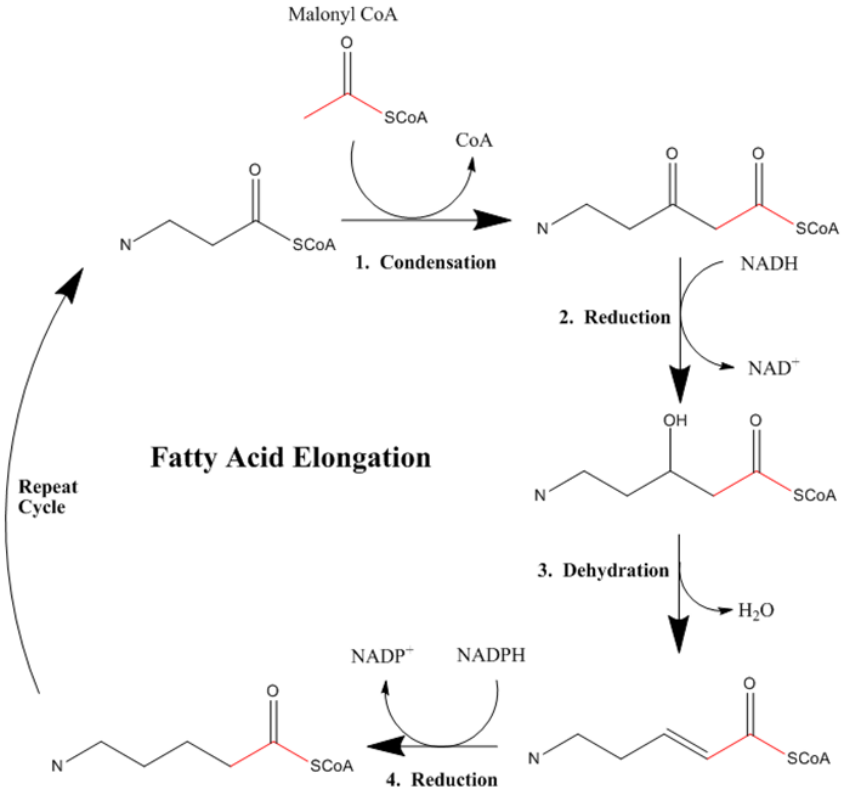

Figure 1-5 Schematic of fatty acid elongation. Shown are the four major cyclic steps and intermediates. The two carbons that elongate the acyl chain are shown in red.

In eukaryotes, the enzymes responsible for fatty acid synthesis reside on a large, multi-enzyme complex called fatty acid synthase (FAS) (Maier et al. 2010). In humans, FAS is composed of a single polypeptide that forms a homodimer (Semenkovich 1997). In yeast, FAS is composed of two separate genes: *FAS1* and *FAS2*. Six copies of each protein are incorporated into a single FAS complex to form a heterododecamer (Schweizer et al. 1978). An overview of the composition of the yeast and human FAS complex is presented in Table 1-2 in the next section. In both cases, the final FAS complex is roughly half a million Daltons in size. Despite the hydrophobic nature of its products, FAS is a soluble, cytoplasmic complex. FAS migrates close to the endoplasmic reticulum (ER) after synthesis of a fatty acid and transfers its fatty acid product to the membrane bilayer of the ER. Further enzymes in the membrane then incorporate the fatty acid into various lipid products. Mammalian FAS and yeast FAS have strikingly different structures. Dimeric mammalian FAS is X-shaped and features extensions resembling arms and legs extending from a central body, enzyme active sites are facing outward in the cleft formed between each arm and leg and the acyl chain passes between each site during the cycle (Maier et al. 2006). Dodecameric yeast FAS is barrel-shaped and contains 2 large hydrophobic pockets in its center. The inner surface of each pocket contains 3 sets of active sites of the various enzymes required for fatty acid synthesis and 3 anchor points for a growing acyl chain connected to ACP (Jenni et al. 2007). It is thought that as each step in the synthesis is carried out the acyl product is passed to another active site for another reaction while still connected to the same ACP anchor site. Elongation in yeast FAS would be continuous and only terminate after the synthesized fatty acid becomes too long to fit into the inner pocket of the complex. This mechanism usually limits synthesized fatty acids to 16-18 carbons in length that form the majority of yeast fatty acids (Ejsing et al. 2009; Schweizer et al. 1978). Interestingly, the fatty acid synthase enzymes in prokaryotes are each discreet proteins rather than the enormous single complex characteristic of eukaryotic fatty acid synthase (White et al. 2005).

Very-Long-Chain Fatty Acids and the Elongase Complex

In yeast, the typical products of FAS are palmitoleic (C_{16}) and oleic (C_{18}) acid (Ejsing et al. 2009). These two fatty acids make up the majority of the fatty acids in the cell. Certain lipid species contain longer chain fatty acids and for these a separate elongation complex called the elongase complex is required

(Cassagne et al. 1978; Jakobsson et al. 2006; Leonard et al. 2004; Welch and Burlingame 1973). The elongase complex uses CoA-bound fatty acids instead of the ACP-bound fatty acids of the FAS complex. Table 1-2 summarizes the components of the yeast and human elongase and FAS complexes (Table 1-2).

Table 1-2 Genes of FAS and the Elongase Complex in Yeast and Humans. Shown are the genes in each complex and what enzymatic functions they possess. Acetyl/malonyl CoA:ACP transaclyase is not needed by the elongase complex. HSD17B12 and SC2 are also known as KAR and TER respectively. The gene responsible for 3-hydroxyacyl dehydratase activity has not been determined for the human elongase complex.

	FAS Complex		Elongase Complex	
	Yeast	Human	Yeast	Human
Complex Structure:	Heterododecamer	Gomodimer	Separate Enzymes	Separate Enzymes
Enzymes:				
- acetyl CoA:ACP transacylase	FAS1	FAS	N/A	N/A
- malonyl CoA:ACP transacylase			N/A	N/A
- 3-ketoacyl synthetase	FAS2		FEN1/SUR4	ELOVL 1-6
- 3-ketoacyl reductase			YBR159W	HSD17B12 (KAR)
- 3-hydroxyacyl dehydratase	FAS1		PHS1	Unknown
- enoyl reductase			TSC13	SC2 (TER)

In yeast, the elongase complex resides in the ER membrane where it elongates fatty acids received from the cytoplasmic FAS complex to fatty acids greater than 20 carbons in length (Han et al. 2002). Fatty acids greater than 20 carbons are known as very-long-chain fatty acids (VLCFA). The predominant VLCFA in yeast is 26 carbons long and makes up 1-5% of all fatty acids in yeast (Ejsing et al. 2009; Rezanka 1989). The elongase complex uses the same 4 steps (elongation, reduction, dehydration, and reduction) used by FAS to generate VLCFAs. Unlike eukaryotic FAS, each enzyme is encoded by a separate gene in a similar manner to the prokaryotic FAS complex. In addition, the elongase complex is a complex in name only, each member seems to operate independent of the others and no single elongase supermolecule has been identified. Each enzyme performs its specific reaction then passes off the product to another member of the complex by simple diffusion in the lipid bilayer (Leonard et al. 2004). In yeast, the elongase complex is composed of 5 proteins (Table 1-2). The first step, elongation, is performed by both *FEN1* and *SUR4* (Oh et al. 1997; Rossler et al. 2003). Each protein contains a fully functional elongation enzyme and each protein acts independently. Rather than being completely complementary with each other, *FEN1* and *SUR4* prefer different fatty acid precursors (Denic and Weissman 2007). *FEN1* has a high affinity for C_{20} fatty acids and is important for the conversion of C_{20} to C_{22} (Oh et al. 1997). *SUR4* has a broader range of precursor fatty acid sizes but is required for the conversion of C_{24} fatty acids to the final C_{26} fatty acids (Oh et al. 1997). Deletion of either gene singly has few noticeable effects on cells but deletion of both is synthetically lethal (Revardel et al. 1995; Silve et al. 1996). In humans, six separate genes (ELOVL 1-6) are responsible for the first elongation step in VLCFA synthesis (Jakobsson et al. 2006). The first reduction step and second step overall in VLCFA elongation is carried out by *IFA38*/YBR159W (from here on referred to as YBR159W) (Rossler et al. 2003). The homolog of YBR159W in humans is HSD17B12 or KAR (See proceeding section on YBR159W and HSD17B12 for more detail) (Moon and Horton 2003). The third step in VLCFA synthesis, dehydration, is carried out by *PHS1* (Denic and Weissman 2007; Schuldiner et al. 2005). Deletion of *PHS1* is lethal in yeast (Giaever et al. 2002). A human homolog of *PHS1* is not known. The second reduction reaction and fourth and final step overall in VLCFA synthesis is carried out by *TSC13*. Deletion of *TSC13* is also lethal in yeast (Giaever et al. 2002). SC2 or TER is the human homolog of *TSC13* (Moon and Horton 2003).

.

The Utilization of Very-Long-Chain Fatty Acids

Utilization of VLCFAs varies considerably between species. In plants, VLCFAs form an essential component of seed coatings (Cassagne et al. 1994). For mammals they are used as signaling molecules as well as structural components in membranes (Calder and Yaqoob 2009). In mammals, the VLCFA component of sphingolipids has been linked to fertility of spermatozoa (Sandhoff et al. 2005). VLCFA length in mammals is extremely variable, being anywhere from 28 to 36 carbons in length (Kihara 2012).

In yeast, nearly all VLCFAs are incorporated into sphingolipids (Dickson et al. 2006). Yeast contain 3 classes of sphingolipid: Inositolphosphoceramide (IPC), mannosylinositolphosphoceramide (MIPC), and mannose-(inositol-$P)_2$-ceramide ($M(IP)_2C$) (Dickson et al. 2006). IPC is the most abundant sphingolipid (Ejsing et al. 2009). Figure 1-7 shows the structure of an IPC molecule and its components (Fig. 1-7). A sphingolipid is a class of lipid that is composed of a head group and a ceramide molecule. The head group is one of three types and determines the class of the sphingolipid. Ceramide in turn is composed of a sphingosine molecule and a fatty acid. In yeast, there are 2 primary classes of sphingosine, also known as a long-chain base: phytoshingosine and dihydrosphingosine (Dickson et al. 2006). In yeast, the fatty acid component of ceramide is most commonly a C_{26} VLCFA (Ejsing et al. 2009; Rezanka 1989). The formation of ceramide is catalyzed by the ceramide synthase complex, in yeast composed of *LAC1*/*LAG1* and *LIP1* (Kageyama-Yahara and Riezman 2006). Sphingosine is generated from palmitic acid and the amino acid serine by serine palmitoyltransferase, composed of *LCB1* and *LCB2* in yeast (Gable et al. 2002).

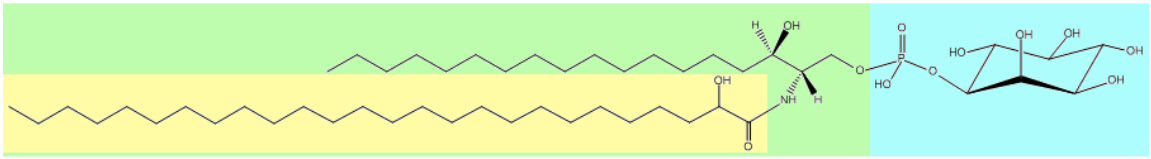

Figure 1-6 Structure of a inositol phospho-ceramide. The head group is shaded blue. The sphingoid base is shaded green. The VLCFA is shaded yellow. The ceramide portion of the sphingolipid is composed of the yellow and green shaded regions.

Sphingolipids in yeast are predominately used in a structural role. The extreme length of the VLCFA component of sphingolipids reduces physical stress on highly curved membrane formations (Schneiter et al. 2004; Schneiter et al. 1996). The VLCFAs themselves have been shown to be important for this stress reduction, a yeast mutant unable to generate sphingolipids but able to incorporate VLCFAs into phospholipids is able to resist many of the symptoms that indicate membrane stress (Gaigg et al. 2006). VLCFA-containing sphingolipids are also important for lipid raft formation (Gaigg et al. 2006). Interestingly, it has been found that sphingolipids containing VLCFAs are not essential in yeast but that both VLCFAs and sphingolipids individually are essential, indicating that they play multiple necessary and independent functions in the cell (Cerantola et al. 2007). In mammals, sphingolipids and ceramides have been linked to a number of essential biological functions. In addition to the previously mentioned role in the fertility of spermatozoa, sphingolipids are also involved in cell proliferation, inflammation, autophagy, and cell differentiation (Bedia et al. 2011; Perrotta et al. 2005; Pettus et al. 2004; Spiegel 1993). Ceramide has been shown to be involved in signaling cascades during apoptosis (Kolesnick et al. 1994).

The 3-Ketoacyl Reductase YBR159W and HSD17B12

Like other members in the elongase complex YBR159W is an integral membrane protein in the ER membrane (Han et al. 2002). It uses NADPH as a cofactor in its 3-ketoacyl reductase activity (Beaudoin et al. 2002; Han et al. 2002). A *ybr159wΔ* deletion leads to temperature sensitivity and extreme slow growth (Breslow et al. 2008; Han et al. 2002). The *ybr159wΔ* mutant fails to grow in the presence of the FAS inhibitor cerulenin and exogenous fatty acids (Omura 1976; Rossler et al. 2003). It is believed that the viability of the deletion mutant is due to the residual activity of the gene *AYR1* compensating for some of the 3-ketoacyl reductase activity of YBR159W (Han et al. 2002). *AYR1* is a 1-acyl dihydroxyacetone phosphate reductase involved in phosphatidic acid biosynthesis (Athenstaedt and Daum 2000). The *AYR1* and YBR159W amino acid sequences share 42% similarity and 23% identity. A *ybr159wΔ, ayr1Δ* double mutant is synthetic lethal (Han et al. 2002). KetoAcyl Reductase (KAR), also known as 17β hydroxysteroid dehydrogenase type 12 (HSD17B12) is the human homolog of YBR159W (Moon and Horton 2003). The amino acid sequences of YBR159W and HSD17B12 share 53% similarity and 32% identity. In addition to its role in VLCFA synthesis, HSD17B12 is responsible for the last step in the synthesis of estradiol from

estrogen (Luu-The et al. 2006). The role of HSD17B12 in estrogen production has led to it being an important marker for a variety of sex-hormone-related-organ cancers (Audet-Walsh et al. 2012; Plourde et al. 2009; Song et al. 2006; Szajnik et al. 2012).

Rationale for Dissertation Research

Recently, using tandem affinity purification and mass spectrometry, a novel protein-protein interaction has been discovered in yeast between all five subunits of eukaryotic initiation factor eIF2B and the 3-ketoacyl reductase YBR159W (Link et al. in preparation). This interaction shows a previously unknown link between protein translation and the VLCFA synthesis pathway. I hypothesize that the interaction with YBR159W represents a new mode of regulation of eIF2B in translation initiation. Furthermore, I hypothesize that this interaction represents only one of many forms of regulation of protein synthesis that have so far gone uncharacterized. The implications of this novel form of protein synthesis regulation provide a clear rational for this dissertation. The interaction would serve to regulate eIF2B activity and overall protein translation in the event of cellular stress or disruptions in VLCFA synthesis. This theory would be best tested by first characterizing the interaction itself, determining any additional factors that aide or mediate the interaction. A genetic and biochemical approach would then be used to determine what effects the interaction is having on cellular processes.

CHAPTER II

THE YEAST eIF2B TRANSLATION INITIATION COMPLEX INTERACTS WITH THE FATTY ACID SYNTHESIS ENZYME YBR159W

The following chapter was adapted from Browne *et al*. Mol. Cell Biol. 2013 Mar 33(5):1041-56 (Browne et al. 2012).

Abstract

Using affinity purifications coupled with mass spectrometry and yeast two-hybrid assays, we show the *Saccharomyces cerevisiae* translation initiation factor complex eIF2B and the very-long-chain-fatty acid (VLCFA) synthesis keto-reductase enzyme YBR159W physically interact. The data show the interaction is specifically between YBR159W and eIF2B and not between other members of the translation initiation or VLCFA pathways. Yeast two-hybrid analysis suggests subunits *GCD6* and *GCD7* as important for the interaction. YBR159Wp is an integral membrane protein localized to the endoplasmic reticulum. A *ybr159wΔ* null strain has a slow growth phenotype and reduced translation rate but a normal *GCN4* response to amino acid starvation. Affinity purifications show the eIF2B complex to be intact in a *ybr159wΔ* null strain though overall expression of the complex is reduced. No VLCFA synthesis defects are seen in a *gcn3Δ* null mutant.

Introduction

In eukaryotic translation initiation, the initiation factor eIF2 bound with GTP is required to interact with the initiator Met_i-tRNA to form the ternary complex. Following start codon recognition, eIF2-GTP is hydrolyzed to GDP and eIF2-GDP dissociates from the translation initiation complex (Preiss and M 2003; Sonenberg 2000). eIF2-GDP must exchange GDP with GTP before it can initiate another round of translation (Fig. 2-1A). The initiation factor eIF2B is an essential guanine nucleotide exchange factor

(GEF) responsible for exchanging GDP for GTP on eIF2 (Pavitt 2005). It is the only known target of eIF2B. This exchange reaction is one of the rate limiting steps in translation initiation and is the target of numerous signaling pathways in yeast as well as higher eukaryotes (Harding et al. 1999; Olsen et al. 1998; Rowlands et al. 1988; Schneider and Mohr 2003; Sood et al. 2000; Wek et al. 1990; Zhan et al. 2004). While the majority of eukaryotic GEFs are monomeric, eIF2B is unique among GEFs in that it is composed of multiple subunits. In *S. cerevisiae*, eIF2B is composed of the five subunits *GCD1*, *GCD2*, *GCN3*, *GCD6*, and *GCD7*. The *GCD6* subunit is necessary and sufficient for catalytic activity, although at a significantly reduced rate compared to the eIF2B complex (Fabian et al. 1997; Gomez and Pavitt 2000; Pavitt et al. 1998). Co-expression of *GCD6* with *GCD1* yields similar GEF activity as the eIF2B holoenzyme (Pavitt et al. 1998). Of the other 3 subunits, previous studies show *GCD2* and *GCD7* to be involved in the stability of the complex and regulatory activity (Bushman et al. 1993; Pavitt et al. 1998; Pavitt et al. 1997). *GCN3* is required for the role of eIF2B in the *GCN4* stress response pathway (Hinnebusch 1985; Kubica et al. 2006). With the exception of *GCN3*, all of the yeast eIF2B genes are essential (Pavitt 2005). Figure 2-1 summarizes the GEF exchange function of eIF2B as well as fatty acid elongation (Fig. 2-1).

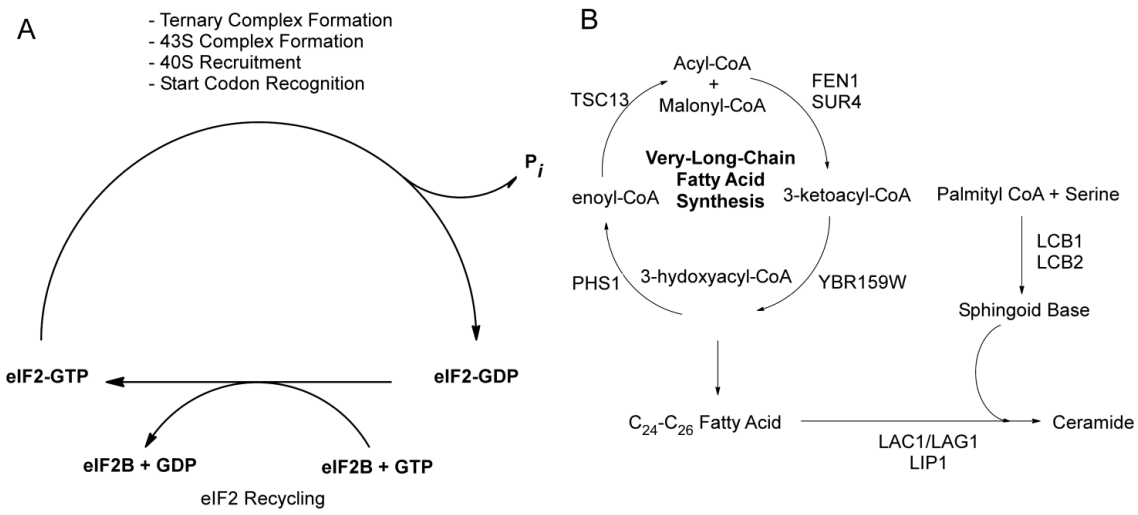

Figure 2-1 eIF2B and the VLCFA Functional Pathways. (A) Diagram showing the GEF pathway of eIF2B that is required for recharging eIF2 with GTP to begin a new round of translation initiation. (B) Diagram showing the cyclical VLCFA elongase pathway and the genes required for the catalytic steps. Also depicted is the pathway utilizing VLCFAs by the ceramide synthase complex *LAC1*/*LAG1* and *LIP1* to make ceramide. Ceramide is later modified to generate various sphingolipids.

In eukaryotes two distinct complexes are responsible for the synthesis of fatty acids (Rossler et al. 2003; Stoops and Wakil 1978). The cytoplasmic fatty acid synthase complex (FAS) elongates fatty acids from 2 to 20 carbons in length in a four reaction cycle. A second fatty acid synthesis complex, the elongase complex, is responsible for the elongation of fatty acids from 20-26 carbons (Fig. 2-1B) (Kihara 2012; Rezanka 1989). The longer chain fatty acids are known as very-long-chain fatty acids (VLCFA). In *S. cerevisiae*, VLCFAs make up 1-5% of total fatty acids (Dittrich et al. 1998; Welch and Burlingame 1973) and the predominant VLCFA is 26 carbons long (Dickson et al. 2006). VLCFAs are crucial for membrane stability and the formation of lipid rafts in yeast (Gaigg et al. 2006). Although the FAS and elongase complexes share very similar catalytic steps, different sets of enzymes catalyze the elongation reactions in the two pathways (Fig. 2-1B). The enzymes of the elongase complex localize to the endoplasmic reticulum membrane (ER) (Abraham et al. 1961; Klein 1957). The complex receives fatty acids from the cytoplasmic FAS complex and elongates them to VLCFAs (Tehlivets et al. 2007). Previous studies show YBR159W, also known as *IFA38*, is a keto-acyl reductase required for the second step in the yeast elongase pathway (Fig. 2-1B) (Beaudoin et al. 2002; Han et al. 2002). A *ybr159wΔ* null yeast strain has a slow growth phenotype and altered VLCFA lipid composition (Han et al. 2002). Though both *FEN1* and *SUR4* catalyze the first enzymatic step in the elongase pathway, they are not redundant and are responsible for different chain-length precursor fatty acids. *FEN1* prefers 20 carbon long precursors while *SUR4* has a broader range of chain-length specificity but is required to convert 24 carbon long VLCFAs to their final 26 carbon long form (Oh et al. 1997). The elongase enzymes *TSC13* and *PHS1* are both essential (Schuldiner et al. 2005; Tuller et al. 1999). In yeast, newly synthesized VLCFAs are predominately incorporated first into ceramide and eventually into sphingolipids (Dickson et al. 2006). *LIP1* is a component of the ceramide synthase complex required for the formation of ceramide from a VLCFA and a sphingoid base (Vallee and Riezman 2005). Each sphingolipid contains one 24 to 26 carbon long VLCFA in addition to the long-chain base and head group (Dickson 2008). In yeast, VLCFA-containing sphingolipids are used predominately in a structural role. Sphingolipids are important for relieving mechanical stress on highly curved membrane formations (Schneiter et al. 2004; Schneiter et al. 1996). Sphingolipids are also important components of lipid rafts. Lipid rafts are subcompartmentalizations of certain lipids in lipid bilayers that are important in a large number of cellular processes including lipid trafficking, endocytosis, and signaling (Simons and

Ikonen 1997). In yeast, one example of an important function of lipid rafts is in the localization of the plasma membrane ATPase *PMA1*. Disruption of VLCA or sphingolipid synthesis can cause defects in *PMA1* localization and function (Gaigg et al. 2006).

Using protein affinity purifications coupled with mass spectrometry and yeast two-hybrid analysis, we provide direct evidence for an interaction between the *S. cerevisiae* eIF2B complex and YBR159W. The interaction does not include eIF2 or other members of the VLCFA synthesis pathway. The eIF2B subunits *GCD6* and *GCD7* are identified as being possible mediators of the interaction. The *ybr159wΔ* null cells have a lower rate of translation but a normal *GCN4* response to amino acid starvation. Overall, this work shows a novel interaction between the essential yeast translation initiation factor and the fatty acid synthesis enzyme YBR159W.

Materials and Methods

Strains and Media

All yeast media, growth, and genetic manipulation was done using standard techniques (David C. Amberg 2005). To create the *ybr159wΔ* strain AL401, the kanamycin resistance cassette from plasmid pFa6a-kanmx6 was first amplified with primers CGTACGCTGCAGGTCGAC and ATCGATGAATTCGAGCTCG. Using the PCR double fusion approach (David C. Amberg 2005), the primers CGGATTTGGAAGTCCTTTATAG, GTCGACCTGCAGCGTACGCATTTCTTAAGCTGCACCG, CGAGCTCGAATTCATCGATTAGAATTATCGTTCTCG, and GGACTTGGTCCTTCCACC were used to expand the YBR159W genomic regions flanking the kanmx6 cassette. The YBR159W disruption cassette was transformed into strain BY4741 and transformants were selected on YPD + 300 mM G418 plates and screened using Western blotting and α-YBR159W polyclonal antibodies. Candidate BY4741 *ybr159wΔ* strains were crossed with the HIS+ strain H1511 and sporulated to create the *ybr159wΔ* null strain AL401. An isogenic wild type HIS+ control strain AL400 was selected from the same sporulation. The *lip1Δ* strain RH5994 was kindly provided by Howard Riezman (Vallee and Riezman 2005). The

gcn3Δ, fen1Δ, and sur4Δ deletion strains were obtained from the MATa yeast deletion collection (Winzeler et al. 1999). The *fen1Δ* and *sur4Δ* deletion strains from the MATa yeast deletion collection were mated with the HIS+ strain H1511 and sporulated to create the *fen1Δ* and *sur4Δ* strains, AL413 and AL414 respectively. The tandem affinity purification (TAP)-tagged strains were obtained from the yeast TAP-tagged library (Ghaemmaghami et al. 2003). The GFP tagged strains were obtained from a GFP-tagged yeast library (Huh et al. 2003). To make the *ybr159wΔ, GCD7-GFP* strain, we mated the *ybr159wΔ* strain AL401 with the *GCD7-GFP* strain AL429 from the GFP-tagged yeast library and sporulated the diploids to obtain the *ybr159wΔ, GCD7-GFP* strain AL403. The yeast two-hybrid activation-domain strains derived from parent strain PJ69-4A, the binding-domain parent strain PJ69-4alpha, and yeast two-hybrid plasmids were obtained from the Yeast Resource Center (University of Washington) (James et al. 1996). Using the protocol previously described by the Yeast Resource Center (30), the AL408 (YBR159W-BD), AL409 (*GCD1-BD*), AL410 (*GCD2-BD*), AL411 (*GCD6-BD*), and AL412 (*GCD7-BD*) strains expressing yeast two-hybrid binding-domain tagged alleles were generated from parent strain PJ69-4alpha. Briefly, initial forward and reverse primers were used to PCR the target gene from yeast genomic DNA. The PCR product and the common forward and reverse two-hybrid primers were used for a second round of PCR to extend the flanking sequences. The 2nd PCR product and the *PvuII* and *NcoI* linearized pOBD2 plasmid were co-transformed into yeast strain PJ69-4alpha and plated on SC-trp to select for recombinants fusing the target gene to the *GAL4* binding domain. Table 2-1 lists the strains used in this study (Table 2-1).

Table 2-1 Strains used in this study. Abbreviations: Del. lib. = Deletion library, YRC = Yeast Resource Center.

Strain	Genotype	Source or Reference
AL400	*MATa, ura3, leu2, HIS*$^{+}$	This study
AL401	*MATa, ura3, leu2, HIS*$^{+}$*, YBR159W::KanR*	This study
AL402	*MATa, ura3, leu2, HIS*$^{+}$*, YBR159W::KanR, [YCp-YBR159W]*	This study
AL403	*MATa, ura3, leu2, HIS*$^{+}$*, YBR159W::KanR, GCD7-GFP*	This study
AL404	*MATa, ura3, leu2, HIS*$^{+}$*, YBR159W::KanR, GCD7-GFP, [YCp-YBR159W]*	This study
AL405	*MATa, leu2, ura3, met15, GCD1-GFP, [YCp-YBR159W-dsRed]*	This study
AL406	*MATa, leu2, ura3, met15, GCD6-GFP, [YCp-YBR159W-dsRed]*	This study
AL407	*MATa, leu2, ura3, met15, GCD7-GFP, [YCp-YBR159W-dsRed]*	This study
AL408	*MATalpha, trp1-901, leu2-3,112, ura3-52, his3-200, gal4Δ, gal80Δ, LYS2::GAL1-HIS3, GAL2-ADE2, met2::GAL7-lacZ, [YBR159W-GAL4DBD]*	This study
AL409	*MATalpha, trp1-901, leu2-3,112, ura3-52, his3-200, gal4Δ, gal80Δ, LYS2::GAL1-HIS3, GAL2-ADE2, met2::GAL7-lacZ, [GCD1-GAL4DBD]*	This study
AL410	*MATalpha, trp1-901, leu2-3,112, ura3-52, his3-200, gal4Δ, gal80Δ, LYS2::GAL1-HIS3, GAL2-ADE2, met2::GAL7-lacZ, [GCD2-GAL4DBD]*	This study
AL411	*MATalpha, trp1-901, leu2-3,112, ura3-52, his3-200, gal4Δ, gal80Δ, LYS2::GAL1-HIS3, GAL2-ADE2, met2::GAL7-lacZ, [GCD6-GAL4DBD]*	This study
AL412	*MATalpha, trp1-901, leu2-3,112, ura3-52, his3-200, gal4Δ, gal80Δ, LYS2::GAL1-HIS3, GAL2-ADE2, met2::GAL7-lacZ, [GCD7-GAL4DBD]*	This study
AL413	*MATa, leu2, ura3, met15, HIS*$^{+}$*, FEN1::KanR*	This study
AL414	*MATa, leu2, ura3, met15, HIS*$^{+}$*, SUR4::KanR*	This study
AL415	*MATa, ura3, leu2, HIS*$^{+}$ *[p180]*	This study
AL416	*MATa, ura3, leu2, HIS*$^{+}$*, YBR159W::KanR, [p180]*	This study
AL417	*MATa, ura3, leu2, HIS*$^{+}$*, YBR159W::KanR, [YCp-YBR159W], [p180]*	This study
AL418	*MATa, leu2, ura3, met15, FEN1::KanR, [p180]*	This study
AL419	*MATa, leu2, ura3, met15, SUR4::KanR, [p180]*	This study
AL420	*MATalpha, ura3-52, gcd1-101, [p180]*	This study
AL421	*MATalpha, ura3-52, trp1-63, leu2-3, leu2-112, GAL2*$^{+}$*, gcn2Δ, [p180]*	This study
AL422	*MATa, leu2, ura3, met15, FEN1-GFP, [YCp-YBR159W-dsRed]*	This study
AL423	*MATa, leu2, ura3, met15, DPM1-GFP, [YCp-YBR159W-dsRed]*	This study
AL424	*MATa, leu2, ura3, met15, his3, GCN3::KanR*	Del. lib. (Winzeler et al. 1999)
AL425	*MATa, leu2, ura3, met15, YBR159W-GFP*	GFP lib. (Huh et al. 2003)
AL426	*MATa, leu2, ura3, met15, FEN1-GFP*	GFP lib. (Huh et al. 2003)
AL427	*MATa, leu2, ura3, met15, GCD1-GFP*	GFP lib. (Huh et al. 2003)
AL428	*MATa, leu2, ura3, met15, GCD6-GFP*	GFP lib. (Huh et al. 2003)
AL429	*MATa, leu2, ura3, met15, GCD7-GFP*	GFP lib. (Huh et al. 2003)
AL430	*MATa, leu2, ura3, met15, GCD2-TAP*	TAP lib. (Ghaemmaghami et al. 2003)
AL431	*MATa, leu2, ura3, met15, GCD7-TAP*	TAP lib. (Ghaemmaghami et al. 2003)
AL432	*MATa, leu2, ura3, met15, YBR159W-TAP*	TAP lib. (Ghaemmaghami et al. 2003)
AL433	*MATa, leu2, ura3, met15, FEN1-TAP*	TAP lib. (Ghaemmaghami et al. 2003)
AL434	*MATa, leu2, ura3, met15, SUR4-TAP*	TAP lib. (Ghaemmaghami et al. 2003)
AL435	*MATa, leu2, ura3, met15, TSC13-TAP*	TAP lib. (Ghaemmaghami

		et al. 2003)
AL436	*MATa, leu2, ura3, met15, his3, FEN1::KanR*	Del. lib. (Winzeler et al. 1999)
AL436	*MATa, leu2, ura3, met15, DPM1-GFP*	GFP lib. (Huh et al. 2003)
AL437	*MATa, leu2, ura3, met15, his3, SUR4::KanR*	Del. lib. (Winzeler et al. 1999)
F98	*MATalpha, ura3-52, gcd1-101*	A. Hinnebusch
H1511	*MATalpha, ura3-52, trp1-63, leu2-3, leu2-112, GAL2^{+}*	A. Hinnebusch
H2557	*MATalpha, ura3-52, trp1-63, leu2-3, leu2-112, GAL2^{+}, gcn2Δ*	A. Hinnebusch
pAD-(GCD7)	*MATa, trp1-901, leu2-3,112, ura3-52, his3-200, gal4Δ, gal80Δ, LYS2::GAL1-HIS3, GAL2-ADE2, met2::GAL7-lacZ, [GCD7-AD]*	YRC (James et al. 1996)
PJ69-4a	*MATa, trp1-901, leu2-3,112, ura3-52, his3-200, gal4Δ, gal80Δ, LYS2::GAL1-HIS3, GAL2-ADE2, met2::GAL7-lacZ*	YRC (James et al. 1996)
PJ69-4alpha	*MATalpha, trp1-901, leu2-3,112, ura3-52, his3-200, gal4Δ, gal80Δ, LYS2::GAL1-HIS3, GAL2-ADE2, met2::GAL7-lacZ*	YRC (James et al. 1996)
pOAD-(GCD1)	*MATa, trp1-901, leu2-3,112, ura3-52, his3-200, gal4Δ, gal80Δ, LYS2::GAL1-HIS3, GAL2-ADE2, met2::GAL7-lacZ, [GCD1-AD]*	YRC (James et al. 1996)
pOAD-(GCD2)	*MATa, trp1-901, leu2-3,112, ura3-52, his3-200, gal4Δ, gal80Δ, LYS2::GAL1-HIS3, GAL2-ADE2, met2::GAL7-lacZ, [GCD2-AD]*	YRC (James et al. 1996)
pOAD-(GCD6)	*MATa, trp1-901, leu2-3,112, ura3-52, his3-200, gal4Δ, gal80Δ, LYS2::GAL1-HIS3, GAL2-ADE2, met2::GAL7-lacZ, [GCD6-AD]*	YRC (James et al. 1996)
pOAD-(GCN3)	*MATa, trp1-901, leu2-3,112, ura3-52, his3-200, gal4Δ, gal80Δ, LYS2::GAL1-HIS3, GAL2-ADE2, met2::GAL7-lacZ, [GCN3-AD]*	YRC (James et al. 1996)
pOAD-(SUI2)	*MATa, trp1-901, leu2-3,112, ura3-52, his3-200, gal4Δ, gal80Δ, LYS2::GAL1-HIS3, GAL2-ADE2, met2::GAL7-lacZ, [SUI2-AD]*	YRC (James et al. 1996)
pOAD (TDH1)	*MATa, trp1-901, leu2-3,112, ura3-52, his3-200, gal4Δ, gal80Δ, LYS2::GAL1-HIS3, GAL2-ADE2, met2::GAL7-lacZ, [TDH1-AD]*	YRC (James et al. 1996)
pOAD-(YBR159W)	*MATa, trp1-901, leu2-3,112, ura3-52, his3-200, gal4Δ, gal80Δ, LYS2::GAL1-HIS3, GAL2-ADE2, met2::GAL7-lacZ, [YBR159W-AD]*	YRC (James et al. 1996)
RH5994	*MATalpha, leu2, ura3, trp1, bar1, LIP1::HIS3*	H. Riezman

Plasmids

The plasmid pOBD2 used in generating yeast 2-hybrd binding-domain strains has been previously described (Hudson et al. 1997). To create a plasmid expressing endogenous level of YBR159W, we used PCR to amplify the YBR159W gene along with 600 bp of the genomic region upstream of the start codon of the gene and the stop codon of YBR159W using the primers CACCATGGTTTTTGTGACTTTACCTATAAATAGTACACAAC and CTATTCCTTTTTAACCTGTCTTGCGGCTTTTTTTAAGGC. The PCR product was cloned into the pENTR entry vector using Directional TOPO Cloning (Invitrogen) to create pENTR-YBR159W 5' UTR-YBR159W. The YBR159W cassette was transferred to the pAG415GAL-ccdB yeast destination vector using LR Clonase recombination (Invitrogen) (Alberti et al. 2007) . To eliminate possible promoter interference, the endogenous GAL promoter of the vector was deleted using the restriction enzymes *SacI* and *SpeI* and replaced with the primer insert GGGAGCTCCATACTGATTAGTACACTAGTGG and CCACTAGTGTACTAATCAGTATGGAGCTCCC to create the YBR159W expression plasmid YCp-YBR159W. To create a plasmid expressing RFP-tagged YBR159W, the YBR159W ORF without the stop codon was amplified by PCR and cloned into the pENTR vector creating pENTR-YBR159W. The YBR159W ORF insert was transferred by recombinational cloning into the pAG415GPD-ccdB-dsRed vector (Addgene) to create the final expression plasmid YCp-YBR159W-dsRed. Tables 2-2 and 2-3 list plasmids and primers used in this study.

Table 2-2 Plasmids used in this study. YRC = Yeast Resource Center

Name	backbone	Notes	Source
pOBD2	pOBD2	ampR, TRP1, CEN4 ORI, GAL4-DBD	YRC (James et al. 1996)
YCp-YBR159W	pAG415GAL-ccdB	ampR, LEU2, CEN ORI, YBR159W 5' UTR-YBR159W	This study
YCp-YBR159W-dsRed	pAG415GPD-ccdB-dsRed	ampR, LEU2, CEN ORI, P_{GPD}-YBR159W-dsRed	This study
p180	YCp50	ampR, URA3, CEN ORI, GCN4 5' UTR-LacZ	A. Hinnebusch
pFa6a-kanmx6	pFa6a-kanmx6	ampR, KanR2	Addgene
pENTR	pENTR	KanR	Invitrogen
pENTR-YBR159W 5' UTR-YBR159W	pENTR	KanR, YBR159W 5' UTR-YBR159W	this study
pENTR-YBR159W	pENTR	KanR, YBR159W	this study
pAG415GAL-ccdB	pAG415GAL-ccdB	ampR, LEU2, CEN ORI ccdB	Addgene
pAG415GPD-ccdB-dsRed	pAG415GPD-ccdB-dsRed	ampR, LEU2, CEN ORI ccdB-dsRed	Addgene

Table 2-3 Primers used in this study. Key: Dir = primer direction, F = forward, R = reverse.

Primers	Dir	Primer Sequence (5'-3')
YBR159W deletion primer set		
	F	CGTACGCTGCAGGTCGAC
	R	ATCGATGAATTCGAGCTCG
5' homology extension primer set		
	F	CGGATTTGGAAGTCCTTTATAG
	R	GTCGACCTGCAGCGTACGCATTTCTTAAGCTGCACCG
3' homology extension primer set		
	F	CGAGCTCGAATTCATCGATTAGAATTATCGTTCTCG
	R	GGACTTGGTCCTTCCACC
two-hybrid common primer set		
	F	CTATCTATTCGATGATGAAGATACCCCACCAAACCCAAAAAAAGAGATCGAATTCCAGCTGACCACCATG
	R	GTACCGTTAAGGGCCCCTAGGCAGCTGGACGTCTCTAGATACTTAGCATCTATGACTTTTTGGGGCGTTC
two-hybrid YBR159W primer set		
	F	AATTCCAGCTGACCACCATGACTTTTATGCAACAGCTTCAAGAGGCTGG
	R	GATCCCCGGGAATTGCCATGCTATTCCTTTTTAACCTGTCTTGCGGCTTTTTTTAAGG
two-hybrid GCD1 primer set		
	F	AATTCCAGCTGACCACCATGTCAATTCAGGCTTTTGTCTTTTGCGGTAAAGG
	R	GATCCCCGGGAATTGCCATGTTAACGCTCAAATAATCCGTCATCTTCGTACTCGTAC
two-hybrid GCD2 primer set		
	F	AATTCCAGCTGACCACCATGAGCGAATCGGAAGCCAAATCTAGGTCG
	R	GATCCCCGGGAATTGCCATGTTATGCGGAACCTTTGTACTCTCTTAAAATAACAGGGAC
two-hybrid GCD6 primer set		
	F	AATTCCAGCTGACCACCATGGCTGGAAAAAAGGGACAAAAGAAAAGTGGACTAG
	R	GATCCCCGGGAATTGCCATGTTATTCCTCTTCTGAGGAAGATTCTTCGTCAGCATTC
two-hybrid GCD7 primer set		
	F	AATTCCAGCTGACCACCATGTCCTCTCAAGCATTCACTTCAGTACATCCG
	R	GATCCCCGGGAATTGCCATGTCACGCCTTATTTTTATCCAAATGCACATCAATTTGC
600 bp upstream YBR159W primer set		
	F	CACCATGGTTTTTGTGACTTTACCTATAAATAGTACACAAC
	R	CTATTCCTTTTTAACCTGTCTTGCGGCTTTTTTTAAGGC
pAG415GAL-ccdB promoter remover insert 1		
		GGGAGCTCCATACTGATTAGTACACTAGTGG
pAG415GAL-ccdB promoter remover insert 2		
		CCACTAGTGTACTAATCAGTATGGAGCTCCC

Antibodies

The α-YBR159W polyclonal antibodies were generated by inoculation of a rabbit with the synthetic peptide CETVKAENKKSGTRG (Covance). The peptide was covalently bound to cyanogen bromide beads (Sigma-Aldrich) to affinity purify α-YBR159W from rabbit whole blood. The polyclonal antibody to yeast *GCD6* was kindly provided by Dr. Alan Hinnebusch. The antibody to recognize yeast *TDH1*, *TDH2*, and *TDH3* was obtained from Millipore.

Mass Spectrometry-Proteomics

For yeast TAP experiments, TAP-tagged protein complexes were purified as previously described (Powell et al. 2004; Sanders et al. 2002). For each TAP strain, a 2 L culture was grown to an optical density at 660 nm (OD_{660}) 1-2 in YPD. The purified TAP complexes were reduced with 1/10 volume of 50 mM DTT at 65 °C for 5 min, and cysteines were alkylated with 1/10 volume of 100 mM iodoacetamide at 30 °C for 30 min. The proteins were digested overnight at 37 °C with modified sequencing grade trypsin at ~25:1 subtrate:enzyme ratio (Promega, Madison, WI). Proteins were identified using Multidimensional Protein Identification Technology (MudPIT) and a LTQ linear ion trap mass spectrometer (ThermoFisher) (Link et al. 1999; Link et al. 2005). A fritless, microcapillary (100 μm-inner diameter) column was packed sequentially with 12 cm of 5 μm C_{18}reverse-phase packing material (Synergi 4 μ Hydro RP80a, Phenomenex) and 3 cm of 5 μm strong cation exchange packing material (Partisphere SCX, Whatman). The entire trypsin-digested samples were loaded onto the biphasic column equilibrated in 0.1% formic acid, 2% acetonitrile, which was then placed in-line with an LTQ linear ion trap mass spectrometer. An automated six-cycle multidimensional chromatographic separation was performed using buffer A (0.1% formic acid, 5% acetonitrile), buffer B (0.1% formic acid, 80% acetonitrile) and buffer C (0.1% formic acid, 5% acetonitrile, 500 mM ammonium acetate) at a flow rate of 300 nL/min. Cycles 1−6 consisted of 3 min of buffer A, 2 min of 0−100% buffer C, 5 min of buffer A, followed by a 60-min linear gradient to 60% buffer B. In cycles 1−6, the percent of buffer C was increased incrementally from 0, 15, 30, 50, 70, and 100% in each cycle. During the linear gradient, the eluting peptides were analyzed by one full MS scan (300−2000 *m*/*z*), followed by five MS/MS scans on the five most abundant ions detected in the full MS scan while operating under dynamic exclusion.

GFP Affinity Purification

Two liters of the *GCD7-GFP ybr159wΔ* strain AL403, *GCD7-GFP* strain AL429, and untagged *ybr159wΔ* strain AL401 were grown to OD_{660} 1-2 in YPD. Yeast cells were harvested by centrifuging at 1500 xg for 5 min, and resuspended in 10 mL ice-cold NP-40 lysis buffer (6 mM Na_2HPO_4, 4 mM NaH_2PO_4, 1% NP-40, 150 mM NaCl, 2 mM EDTA, 50 mM NaF, 4 µg/mL leupeptin, 0.1 mM Na_3VO_4). Cells were lysed for 10 min with glass beads in NP-40 lysis buffer. The lysates were centrifuged at 500 xg for 5 min. The cleared supernatant was brought up to 25 mL with ice-cold lysis buffer. Five hundred µL bed volume of protein A/G agarose beads (Thermo Scientific) and 50 µg of anti-GFP antibody (ThermoFisher) were added simultaneously and allowed to incubate for 1 h at RT. The beads were centrifuged at 300 xg for 5 min, transferred to a Poly Prep Chromatography Column (Bio Rad) and washed at 4^{o}C with 50 column volumes of wash buffer (10 mM Tris pH 8.0, 150 mM NaCl, 0.1% NP-40). Protein digestion was carried out directly on the agarose beads. The beads were suspended in 1 mL of digestion buffer (10 mM Tris pH 8.0, 150 mM NaCl, 0.5 mM EDTA, 1 mM DTT) and transferred to a 1.5 mL microcentrifuge tube. The resuspended beads were trypsin digested as described for yeast TAP complexes. After digestion the beads were centrifuged at 13,000 xg for 1 min and the supernatant was transferred to a fresh microcentrifuge tube. MudPIT was performed identical as described for the TAP purifications. Mass spectrometry data was analyzed as previously described using C_n scoring filters of 1.5 (+1), 3.5 (+2) and 3.5 (+3) (McAfee et al. 2006).

Fatty Acid Profiling

The protocol for extracting lipids from yeast cells was adapted from Ejsing *et al.* 2008 (Ejsing et al. 2009). Each yeast strain was grown to OD_{660} 1.0-1.5 in YPD media at 30 ^{o}C. Fifty mg of wet weight yeast cells was incubated in 200 µL PBS with 100µg/mL lyticase (Sigma) for 1 h at 37°C. Next, 990 µL of chloroform/methanol (17:1 V/V) was added and incubated for 2 h at 37°C. The lower organic layer was collected and vacuum evaporated. Next, 990 µL of chloroform/methanol (2:1 V/V) was added to the upper aqueous layer and incubated for 2 h at 37°C. The lower layer was collected and pooled with the evaporated fraction taken from the first extraction and vacuum evaporated. The sample was solubilized with 100µL

chloroform/methanol (1:2 V/V) and mixed 1:1 with 0.4 mM methylamine in methanol. Samples were directly injected into an ESI-LTQ OrbitrapXL at 2 μL/min and precursor ions were scanned using the Orbitrap analyzer at a resolution of 30,000 in negative ion mode. Using published inositolphosphoceramide (IPC) precursor *m/z* values, precursor ion peaks were identified using a mass tolerance of 10 ppm (Ejsing et al. 2006; Sud et al. 2007). The following nomenclature was used for sphingolipid species: <lipid class> <carbons in fatty acid (FA) moiety> : <double bonds in FA moiety> ; <hydroxyl groups in FA moiety>. Using inositolphosphoceramide (IPC) structure data at the LIPID MAPS Lipidomics Gateway (Sud et al. 2007), the following theoretical precursor $[M-H]^-$ ion *m/z* values were used to identify the IPC ions in the high resolution scan: IPC 46:0;4 (980.717), IPC 44:0;4 (952.686), IPC 42:0;4 (924.655), IPC 40:0;4 (896.623), IPC 38:0;4 (868.592). To validate the identity of these IPC ions, the IPC precursor ions were fragmented by CID in the linear ion trap. The observed *m/z* values of the MS/MS fragment ions for each IPC precursor was compared to predicted $[\text{ceramide phosphate} - H_2O]^-$ and $[\text{ceramide phosphate}]^-$ *m/z* values at a mass tolerance of 0.1 Da. The following theoretical *m/z* $[\text{ceramide phosphate} - H_2O]^-$ and $[\text{ceramide phosphate}]^-$ fragment ions were used to validate the IPC lipids: IPC 38:0;4 (688.53, 706.54), IPC 40:0;4 (716.56, 734.57), IPC 42:0;4 (744.59, 762.60), and IPC 46:0;4 (800.65, 818.66). In addition, to validate the identification of IPC 44:0;4, the fragmentation spectrum of precursor *m/z* 952.68 at a mass tolerance of 0.1 Da was compared to the previously published fragment ions $[\text{ceramide phosphate} - H_2O]^-$, *m/z* 772.62 and $[\text{ceramide phosphate}]^-$, *m/z* 790.63 values (Ejsing et al. 2006). To compare the observed abundance for each IPC species between strains, the precursor ion signal intensity for each identified IPC species was normalized to the signal intensity of the *m/z* 835.53 base peak corresponding to the phosphatidyl inositol (PI) species PI 16:1-18:0 and PI 16:0-18:1. The following nomenclature was used for PI species: <lipid class> <carbons in 1st FA moiety> : <double bonds in 1st FA moiety> - <carbons in 2nd FA moiety> : <double bonds in 2nd FA moiety>.

Growth Rate Analysis

Yeast strains were grown overnight at 30 °C in YPD. Relative cell number was measured at OD_{660} using a Beckman DU 530 Spectrophotometer. Cells were diluted in 50 mL of fresh YPD to ~0.05 OD_{660} units/mL. Individual strains were grown at 30 °C and an OD_{660} measurement was taken every 2 h. The formula for

used for converting OD_{660} readings to cell numbers was $y = 1.1564x^3 - 0.6815x^2 + 1.3996x$ with y = cell number/mL and x = OD_{660} value (David C. Amberg 2005). Cell doubling time was determined by plotting the growth curve for each strain and measuring the maximum rate of cell growth during logarithmic growth.

Yeast Two-Hybrid

Mating type A strains containing AD tagged alleles and mating type α strains containing BD tagged alleles have been previously described (Fields and Song 1989). The A and α strains were allowed to mate in liquid YPD at 30°C overnight. Relative cell number was determined by measuring OD_{660} and 4 μL of a $1x10^7$ cells/mL solution was plated onto SC -leu, -trp, -his, 1.5 mM 3-AT agar plates. Plates were scanned after 48 h.

***GCN4-LacZ* Induction**

The yeast reporter plasmid p180 containing the *GCN4 5′* untranslated region (UTR) coupled to a -*lacZ* reporter has been previously described (Hinnebusch 1985). Yeast strains transformed with p180 were grown overnight at 30 °C in SC-ura. Cultures were diluted 1:10 and allowed to continue growing for 2 h in SC -ura, -his. Cells were spun down and split into two tubes containing 10 mL of SC -ura, -his media. A 1 M 3-AT solution was added to the starvation tube to a final concentration of 10 mM. The cells continued to grow for 4 h at 30 °C. β-galactosidase assays were performed as previously described (Rose and Botstein 1983). Cells were centrifuged at 1500 xg for 5 min and lysed with glass beads in 1 mL of ice-cold breaking buffer (100mM Tris pH 8.0, 1mM DTT, 20% glycerol). Twenty microliters of whole cell extract was added to 900 μL of Z buffer (16.1 g/L Na_2HPO_4-$7H_2O$, 5.5 g/L NaH_2PO_4-H_2O, 0.75 g/L KCl, 0.246 g/L $MgSO_4$-$7H_2O$, 2.7 mL/L βME, pH 7.0) and incubated at 28 °C for 5 min. The reaction was initiated by adding 200 μL of 4 mg/mL ONPG in Z buffer and incubated at 28 °C. After the reaction turned a pale yellow color, 0.5 mL of 1 M Na_2CO_3 was added. LacZ expression was determined by measuring the absorbance at 420 nm using a Beckman DU 530 Spectrophotometer. Protein concentration of the extracts was determined using the BioRad Dc protein assay. LacZ specific activity was determined using the equation: (OD_{420} x

1.7)/(0.0045 x protein conc. (mg/mL) x extract volume(mL) x time (min)) (David C. Amberg 2005). Values were normalized to wild type.

^{35}S-Met Incorporation

Overnight cultures of yeast grown in YPD were diluted 1:10 in 10 mL of SC-Met and grown for 3 h at 30 ^{o}C. The OD_{660} of the culture was measured to determine cell numbers. For labeling, ^{35}S-methionine (MP Biomedicals) was added to 5 mL of the cell culture to a final concentration of 10 μCi/mL. Samples were incubated with shaking for 30 min at 30 ^{o}C. Labeling was stopped by the addition of 1/10 volume 100% TCA and heating to 100 ^{o}C for 30 min. TCA precipitates were collected on GFC filters (Whatman) then washed sequentially with 5 mL each of 10% TCA and 95% ethanol. Filters were then placed in 5 mL EcoLume scintillation fluid (MP Biomedicals) and ^{35}S-Met incorporation was measured using a Beckman LS 6500 scintillation counter. Values were reported as (Counts per minute) / (OD_{660} unit).

Microscopy

Epifluorescence microscopy was performed using live yeast cells grown in SC media to an OD_{660} 1.0-1.5 at 30 ^{o}C. Cells were mounted on slides and visualized using a Zeiss Axiophot brightfield microscope with a 63x / 1.40 Plan-Apochromat oil DIC lense. Images were analyzed with MetaMorph imaging software (Molecular Devices). Live yeast cells imaged using confocal microscopy were grown in SC media to an OD_{660} 1.0-1.5 at 30 ^{o}C., Cells were visualized with a Zeiss LSM 510 META inverted confocal microscope using a 63x / 1.40 Plan Apochromat oil immersion lens.

Polysome Profiling

Polysome analysis was performed as previously described (Gerbasi et al. 2004). Yeast strains were grown in YPD to an OD_{660} of ~1. Cells were lysed with glass beads in ice-cold breaking buffer (10 mM Tris pH 7.0, 100 mM NaCl, 30 mM $MgCl_2$, 50 μg/mL cycloheximide, 200 μg/mL heparin). The crude lysate was cleared by centrifugation at 500 xg for 3 min and 20 OD_{660} units of cells was loaded on top of a 7 to 47% continuous sucrose gradient (wt/vol) cast in 50 mM Tris pH 7.0, 50 mM NH_4Cl, 12 mM $MgCl_2$, 50 μg/mL cycloheximide in a 14 x 89 mm ultracentrifuge tube (Beckman). Gradients were centrifuged in a Beckman

SW-41 rotor at 14,000 rpm for 18 h at 4 ^{o}C. Absorbance profile at 254 nm was collected from the gradients as previously described (16). One mL fractions were used for Western blotting. Monosome and polysome peak areas were determined using ImageJ software (Schneider et al. 2012). A moving baseline for each profile was established by connecting the minima between each peak and the area under each peak above this line was calculated. The polysome peak areas were summed and compared to the monosome peak area.

Results

In a tandem affinity purification proteomics screen of *S. cerevisiae* translation initiation factors followed by liquid-chromatography mass spectrometry analysis, we discovered that all five subunits of eIF2B co-purified with the VLCFA enzyme YBR159W (Link et al, in preparation; and Fig. 2-2A). Subsequent LC-MS/MS analysis of TAP-YBR159W affinity purification showed YBR159W co-purified with all five subunits of the eIF2B complex and several members of the VLCFA synthesis pathway. In this study, additional TAP experiments examined whether other members of the VLCFA synthesis pathway also interact with eIF2B subunits. With the exception of YBR159W, our data showed that other members of the VLCFA synthesis pathway did not interact with eIF2B (Fig. 2-2A). To rule out the possibility that the YBR159W-eIF2B interaction was due to an artifact of the TAP-tagged strains, we performed a GFP affinity purification using the *GCD7-GFP* strain AL429. LC-MS/MS analysis identified YBR159W co-purifying with all five subunits of eIF2B (Fig. 2-4E). Next, we utilized yeast two-hybrid to identify interactions between eIF2B subunits and YBR159W. The activation-domain tagged strains pOAD(YBR159W), pOAD(*GCD1*), pOAD(*GCD2*), pOAD(*GCN3*), pOAD(*GCD6*), pOAD(*GCD7*), pOAD(*SUI2*), and pOAD(*TDH1*) were mated with binding-domain tagged strains AL408 (YBR159W), AL409 (*GCD1*), AL410 (*GCD2*), AL411 (*GCD6*) and AL412 (*GCD7*). The positive interactions between different subunits of the eIF2B complex validated the ability of the experiment to detect previously described interactions (Fig. 2-2B). The two-hybrid analysis showed that YBR159W positively interacted with both the *GCD6* and *GCD7* subunits of eIF2B (Fig. 2-2B).

A

Gene	TAP-GCD2	TAP-YBR159W	TAP-FEN1	TAP-SUR4	TAP-TSC13
GCD1	10(28.72)	10(23.49)	-	-	-
GCD2	7(20.58)	10(21.47)	-	-	-
GCN3	7(47.54)	4(17.97)	-	-	-
GCD6	13(30.34)	16(30.58)	-	-	-
GCD7	8(34.91)	6(21.47)	-	-	-
YBR159W	6(23.92)	10(27.59)	-	-	-
FEN1	-	-	2(6.63)	-	-
SUR4	-	-	-	2(5.20)	1(5.49)
TSC13	-	1(2.89)	-	1(3.22)	2(5.79)

B

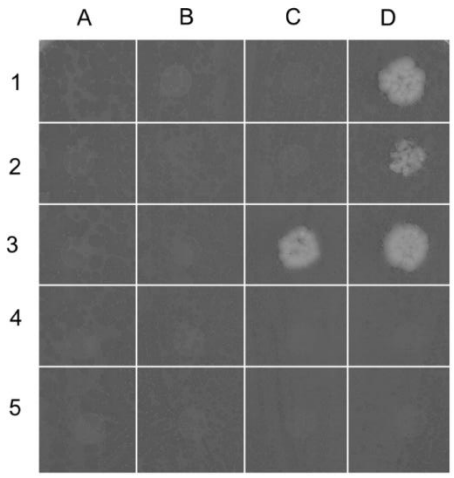

	A	B	C	D
1	YBR : GCD1	YBR : GCD2	YBR : GCD6	YBR : GCD7
2	GCD1 : YBR	GCD2 : YBR	GCN3 : YBR	GCD6 : YBR
3	GCD7 : YBR	GCD6 : GCD1	GCD6 : GCD7	GCD1 : GCD7
4	GCD1 : GCD6	GCD2 : GCD6	GCN3 : GCD6	GCD7 : GCD6
5	SUI2 : GCD1	SUI2 : YBR	TDH1 : GCD1	TDH1 : YBR

KEY

BAIT : PREY

YBR = YBR159W

Positive interaction

Figure 2-2 YBR159W's interaction with eIF2B is unique among VLCFA genes. (A) Mass spectrometry analysis of the affinity-purified *TAP-GCD2*, TAP-YBR159W, and other TAP-tagged VLCFA protein complexes. Listed are unique peptide identifications with the percent coverage of identified peptides in the protein in parentheses. A "-" indicates no peptides were identified for the gene. (B) Yeast two-hybrid (Y2H) analysis of interactions between YBR159W and eIF2B subunits *GCD6* and *GCD7*. Shown is both the assay plate used for scoring the Y2H interactions and a table of the interactions tested at each spot. Shading on the table corresponds to a positive interaction on the plate.

The GFP-tagged YBR159W strain AL425 showed the YBR159W protein localizes to the ER membrane using epifluorescence microscopy (Fig. 2-3A). *DPM1* encodes the enzyme dolichol phosphate mannose synthase which adds a mannose moiety to dolichyl phosphate on the cytosolic side of the endoplasmic reticulum (Orlean 1990; Orlean et al. 1988). Dpm1p is an ER membrane protein unrelated to VLCFA synthesis or utilization (Orlean et al. 1988). Confocal microscopy using the *FEN1-GFP*, YBR159W-RFP strain AL422 and the *DPM1-GFP*, YBR159W-RFP strain AL423 confirmed that RFP-tagged YBR159W expressed from a low-copy plasmid co-localizes with the VLCFA protein Fen1p and ER protein Dpm1p (Fig. 2-3B).

We constructed a *ybr159wΔ* yeast strain AL401 to examine the null phenotype. The mutant strain had a slow growth phenotype (Fig. 2-3C) and was temperature sensitive at 37^{o} C (data not shown). To show the slow growth phenotype was due to the deletion of *ybr159wΔ* and not a second site mutation in the strain, the *ybr159wΔ* null yeast strain was complemented in strain AL402 expressing YBR159W from the low-copy plasmid YCp-YBR159W (Fig. 2-3C). Our results agreed with previous studies using an unrelated *ybr159wΔ* null strain (Beaudoin et al. 2002).

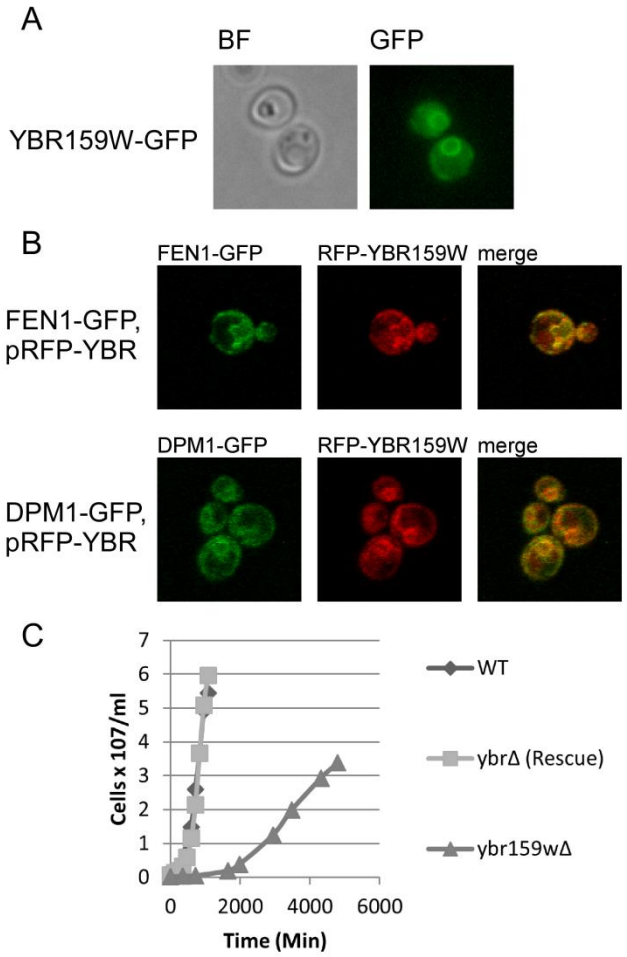

Figure 2-3 Cellular analysis of YBR159W. (A) Live cell epifluorescence imaging of endogenously tagged YBR159W-GFP indicates YBR159W localizes mainly to the ER membrane. (B) Live cell confocal microscopy showing the co-localization of YBR159W with the VLCFA pathway enzyme Fen1p and ER membrane protein Dpm1p. YBR159W is expressed on a low-copy plasmid and tagged with dsRed. *FEN1* and *DPM1* are endogenously expressed and tagged with GFP. (C) Deletion of YBR159W results in a very slow growth rate.

To determine if YBR159W has a role in translation, we examined if the *ybr159wΔ* strain AL401 causes a defect in protein synthesis. We used ^{35}S-methionine incorporation to quantify the global translation rate. The ^{35}S-methionine incorporation experiments showed that the *ybr159wΔ* strain has a reduced translation rate (Fig. 2-4A). The ceramide synthase mutant *lip1Δ* strain RH5994 also showed a reduction in the rate of translation. The *lip1Δ* strain had a similar slow growth rate as the *ybr159wΔ* strain. However, the VLCFA mutant strains AL413 (*fen1Δ)* and AL414 (*sur4Δ)* showed no reduction in translation or growth rates (Fig. 2-4A).

Next, we performed polyribosome profiling to examine the distribution of 40S, 60S, 80S, and polyribosomes in the *ybr159wΔ* strain AL401. Compared to the WT strain, we observed the polysome profiles for the *ybr159wΔ* strain showed an increase in the 80S monosome peak and a decrease in polysome peaks (Fig. 2-4B). As expected, the complemented *ybr159wΔ* strain AL402 showed a similar polysome profile to WT. To normalize and quantify the observed differences in the peak areas, the ratio of the 80S monosome to polysome peak areas was calculated. The monosome:polysome ratio significantly increased for the *ybr159wΔ* strain compared to the WT and complemented strains (Fig 2-4D). Polysome profiles of the *lip1Δ* strain RH5994 showed similar defects to the *ybr159wΔ* strain (Fig. 2-4B and 2-4D). Polysome profiling of the *fen1Δ* strain AL413 and *sur4Δ* strain AL414 showed no noticeable differences from wild type strain AL400 (Fig. 2-4B and 2-4D). These polysome distributions were consistent with the reduced global translation rates seen previously in the ^{35}S-methionine labeling experiments.

We next examined the effect of *ybr159wΔ* deletion on eIF2B activity. We used a *GCN4-lacZ* expression assay to examine *GCN4* expression during the starvation response (Hinnebusch 1994). Strains AL400 (HIS+ control strain), AL401 (*ybr159wΔ),* AL402 (*ybr159wΔ* +YCp-YBR159W), AL413 (*fen1Δ)*, AL414 (*sur4Δ),* RH5994 (*lip1Δ)*, H2557 (*gcn2Δ*) and F98 (*gcd1*) were transformed with the *GCN4-lacZ* reporter plasmid p180. Our results showed that the *ybr159wΔ, fen1Δ*, *sur4Δ*, and *lip1Δ* null strains did not affect the induction of *GCN4* during amino acid starvation (Fig. 2-4C). This suggested that the role of eIF2B in the regulation of *GCN4* response is not affected by the *ybr159wΔ* null or other VLCFA pathway mutation.

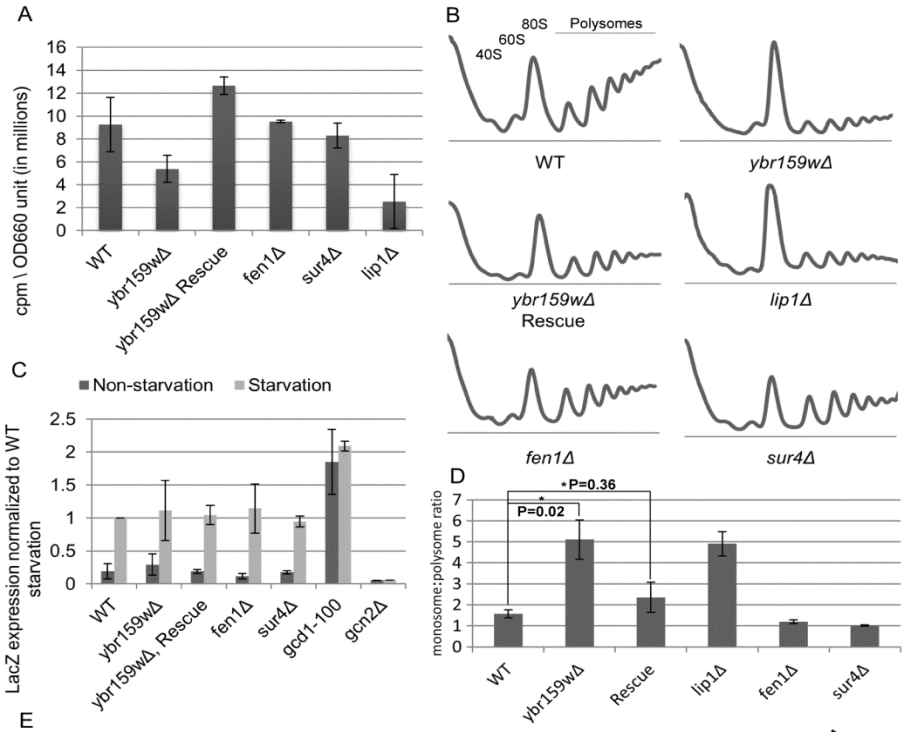

E

Gene	*ybr159wΔ*	GCD7-GFP	GCD7-GFP, *ybr159wΔ*
YBR159W	-	15(47.55)	-
GCD1	-	33(60.21)	13(33.39)
GCD2	-	30(36.41)	10(25.96)
GCN3	-	13(58.36)	8(50.49)
GCD6	-	34(54.63)	16(30.76)
GCD7	-	21(55.12)	11(38.58)

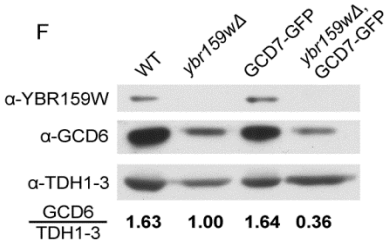

Figure 2-4 Translation assays on the ybr159wΔ strain. (A) Translation efficiency as measured by ^{35}S-methionine incorporation. Values are counts per minute per OD_{660} unit of cells. Results shown are from at least three replicates. (B) Polysome profiling of *ybr159wΔ* and other VLCFA null strains. At least three replicates were performed for each strain. Though the example *ybr159wΔ* plot does not show a 40S ribosome peak, all other replicates of the strain showed a 40S peak similar to WT. (C) Assay for *GCN4* pathway competence by *GCN4-LacZ* induction. Results are LacZ expression per mg of protein per min normalized to the WT starvation condition. Starvation conditions were induced by 10 mM 3-AT in synthetic complete minus histidine media for 4 h. The *gcd1-100* strain has a constitutively derepressed *GCN4* pathway and constant Gcn4p protein translation while the *gcn2Δ* strain is incapable of derepression of *GCN4* and cannot produce significant amounts of Gcn4p protein. (D) Ratio of monosome:polysome peak areas for the polysome profiles. P values were generated using a Student's *t*-test from at least 3 individual replicates. (E) GFP pull-down of eIF2B complexes in a *ybr159wΔ* background. Following pull-down LC-MS/MS was performed to identify the proteins. An untagged *ybr159wΔ* strain and *GCD7-GFP* tagged strain were used as controls. Displayed are unique peptide hits and percentage coverage as described in Figure 2-2A. (F) Western blot analysis of WT, *ybr159wΔ*, and *GCD7-GFP* strains. Yeast strains in Fig. 2-4D and WT strain AL400 were used. Equivalent amounts of whole cell extracts were loaded on the SDS-PAGE gel. The Western signals for *GCD6* and *TDH1-3* were determined by densitometry. The ratio of the α-GCD6/α-TDH1-3 signal is shown for each strain. The α-TDH1-3 antibody does not distinguish between the three GAPDH gene duplications in yeast.

We next tested if the *ybr159wΔ* mutation affected the composition of the eIF2B complex. Using the *ybr159wΔ*, *GCD7-GFP* tagged strain AL403, the untagged *ybr159wΔ* strain AL401, and the *GCD7-GFP* strain AL429, we performed GFP affinity purifications and LC-MS/MS mass spectrometry analysis of the affinity purified complexes. All five subunits of eIF2B were identified in the *ybr159wΔ, GCD7-GFP* strain and the *GCD7-GFP* strain (Fig. 2-4E). No subunits of eIF2B were identified in the untagged *ybr159wΔ* control strain AL401. These results suggested that the composition of eIF2B is not dependent upon presence of YBR159W.

While the composition of eIF2B appeared to be independent of YBR159W, the consistently lower number of identified peptides for each eIF2B subunit from the mass spectrometry data for the *GCD7-GFP*, *ybr159wΔ* null strain compared to the *GCD7-GFP* strain suggested that the cellular abundance of eIF2B was lower in the *ybr159wΔ* null background (Fig. 2-4E). To determine if the cellular abundance of eIF2B is lower in a *ybr159wΔ* null strain, Western analysis was performed on the yeast strains used in the *GCD7-GFP* affinity purification of eIF2B complexes. Lack of signal for YBR159W in the *ybr159wΔ* strains confirmed the expected null genotype (Fig. 2-4F). In concordance with the mass spectrometry results, the *GCD7-GFP*, *ybr159wΔ* strain had a lower abundance of eIF2B compared to *GCD7-GFP* strain (Fig. 2-4E). To validate this observation in untagged strains, Western analysis was also performed using the WT strain AL400 and the untagged *ybr159wΔ* null strain AL401. The *ybr159wΔ* null strain again showed lower abundance of eIF2B compared to the WT strain (Fig. 2-4F)

We next tested whether eIF2B played a role in VLCFA synthesis. Previous studies had shown a *ybr159wΔ* null strain had an altered VLCFA lipid composition (Han et al. 2002). Since four of the five subunits of eIF2B are essential, we used a *gcn3Δ* strain AL424 to test for VLCFA defects. WT strain AL400, *ybr159wΔ* strain AL401, *ybr159wΔ* rescue strain AL402, *sur4Δ* strain AL414, and *lip1Δ* strain RH5994 were used as positive and negative controls. To profile the VLCFAs, lipids were extracted from yeast cells and directly infused into an ESI-LTQ-OrbitrapXL mass spectrometer while scanning at high resolution in negative ion mode. Several inositolphosphoceramides (IPC), a class of VLCFA-containing sphingolipid, were identified using previously published *m/z* values at 10 ppm mass accuracy (Ejsing et al. 2009; Sud et al. 2007). We validated the identification of the IPC species using either previously observed

fragmentation spectrum or expected *m/z* values for the [ceramide phosphate – H_2O]$^-$ and [ceramide phosphate]$^-$ fragment ions of the IPCs (Fig. 2-5) (Ejsing et al. 2006).

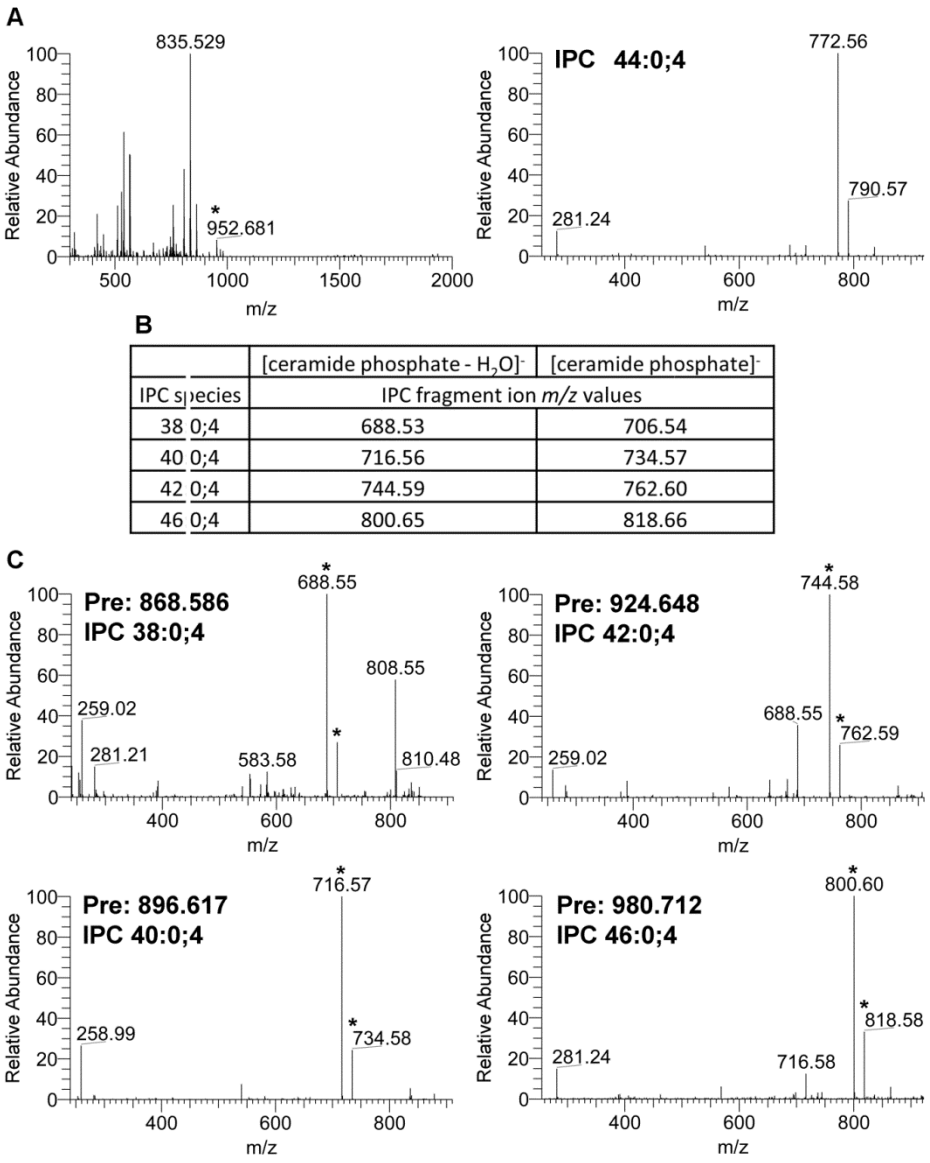

IPC species	[ceramide phosphate - H_2O]$^-$	[ceramide phosphate]$^-$
	IPC fragment ion *m/z* values	
38:0;4	688.53	706.54
40:0;4	716.56	734.57
42:0;4	744.59	762.60
46:0;4	800.65	818.66

Figure 2-5 Validation and Identification of IPCs. (A) Mass spectrometry precursor and MS/MS fragmentation spectrum for IPC 44:0;4 from WT yeast. The observed precursor ion *m/z* 952.681 represents the expected ion IPC 44:0;4 (952.686). The observed *m/z* 835.529 corresponds to the phosphotidyl inositols PI 16:0-18:1 and PI 16:1-18:0 used to normalize the relative abundance of each IPC species. In the lower MS/MS spectra of the 952.681 precursor ion, the first and second most abundant peaks correspond to the expected IPC 44:0;4 fragment ions [Ceramide Phosphate – H_2O]$^-$, *m/z* 772.62 and [Ceramide Phosphate]$^-$, *m/z* 790.63. (B) Theoretical fragmentation database for IPCs 38:0;4, 40:0;4, 42:0;4, and 46:0;4. Shown are the theoretical *m/z* values for fragment ions [ceramide phosphate – H_2O]$^-$ and [ceramide phosphate]$^-$ for IPCs 38:0;4, 40:0;4, 42:0;4, and 46:0;4. (C) MS/MS fragmentation spectra for IPCs 38:0;4, 40:0;4, 42:0;4, and 46:0;4. The observed precursor *m/z* values "Pre" of 868.586, 896.617, 924.648, and 980.712 correspond to the expected *m/z* values of IPC 38:0;4 (868.592), IPC 40:0;4 (896.623), IPC 42:0;4 (924.655), and IPC 46:0;4 (980.717) respectively. In the MS/MS spectra, the peaks corresponding to the expected theoretical IPC fragment ions [Ceramide Phosphate – H_2O]$^-$ and [Ceramide Phosphate]$^-$ are mark with a "*". In each case, the peak corresponding to the expected [Ceramide Phosphate – H_2O]$^-$ fragment ion was the most intense ion in the MS/MS spectrum.

The IPC 44:0;4 and IPC 46:0;4 sphingolipids contain full-length VLCFAs and are the most abundant yeast sphingolipid species (Dickson et al. 2006). Compared to WT, the *gcn3Δ*, *ybr159wΔ,* and other VLCFA and ceramide synthase mutant strains all showed a reduction in the IPC 44:0;4 and IPC 46:0;4 sphingolipids containing full-length VLCFAs (Fig. 2-6A). The IPC sphingolipid species IPC 38:0;4, IPC 40:0;4, and IPC 42:0;4 contain shorter-chain fatty acids and are typically only detected in VLCFA biosynthesis mutant strains (Dickson et al. 2006). As previously observed, the *sur4Δ* strain had elevated shorter-chain fatty acid-containing IPC species 38:0;4, 40:0;4, and 42:0;4 (36). We observed IPC 38:0;4 and IPC 42:0;4 were also elevated in the *ybr159wΔ* strain. The *gcn3Δ* strain showed no significant changes in the levels of the shorter-chain fatty acid sphingolipids IPC 38:0;4, 40:0;4, and 42:0;4 (Fig. 2-6B). The *lip1Δ* strain contained barely perceptible levels of any IPC, supporting its requirement for ceramide synthesis (Vallee and Riezman 2005).

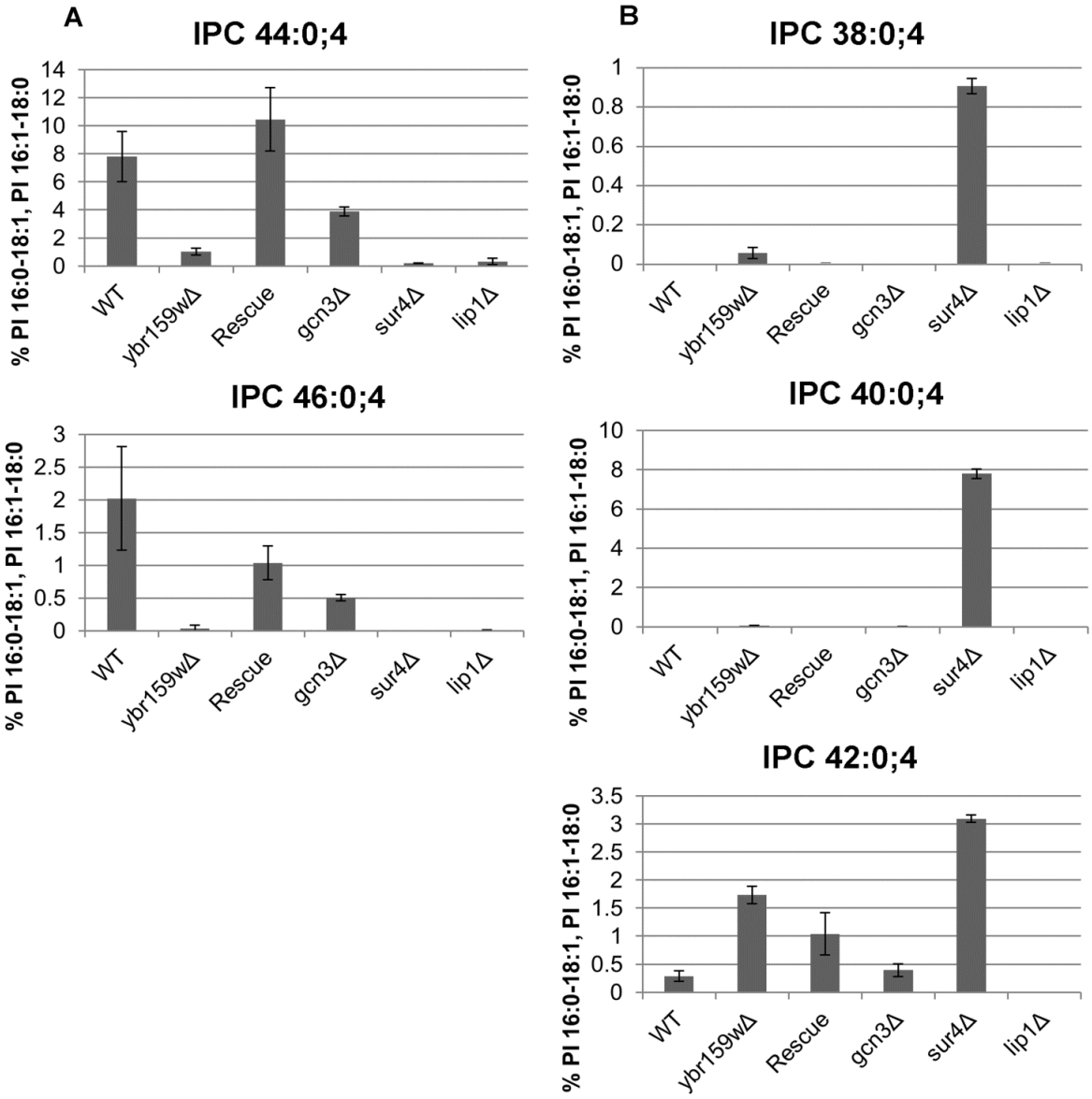

Figure 2-6 Fatty Acid profiling of WT and mutant yeast strains. (A) Longer-chain fatty acid-containing sphingolipid species. IPC species with 44 and 46 carbon-containing acyl chains are shown. The VLCFA and ceramide synthase mutants *sur4Δ* and *lip1Δ* are included as controls. (B) Shorter-chain fatty acid-containing sphingolipid species. Three IPC species with 38, 40, and 42 carbon-containing acyl chains are shown. For both A and B, data represents percentage of signal of each lipid species normalized to the signal of the PI 16:0-18:1 and PI 16:1-18:0 ion.

Discussion

Previous large-scale yeast interactions studies failed to show eIF2B interacting with the VLCFA pathway (Gavin et al. 2002; Krogan et al. 2006; Miller et al. 2005). We show using TAP-tagged and GFP-tagged affinity purifications as well as yeast-two-hybrid that the VLCFA keto-reductase YBR159W interacts with the translation initiation factor complex eIF2B. Because our unpublished proteomic screen of translation factor interactions identified YBR159W interacting with eIF2B, we named the *S. cerevisiae* locus Initiation Factor Associated protein of 38 kD or *IFA38* (Link et al., unpublished). Affinity purification and LC-MS/MS experiments show that YBR159W co-purifies with all five subunits of eIF2B and not with controls. No other member of the VLCFA pathway co-purifies in the eIF2B affinity purifications. Interestingly, the TAP-tagged members of the VLCFA pathway do not seem to strongly interact with each other. Our Y2H data suggest the eIF2B subunits *GCD6* and *GCD7* physically interact with YBR159W.

Several models for the eIF2B-YBR159W interaction can be hypothesized. Figure 2-7 presents several models for the interaction at the ER membrane (Fig. 2-7). One argument is for a direct interaction between eIF2B and YBR159W (Fig. 2-7A). The simplest model, this could be tested by pull-down of eIF2B subunits by YBR159W in an unrelated organism. Additionally, if eIF2B associates indirectly with lipid membranes via YBR159W, a deletion of *ybr159wΔ* should abolish this membrane association. Another possibility is that eIF2B subunits can be lipid modified and so directly localize to the ER membrane for interaction with YBR159W (Fig. 2-7B). This would mean eIF2B would still be membrane bound in the absence of YBR159W. Yeast cells possess several mechanisms for lipid modification including myristoylation and palmitoylation (Boutin 1997; Dietrich and Ungermann 2004). As myristoylation requires an N-terminal glycine, this form of lipid modification is unlikely for any of the eIF2B subunits. Targets of palmitoylation are much less specific; no clear consensus sequence for the modification exists. Palmitoylation is also reversible, with proteins being directed on or off the membrane depending on cellular events (Bijlmakers and Marsh 2003). Use of the palmitoylation prediction software tool CSS-Palm shows some evidence for a number of possibly modified sites on eIF2B subunits *GCD1*,

GCD2 and *GCD6* (Table 2-4) (Zhou et al. 2006). Two subunits of eIF2 are also predicted to contain possible palmitoylation sites. The unreliability of software prediction tools means experiments looking specifically for eIF2B palmitoylation *in vivo* are required.

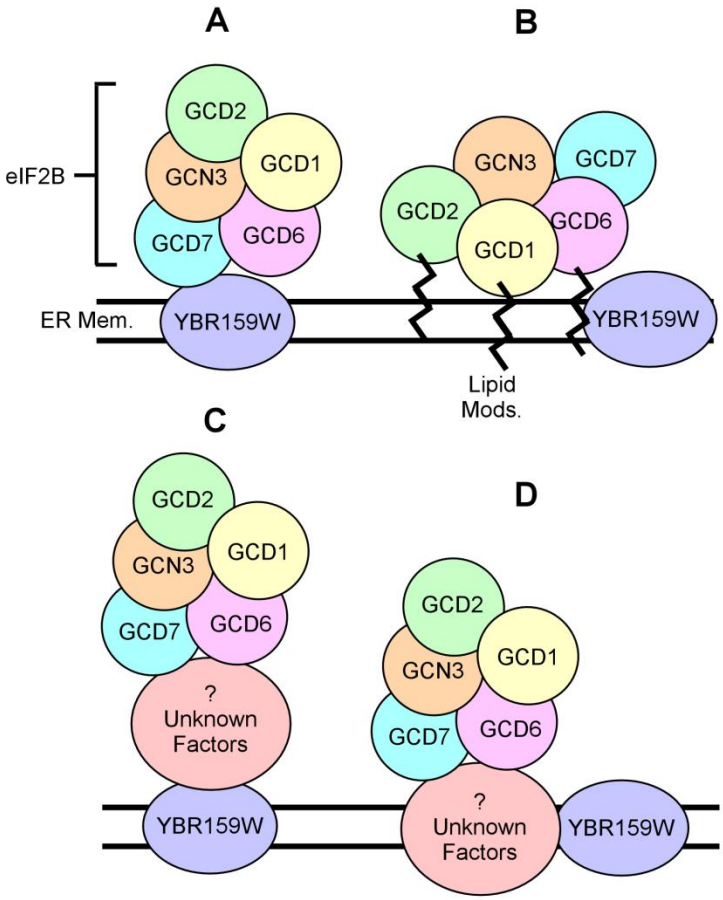

Figure 2-7 Models for the interaction between eIF2B and YBR159W. (A,B) Direct interaction models between ER bound YBR159W (A) and the ER membrane (B). (C,D) Indirect interaction models between YBR159W (C) and the ER membrane (D). In both C and D an as yet unknown factor(s) mediates the interaction seen between eIF2B and YBR159W.

Table 2-4 Putative palmitoylation sites on eIF2B and eIF2 subunits as predicted by CSS-Palm. Position is for the predicted modified cysteine residue. For details on CSS-Palm and CSS scoring see (Zhou et al. 2006).

Gene	Peptide	Position	CSS Score
GCD1			
	SIQAFVFCGKGSNLA	9	3.31
	LNSFIYFCSFELCQL	280	2.64
GCD2			
	KAAKKDLCEKIGQFA	368	2.69
	RNIPVLVCCESLKFS	506	3.41
	NIPVLVCCESLKFSQ	507	5.15
GCD6			
	QSCKIGKCTAIGSGT	342	3.77
SUI3			
	YILEYVTCKTCKSIN	236	3.54
	EYVTCKTCKSINTEL	239	3.15
	NRLFFMVCKSCGSTR	259	3.87
	FFMVCKSCGSTRSVS	262	4.62
GCD11			
	LIAGNESCPQPQTSE	224	4.08

An additional explanation for the eIF2B-YBR159W interaction is that it is indirect, with an as yet unidentified factor or set of factors mediating the interaction. This factor could be either soluble and bind both the eIF2B complex and YBR159W (Fig. 2-7C) or membrane bound (Fig. 2-7D). Figure 2-7D depicts this unknown factor as integral to the ER membrane. The model does not rule out the possibility that the unknown factor is peripherally association with the ER membrane. Statistical analysis of the LC-MS/MS data did not identify any particular factors, either cytoplasmic or membrane bound, that also showed a significant interaction with both eIF2B subunits and YBR159W. This does not mean such a factor does not exist; only that TAP purifications and mass spectrometry analysis did not identify it. It is possible the amino acid sequence of the factor does not allow for easily identifiable trypsin digested peptides or the factor(s) is not soluble during the TAP enrichment. Though use of alternative proteases may solve this problem, it is still possible it would be missed. A final theory for the interaction could be a combination of the previous models. eIF2B could have multiple redundant interaction sites with YBR159W, some direct and some indirect. More intense biochemical analysis of the interaction between eIF2B and YBR159W is needed to determine the exact sites on the proteins important for the interaction and to identify any additional factors that mediate it.

Theorizing about the function of the interaction between the VLCFA synthesis pathway and the eIF2B translation initiation pathway raises a number of possibilities. Is one pathway regulating the other or vice versa? It can be hypothesized that the cell might need to regulate VLCFA synthesis if translation is disrupted. Alternatively, it might be advantageous to reduce translational activity if VLCFAs are being down regulated. Finally, the YBR159W-eIF2B complex could be involved in a novel function. A link between a translation initiation factor and lipid membranes is not totally unique. Experiments in human cells have shown an interaction between the translation initiation factor eIF4E and the Golgi apparatus (Willett et al. 2011).

To test the hypothesis that YBR159W and VLCFA synthesis play a role in translation, we used ^{35}S-methionine incorporation and polysome profiling to assay translation activity in mutant strains. Both experiments show a reduction in the translation rate for the *ybr159wΔ* strain. However, a similar phenotype is seen for the slow growing *lip1Δ* strain. The VLFCA mutant *fen1Δ* and *sur4Δ* strains have wild type growth rates and do not share a translation defect with the slower growing members of the pathway. It is

not known if the cause of the translation defect seen in the *ybr159wΔ* strain is directly related to its interaction with eIF2B or is an indirect consequence of slow growth or a VLCFA defect.

When Gcn4p expression is examined using the *GCN4-LacZ* assay, the *ybr159wΔ* strain has WT levels of *GCN4* induction. The *GCN4-LacZ* assay was normalized to protein concentration so the slow growth rate of *ybr159wΔ* should not affect the results. The data indicates that the *ybr159wΔ* strain does not have a defect in the *GCN4* pathway. We cannot rule out the possibility that the slow growth of *ybr159wΔ* may be masking a subtle defect in the GEF activity of eIF2B unrelated to the *GCN4* pathway. Our affinity purification experiments of eIF2B in a *ybr159wΔ* deletion background showed that the eIF2B complex is intact. A Western blot of *ybr159wΔ* strains showed that the overall abundance of eIF2B was lower in the deletion background compared to WT. It is not clear if the lower level of eIF2B is caused by the slow growth phenotype of the *ybr159wΔ* null background or some other factor.

An unusual and poorly understood property of the eIF2B catalytic ε subunit (*GCD6* in yeast, eIF2B5 in humans) is its inhibition by high concentrations of nicotinamide adenine dinucleotide phosphate ($NADP^+$) and the subsequent rescue from inhibition by equal concentrations of the reduced form of $NADP^+$ (NADPH) (Dholakia et al. 1986; Oldfield and Proud 1992; Wang et al. 2012). A predicted dinucleotide binding site exists on eIF2Bε but *in vivo* binding of $NADP^+$/NADPH has not been shown. The fact that equimolar concentrations of NADPH counteract the inhibiting effect of $NADP^+$ has led researchers to assume the effect is not significant *in vivo*. NADPH is often several fold more abundant in the cell than $NADP^+$. $NADP^+$ also typically exists in the cell at much lower concentrations than those needed to see eIF2B inhibition (Veech et al. 1969). YBR159W specifically binds NADPH as a cofactor in its enzyme function (Beaudoin et al. 2002). This presents a possible model for the function of the interaction. By being in close proximity to $NADP^+$/NADPH bound YBR159W via the interaction eIF2B might experience an increased local concentration of the dinucleotide. Following its reduction reaction, if $NADP^+$ does not immediately dissociate from YBR159W, eIF2B could be inhibited by the YBR159W-bound $NADP^+$. YBR159W in a $NADP^+$-bound state for an extended period of time could represent either a disruption of VLCFA synthesis or an unfavorable redox state in the cell. Either possibility could be reasons to limit protein synthesis via regulation of eIF2B. Figure 2-8 illustrates several models for eIF2B inhibition by binding of $NADP^+$ to *GCD6* (Fig. 2-8). One model depicts an oxidizing environment and a corresponding

increase in YBR159W bound with $NADP^+$ (Fig. 2-8B). This model could be tested by examination of the translation response of *ybr159wΔ* null cells to oxidative stress. The model would predict a lessened response to the stress. A second model depicts how a disruption in VLCFA synthesis could lead to an increase in enzymatically inactive YBR159W bound with $NADP^+$ and thus inhibition of eIF2B activity (Fig. 2-8C). This model could be tested by examination of translation initiation rates in cells with a deletion of either *fen1Δ* or *sur4Δ* and a conditional allele for the other second gene. This would deplete the precursors for YBR159W catalytic activity and leave it in an inactive state.

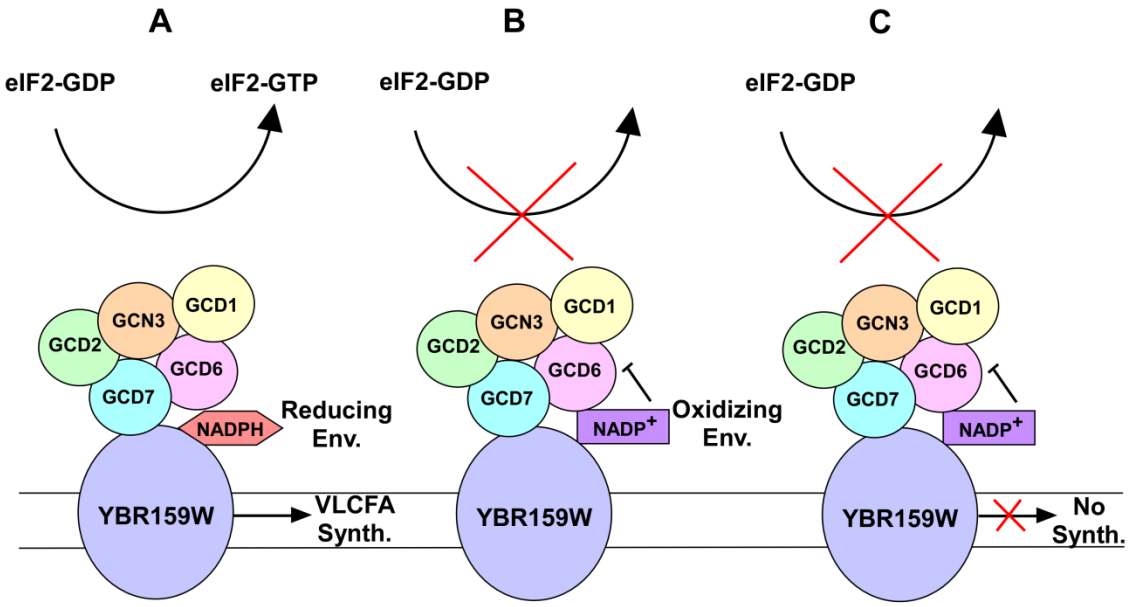

Figure 2-8 Functional models of the interaction between eIF2B and YBR159W. (A) Normal cellular conditions allow for synthesis of both VLCFAs and proteins via interactions between NADPH bound YBR159W and eIF2B. (B) During oxidation stress, $NADP^+$ bound to YBR159W could inhibit eIF2B GEF exchange via eIF2B subunit *GCD6*. It is not known if an oxidizing environment also inhibits YBR159W. (C) Disruptions in VLCFA synthesis could inhibit eIF2B activity. Downregulation of YBR159W activity could increase the occupancy of $NADP^+$ over NADPH and thus inactivate *GCD6*.

To test the hypothesis that eIF2B plays a role in VLCFA synthesis, several limitations arose that made answering the question problematic. Of the 5 yeast eIF2B subunits, only *GCN3* is nonessential. The *gcn3Δ* strain did not show a defect in VLCFA production or utilization. While the *gcn3Δ* strain showed a reduction in the sphingolipid species IPC 44:0;4 and IPC 46:0;4, it did not show a concomitant rise in shorter-chain fatty acid-containing IPC species indicative of a defect in VLCFA production. The presence of shorter-chain sphingolipids would indicate the cell is trying to compensate for a lack of VLCFAs. Therefore, we postulate the lower levels of IPC 44:0;4 and IPC 46:0;4 seen in the *gcn3Δ* strain are unrelated to a defect in VLCFA production. The VLCFA defect in *ybr159wΔ* is modest; with only a small rise in the shorter-chain fatty acid-containing sphingolipids. The loss of IPC 46:0;4 is the most striking characteristic of the strain. Previous work suggests that Ayr1p is able to perform 3-ketoacyl activity in the absence of YBR159W (Han et al. 2002). The same study showed *ayr1* and *ybr159w* are synthetically lethal (Han et al. 2002).

A *gcn3Δ* null strain is unable to fully derepress Gcn4p expression during amino acid starvation (Hannig and Hinnebusch 1988). *GCN4* is a transcription factor involved in the expression of several hundred genes during a wide variety of cellular stresses (Natarajan et al. 2001). Though growth conditions for the *gcn3Δ* strain should not have activated a stress response, we suspected analysis of the lipid content of the *gcn3Δ* strain could prove problematic if the VLCFA pathway was a downstream target of the *GCN4* transcription factor. We examined the effects of loss of *GCN4* using expression data for *gcn4Δ* strains from the Gene Expression Omnibus (GEO) Database (Barrett et al. 2011). Two separate datasets showed no significant changes in the expression of various VLCFA genes (data not shown, GEO Accession GSE24057 (Fendt et al. 2010) and GSE25582). We concluded that under the conditions used for the analysis of sphingolipids, loss of *GCN4* did not significantly alter VLCFA gene expression. We concluded our *gcn3Δ* strain was not experiencing alterations in VLCFA gene expression due to repression of *GCN4*. The lack of a direct translation defect in the *ybr159wΔ* strain and the lack of a VLCFA defect in the *gcn3Δ* strain suggest there is no significant cross-talk between the GEF and VLCFA pathways.

It remains to be determined if the translation defect seen in the *ybr159wΔ* strain is the cause of the slow growth of the strain or vice versa. Further experiments are required to determine the functional role of YBR159W interacting with eIF2B. Up until now, the interaction between eIF2B and YBR159W has been

assumed to occur on the ER membrane. Our data indicates that YBR159W is ER bound while eIF2B is thought to be a soluble cytoplasmic complex. Because eIF2B is the more mobile component of the interaction, it is assumed that it moves relative to YBR159W. From the interaction it can be theorized that there would be a fraction of eIF2B interacting with YBR159W at the membrane. Experiments need to be performed to see if membrane-associated eIF2B is visible using other methods such as fluorescent microscopy or subcellular fractionation. It would be expected that membrane-associated eIF2B would co-fractionate with membranes. If this were not seen it might be that YBR159W has a soluble form and that the interaction is occurring in the cytoplasm. Another approach is to see if eIF2B co-localizes with the ER membrane using fluorescent confocal microscopy. If co-localization is seen between eIF2B and YBR159W that would indicate a substantial amount of the proteins are interacting. Lack of co-localization under fluorescent microscopy would not necessarily indicate that the interaction is not happening, just that the total amount of eIF2B and YBR159W interacting are well below the levels of non-interacting proteins and thus the interaction is too small to properly visualize with microscopy. As eIF2B has been shown to localize to eIF2B bodies in yeast, it needs to be seen if these bodies also display any membrane localization. These findings could show a never before seen characteristic of the eIF2B complex and strengthen the impact of the novel interaction between eIF2B and YBR159W.

Acknowledgements

CB was supported by NIH training grant T32 AI007611. PS and AL were supported by NIH grant GM64779**.** We thank Dr. Tom Dever, Dr. Alan Hinnebusch, and Dr. Howard Riezman, for reagents and yeast strains. Experiments, data analysis, and presentation of fluorescent microscope images were performed in part through the use of the VUMC Cell Imaging Shared Resource, which is supported by NIH grants CA68485, DK20593, DK58404, HD15052, DK59637.

CHAPTER III

THE YEAST eIF2B TRANSLATION INITIATION COMPLEX SHOWS INTERACTIONS WITH ER MEMBRANES AND ABNORMAL CELLULAR LOCALIZATION FOLLOWING DELETION OF VLCFA PATHWAY GENES

The following chapter was adapted from Browne *et al*. Mol. Cell Biol. 2013 Mar 33(5):1041-56.

Abstract

Previous work has shown that the eukaryotic translation factor eIF2B interacts with the very-long-chain fatty acid 3-ketoacyl reductase enzyme YBR159W. YBR159W is an integral membrane protein of the endoplasmic reticulum. The eIF2B complex shows two different forms of cellular localization; one form is diffuse, cytoplasmic localization, the other is in distinct foci termed eIF2B bodies. Up to now, eIF2B bodies have been thought to be mobile cytoplasmic complexes that appear as one to two large cytoplasmic bodies. Our work confirms that YBR159W localizes to the ER membrane. Using subcellular fractionation experiments, I have found that a pool of eIF2B cofractionates with lipid membranes in a ribosome-independent and YBR159W-independent manner. Though the majority of cellular eIF2B and YBR159W do not appear to colocalize under fluorescent microscopy, confocal imaging strongly suggests that eIF2B bodies have an affinity for ER membranes. We show that a *ybr159wΔ* yeast strain and other strains with null mutations in the VLCFA pathway disrupt the normal localization of eIF2B in the cell and cause eIF2B to appear as numerous small foci throughout the cytoplasm.

Introduction

In eukaryotes, the translation initiation guanine-nucleotide exchange factor (GEF) eIF2B is responsible for exchanging GDP with GTP on eIF2. eIF2-GDP is unable to bind initiator tRNA or interact

with the 40S ribosomal subunit during translation initiation (Merrick W. C.). eIF2B is the only GEF of eIF2 and eIF2 is the only target of eIF2B (Pavitt 2005). eIF2B exists in the cell as a complex of 5 protein subunits. These 5 subunits are conserved from yeast to humans. In yeast, the subunits are *GCN3* (α), *GCD7* (β), *GCD1* (γ), *GCD2* (δ) and *GCD6* (ε). Only *GCN3* is nonessential in yeast; all 5 subunits are essential in humans. Studies in yeast have shown the ε subunit *GCD6* to be responsible for eIF2B GEF activity. The γ subunit *GCD1* aids *GCD6* and greatly increases the nucleotide exchange rate of *GCD6* (Pavitt et al. 1998). The α subunit *GCN3* serves a regulatory role in a number of stress response pathways. The δ and β subunits *GCD2* and *GCD7* share homology with regions of *GCN3* that allow for intersubunit interactions; all three subunits form a regulatory subcomplex (Pavitt et al. 1998).

Recent studies show that a significant fraction of yeast eIF2B resides in distinct foci in the cytoplasm known as eIF2B bodies (Campbell and Ashe 2006; Campbell et al. 2005). During logarithmic growth, yeast cells often contain 1 to 2 eIF2B bodies. The presence of eIF2B bodies under normal growth conditions is a striking difference between eIF2B bodies and the stress-induced processing-bodies (P-bodies) and stress granules. GFP fluorescence microscopy shows the eIF2B bodies contain both eIF2B and eIF2 (Buchan and Parker 2009; Parker and Sheth 2007). As more evidence eIF2B bodies are unique structures, eIF2B and eIF2 are not present in P-bodies or stress granules. The initiation factor eIF2 appears to shuttle in and out of the eIF2B bodies (Campbell et al. 2005). The shuttling occurs quickly during logarithmic growth and slower following disruptions of translation initiation. The presence of eIF2B in the bodies is more stable. These findings have created a model where eIF2 moves into the eIF2B body for nucleotide exchange and then leaves it to complete its translation initiation function. The eIF2B bodies are thus thought to be important sites for the GEF activity of eIF2B.

In eukaryotes, fatty acids longer than 20 carbons in length are synthesized by a special fatty acid synthesis complex known as the elongase complex (see Fig. 2-1B in previous chapter) (Jakobsson et al. 2006; Leonard et al. 2004). Fatty acids longer than 20 carbons are known as very-long-chain fatty acids (VLCFA). In yeast, the elongase pathway is composed of the 3-ketoacyl synthetases *FEN1* and *SUR4*, the 3-ketoacyl reductase YBR159W, the 3-hydroxyacyl dehydratase *PHS1*, and the enoyl reductase *TSC13* (Oh et al. 1997; Rossler et al. 2003; Schuldiner et al. 2005). The pathway predominately synthesizes 26-carbon

long VLCFAs. These VLCFAs are incorporated into sphingolipids in yeast where they largely serve a structure role by both relieving mechanical stress in highly-curved membranes and stabilizing lipid rafts (Dickson et al. 2006; Gaigg et al. 2006; Schneiter et al. 2004; Schneiter et al. 1996). VLCFAs are synthesized in the ER membrane where the elongase complex resides. Both *PHS1* and *TSC13* are essential genes. Deletion of *FEN1* along with *SUR4* is synthetically lethal (Revardel et al. 1995; Silve et al. 1996). While a *ybr159wΔ* null mutant is viable, it is thought the reductase gene *AYR1* can compensate for the loss of ketoacyl reducatase activity in the mutant (Han et al. 2002). A *ybr159wΔ, ayr1Δ* double null mutant is synthetically lethal.

YBR159W, also known as *IFA38*, is responsible for the second step in VLCFA synthesis, the reduction of a 3-ketoacyl intermediate to a 3-hydroxyacyl intermediate. YBR159W binds NADPH as a cofactor and oxidizes it as part of its enzymatic activity. A *ybr159wΔ* null yeast strain is extremely slow growing, temperature-sensitive, and has reduced levels of VLCFA-containing sphingolipids (Beaudoin et al. 2002; Han et al. 2002). In *ybr159wΔ* null cells, sphingolipids contain shorter-chain fatty acids instead of the wild-type VLCFA. Like other members of the elongase pathway, YBR159W is an integral ER membrane protein.

The ER in budding yeast is composed of the classical membrane network connected to the nuclear envelope as well as a network of tubules known as the cortical ER. The cortical ER extends throughout the cell and encases the inner face of the entire plasma membrane (Preuss et al. 1991). In microscopy, the cortical ER can often be mistaken as the plasma membrane itself (Preuss et al. 1991). While the bulk of yeast cortical ER lies under the plasma membrane, in most metazoan cells, including mammalian cells, the ER is continuous with the nuclear envelope and forms a network of tubules throughout the cytoplasm that closely align with microtubules (Lowe and Barr 2007).

Recently, studies in our laboratory have found a novel protein-protein interaction between the eIF2B complex and the 3-ketoacyl reductase YBR159W. The interaction is unique in that eIF2B has been thought to only localize to the cytoplasm and has not been previously shown to strongly interact with any ER membrane proteins. We showed that the interaction is specific for all 5 subunits of eIF2B and YBR159W and does not include either eIF2 or other members of the VLCFA synthesis pathway. Yeast 2-

hybrid (Y2H) data showed the interaction with the eIF2B complex is possibly mediated by subunits *GCD6* and *GCD7*. Functional assays showed that a *ybr159wΔ* null strain has a reduced rate of translation though the exact cause of the phenotype could not be determined. In this study, we examine the effects the interaction of eIF2B and YBR159W have on the localization of each other. Supporting our previous work that shows eIF2B interacting with ER membrane protein YBR159W, we find that in wild-type cells eIF2B co-localizes with lipid membranes. We show that this membrane co-localization is not altered in a *ybr159wΔ* strain, indicating eIF2B is interacting with the membrane in an as yet undetermined manner. Our experiments show that a *ybr159wΔ* mutation causes eIF2B to appear as numerous foci. The appearance of numerous eIF2B foci does not appear to correlate with the cell's translation rate as other VLCFA mutant strains showing multiple eIF2B foci have WT translation rates. We find that all strains displaying multiple eIF2B foci also display abnormal internal membrane structures. This work shows an until now undescribed membrane localization for translation initiation factor eIF2B and presents a possible link between lipid membranes and the eIF2B body.

Materials and Methods

Strains and Media

All yeast media, growth, and genetic manipulation was done using standard techniques (David C. Amberg 2005). To create the *ybr159wΔ* strain AL401, the kanamycin resistance cassette from plasmid pFa6a-kanmx6 was first amplified with primers CGTACGCTGCAGGTCGAC and ATCGATGAATTCGAGCTCG. Using the PCR double fusion approach (David C. Amberg 2005), the primers CGGATTTGGAAGTCCTTTATAG, GTCGACCTGCAGCGTACGCATTTCTTAAGCTGCACCG, CGAGCTCGAATTCATCGATTAGAATTATCGTTCTCG, and GGACTTGGTCCTTCCACC were used to expand the YBR159W genomics flanking the kanmx6 cassette. The YBR159W disruption cassette was transformed into strain BY4741 and transformants were selected on YPD + 300 mM G418 plates and screened using Western blotting and α-YBR159W polyclonal antibodies. Candidate BY4741 *ybr159wΔ*

strains were crossed with the HIS+ strain H1511 and sporulated to create the *ybr159wΔ* null strain AL401. An isogenic wild type HIS+ control strain AL400 was selected from the same sporulation. The *lip1Δ* strain RH5994 was kindly provided by Howard Riezman (Vallee and Riezman 2005). The *fen1Δ, and sur4Δ* deletion strains were obtained from the MATa yeast deletion collection (Winzeler et al. 1999). The *fen1Δ* and *sur4Δ* deletion strains from the MATa yeast deletion collection were mated with the HIS+ strain H1511 and sporulated to create the *fen1Δ* and *sur4Δ* strains, AL413 and AL414 respectively. The TAP tagged strains were obtained from the yeast TAP-tagged library (Ghaemmaghami et al. 2003). The GFP tagged strains were obtained from a GFP-tagged yeast library (Huh et al. 2003). To make the *ybr159wΔ, GCD7-GFP* strain, we mated the *ybr159wΔ* strain AL401 with the *GCD7-GFP* strain AL429 from the GFP-tagged yeast library and sporulated the diploids to obtain the *ybr159wΔ, GCD7-GFP* strain AL403. See Table 2-1 is the last chapter for a full list of strains used in this study.

Plasmids

The plasmid pOBD2 used in generating yeast 2-hybrd binding-domain strains has been previously described (Hudson et al. 1997). To create a plasmid expressing endogenous level of YBR159W, we used PCR to amplify the YBR159W gene along with 600 bp of the genomic region upstream of the start codon of the gene and the stop codon of YBR159W using the primers CACCATGGTTTTTGTGACTTTACCTATAAATAGTACACAAC and CTATTCCTTTTTAACCTGTCTTGCGGCTTTTTTTAAGGC. The PCR product was cloned into the pENTR entry vector using Directional TOPO Cloning (Invitrogen) to create pENTR-YBR159W 5' UTR-YBR159W. The YBR159W cassette was transferred to the pAG415GAL-ccdB yeast destination vector using LR Clonase recombination (Invitrogen) (Alberti et al. 2007) . To eliminate possible promoter interference, the endogenous GAL promoter of the vector was deleted using the restriction enzymes *SacI* and *SpeI* and replaced with the primer insert GGGAGCTCCATACTGATTAGTACACTAGTGG and CCACTAGTGTACTAATCAGTATGGAGCTCCC to create the YBR159W expression plasmid YCp-YBR159W. To create a plasmid expressing RFP-tagged YBR159W, the YBR159W ORF without the stop codon was amplified by PCR and cloned into the pENTR vector creating pENTR-YBR159W. The YBR159W ORF insert was transferred by recombinational cloning into the pAG415GPD-ccdB-dsRed

vector (Addgene) to create the final expression plasmid YCp-YBR159W-dsRed. All plasmids and primers used in this study are listed in Table 2-2 and Table 2-3 respectively in the previous chapter.

Antibodies

The α-YBR159W polyclonal antibodies were generated by inoculation of a rabbit with the synthetic peptide CETVKAENKKSGTRG (Covance). The peptide was covalently bound to cyanogen bromide beads (Sigma-Aldrich) to affinity purify α-YBR159W from rabbit whole blood. Polyclonal antibodies to yeast Sui2 were kindly provided by Dr. Tom Dever. Polyclonal antibodies to yeast Gcd6 and Gcd1 were kindly provided by Dr. Allan Hinnebusch. The mouse α-DPM1 was obtained from Molecular Probes. Antibodies to the yeast Tdh1, 2, 3 proteins were obtained from Millipore. The antibody to yeast Rpl32 was kindly provided by Dr. Jonathan Warner.

Membrane Flotation

Membrane flotation of yeast extracts was performed as previously described (Bergmann and Fusco 1988). Fifty mL of each yeast strain was grown to OD_{660} 1.0-1.5 in YPD media at 30 ^{o}C. The cells were lysed with glass beads in ice-cold breaking buffer (30 mM Tris pH 7.0, 1 mM EDTA). The lysate was cleared by centrifugation at 500 xg for 3 min. Lysate corresponding to 10 OD_{660} units of cells in 222 µL was mixed with 1778 µL of ice-cold 90% sucrose (wt/vol), 10 mM Tris pH 7.0 solution. The 2 mL of lysate/sucrose solution was transferred to the bottom of a 14 x 89 mm ultracentrifuge tube (Beckman, cat. # 344059) and layered with 6 mL of 65% sucrose, 10mM Tris pH7.0 and then 3 mL of 10% sucrose, 10mM Tris pH 7.0. The tubes were centrifuged in a Beckman SW-41 rotor at 24,000 rpm for 18 h. Individual 1.5 mL fractions were collected from the top of the gradient and the proteins TCA precipitated. Ten percent of each fraction was used for SDS-PAGE and Western blotting.

Membrane Flotation Fractions Affinity Purifications

For each TAP strain, a 1 L culture was grown to OD_{600} ~1 in YPD and the cells were split into 6 fractions. Each cell fraction was separated using the membrane flotation gradients as described above. The 10%-65% sucrose interface layer and 80% sucrose layer from each gradient were collected and pooled. TAP

purification was performed as previously described up to TEV protease cleavage (Powell et al. 2004; Sanders et al. 2002).

Mass Spectrometry-Proteomics

For yeast TAP experiments of membrane float membrane and cytoplasmic fractions, a modified MudPIT protocol was utilized (Powell et al. 2004; Sanders et al. 2002). For each TAP strain, a 2 L culture was grown to OD_{660} 1-2 in YPD. The yeast were lysed and split into 6 tubes for membrane floatation. The membrane floatation and affinity purification were performed as described in the previous section. The purified TAP complexes were reduced with 1/10 volume of 50 mM DTT at 65 °C for 5 min, and cysteines were alkylated with 1/10 volume of 100 mM iodoacetamide at 30 °C for 30 min. The proteins were digested overnight at 37 °C with modified sequencing grade trypsin at ~25:1 subtrate:enzyme ratio (Promega, Madison, WI). Proteins were identified using Multidimensional Protein Identification Technology (MudPIT) and a LTQ linear ion trap mass spectrometer (ThermoFisher) (Link et al. 1999; Link et al. 2005). A fritless, microcapillary (100 μm-inner diameter) column was packed sequentially with 12 cm of 5 μm C_{18}reverse-phase packing material (Synergi 4 μ Hydro RP80a, Phenomenex) and 3 cm of 5 μm strong cation exchange packing material (Partisphere SCX, Whatman). The entire trypsin-digested samples were loaded onto the biphasic column equilibrated in 0.1% formic acid, 2% acetonitrile, which was then placed in-line with an LTQ-OrbitrapXL mass spectrometer. An automated twelve-cycle multidimensional chromatographic separation was performed using buffer A (0.1% formic acid, 5% acetonitrile), buffer B (0.1% formic acid, 80% acetonitrile) and buffer C (0.1% formic acid, 5% acetonitrile, 1 M ammonium acetate) at a flow rate of 500 nL/min. Cycles 1−12 consisted of 3 min of buffer A, 2 min of 0−100% buffer C, 5 min of buffer A, followed by a 60-min linear gradient to 60% buffer B. In cycles 1−12, buffer C salt pulses of 0mM, 25mM, 50mM, 75mM, 100mM, 150mM, 200mM, 250mM, 300mM, 500mM, 750mM and 1M ammonium acetate were used. Eluting peptides were analyzed by one full MS scan (300-2000 *m/z*) using an LTQ-OrbitrapXL mass spectrometer with preview mode and monoisotopic precursor selection enabled. The top 10 precursors ions based on intensity were fragmented using CID in the ion trap using 35% normalized collision energy. Dynamic exclusion was enabled for 180s with repeat count of 1 at 30 s

duration, list size of 500, mass tolerance of 10 ppm. Mass spectrometry data was analyzed as previously described (McAfee et al. 2006).

Microscopy

Epifluorescent microscopy was performed using live yeast cells grown in SC media to an OD_{660} 1.0-1.5 at 30 ^{o}C. Cells were mounted on slides and visualized using a Zeiss Axiophot brightfield microscope with a 63x / 1.40 Plan-Apochromat oil DIC lense. Images were analyzed with MetaMorph imaging software (Molecular Devices). Live yeast cells imaged using confocal microscopy were grown in SC media to an OD_{660} 1.0-1.5 at 30 ^{o}C., Cells were visualized with a Zeiss LSM 510 META inverted confocal microscope using a 63x / 1.40 Plan Apochromat oil immersion lens. Microscopic images used for quantitative analysis were analyzed using ImageJ imaging software (Schneider et al. 2012). To quantify the percentage of eIF2B bodies that co-localized with the ER, a eIF2B body was judged to be co-localized with the ER only if the eIF2B body signal overlapped with an area of YBR159W at least half as bright as the brightest YBR159W signal seen in the cell. Cells were pooled into groups of approximately 25 cells to calculate a standard deviation for the percentage of eIF2B bodies co-localized with the ER. The bright regions of the ER were subtracted from the total area of the cell minus the nuclear area to determine the fraction of the cell taken up by the ER. The compound 3,3'-dihexyloxacarbocyanine iodide ($DiOC_6(3)$) was used to stain and image the membranes of wild type strain AL400, and *ybr159wΔ* strain AL401 as previously described (Terasaki et al. 1984). Yeast cells were incubated in media containg 2.5 µg/mL DiOC6(3) for 10 min before imaging.

Subcellular Fractionation

WT yeast strain AL400 was grown to OD_{660} 1.0-1.5 in YPD media at 30 ^{o}C. To isolate subcellular fractions, 45 OD_{660} units of cells were split into three samples: control, puromycin treatment, and EDTA treatment. The control sample was lysed using glass beads in 750 µL of ice-cold control buffer (10 mM Tris pH 8.0, 100 mM NaCl, 1 mM EDTA, 10 mM KCl, 30 mM $MgCl_2$). The puromycin and EDTA treatment samples were lysed using glass beads in 750 µL of ice-cold ribosome dissociation buffer (10 mM Tris pH 8.0, 100 mM NaCl, 1 mM EDTA). The control sample was diluted in 750 µL of control buffer. The puromycin treated sample was diluted with750 µL of ribosome dissociation buffer containing 2 mM

puromycin to a final concentration of 1 mM. The EDTA-treated sample was diluted in Ribosome dissociation buffer (20mM EDTA) to a final concentration of 10 mM EDTA. Lysates were gently mixed at RT for 30 min to facilitate dissociation of ribosomes from the ER. Lysates were centrifuged at 900 xg for 5 min, and the supernatant was centrifuged at 11,000 xg for 20 min. The soluble fraction was recovered from the supernatant. The pellets was resuspended in either control buffer (1 mM puromycin, 10 mM Tris pH 8.0, 100 mM NaCl, 1 mM EDTA) or EDTA solution (10mM EDTA, 10 mM Tris pH 8.0, 100 mM NaCl, 1 mM EDTA) and centrifuged at 11,000 xg for 20 min. The pellets were resuspended in 1.5 mL of resuspension buffer (1 mM puromycin, 10 mM Tris pH 8.0, 100 mM NaCl, 1 mM EDTA, 1% SDS) and 15 µL of each fraction was used for Western blotting.

Results

Given the previously identified interaction between eIF2B and YBR159W, we wanted to look at cellular localization of eIF2B and YBR159W in the cell. Previous work in our laboratory confirmed that YBR159W localizes to the ER membrane (Fig. 2-3A and B). To look for possible co-localization between eIF2B and YBR159W, we used strains with subunits of eIF2B endogenously tagged with GFP and the YBR159W-RFP expression plasmid YCp-YBR159W-dsRed. To show the RFP-tagged YBR159W allele was functional, the plasmid YCp-YBR159W-dsRed complemented the ybr159w*Δ* null strain AL401. Confocal microscopy of the dual-fluorescently-labeled strains was used to look for co-localization between eIF2B and YBR159W (Fig. 3-1). As observed in previous studies and Fig. 2-3, our YBR159W-RFP construct localized to membranes corresponding to the endoplasmic reticulum (Fig. 3-1 and Fig. 2-3). Using strains with different eIF2B subunits tagged with GFP, we observed eIF2B localized as 1-2 large foci (Fig. 3-1). This agrees with previous studies showing eIF2B localization in eIF2B bodies (Campbell et al. 2005). In addition, GFP-tagged eIF2B is seen dispersed throughout the cytoplasm . Surprisingly, the confocal microscopy images did not convincingly show the majority of YBR159W signal co-localizing with eIF2B subunits. Because we observed that the eIF2B body localized in close proximity to ER membrane-bound YBR159W, we performed a statistical analysis to test if eIF2B and YBR159W co-localize. We examined 221 individual eIF2B bodies from 140 dual labeled cells by pooling results from the

YCp-YBR159W-dsRed transformed *GCD1-GFP*, *GCD6-GFP*, and *GCD7-GFP* strains (AL405, AL406, and AL407). We found 60.1% ±6.6% of eIF2B bodies examined showed partial co-localization with a bright area of YBR159W signal. Based on the area of the cell taken up by bright areas of YBR159W signal, it would be expected that only 30.7% ±6.9% of eIF2B bodies would co-localize with YBR159W signal if the two signals were independent of each other. A Student's *t*-test ($P=2.9x10^{-8}$) shows this difference to be significant.

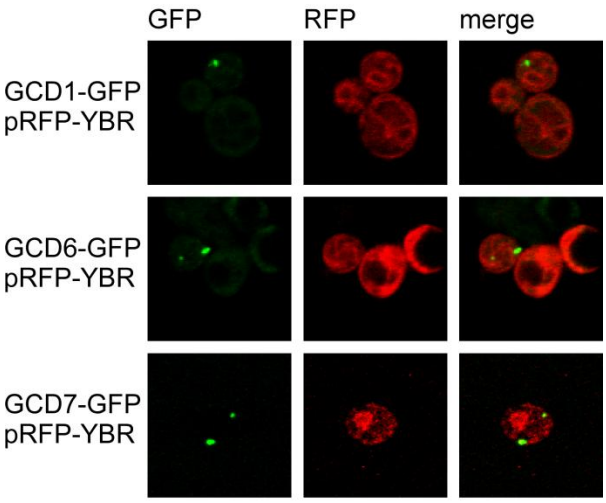

Figure 3-1 eIF2B and YBR159W localization in live cells. Confocal microscopy of live yeast cells showing localization of eIF2B subunits in relation to the localization of YBR159W. eIF2B subunits are endogenously tagged with GFP while YBR159W-RFP is expressed on a centromeric plasmid.

To observe the effects of the *ybr159wΔ* deletion on eIF2B localization, we performed live cell imaging using epifluorescence microscopy on the yeast strains *ybr159wΔ, GCD7-GFP* (AL403), *GCD7-GFP* (AL429), and *ybr159wΔ, GCD7-GFP*, [YCp-YBR159W] (AL404). Cells from the *GCD7-GFP* control strain were found to contain 1 to 2 large eIF2B bodies (Fig. 3-2A). In the *ybr159wΔ* strain AL403, eIF2B appeared as multiple foci (Fig. 3-2A). The *ybr159wΔ* phenotype of AL403 was rescued by expression of plasmid YCp-YBR159W in strain AL404 (Fig. 3-2A). Using these strains, we counted the number of cells containing 1 to 2 large eIF2B bodies compared to the number of cells having the multiple eIF2B foci or diffuse cytoplasmic localization. We found that the majority of *ybr159wΔ* cells had the multiple eIF2B foci phenotype (Table 3-1A). For the *GCD7-GFP* WT control strain, no cells had the multiple eIF2B foci phenotype and a majority of cells had either 1 or 2 eIF2B bodies. The rescued *ybr159wΔ, GCD7-GFP*, [YCp-YBR159W] strain AL404 did not have multiple eIF2B foci (Table 3-1A). To show the eIF2B body phenotype was independent of the GFP-tagged alleles, we performed immunofluorescence microscopy on untagged yeast strains using polyclonal antibody against the eIF2B subunit Gcd6 (Fig. 3-2B). We observed the 1 to 2 large eIF2B body foci phenotype for the majority of the WT control AL400 cells while the majority of the *ybr159wΔ* cells (AL401) displayed multiple eIF2B foci (Table 3-1B). The *ybr159wΔ*, [YCp-YBR159W] rescue strain AL402 showed a majority of cells had eIF2B present as either a single eIF2B foci or no detectable foci (Table 3-1B). The VLCFA and ceramide synthase mutants AL413 (*fen1Δ)*, AL414 (*sur4Δ)*, and RH5994 (*lip1Δ)* were all found to have the multiple eIF2B foci phenotype (Table 3-1B).

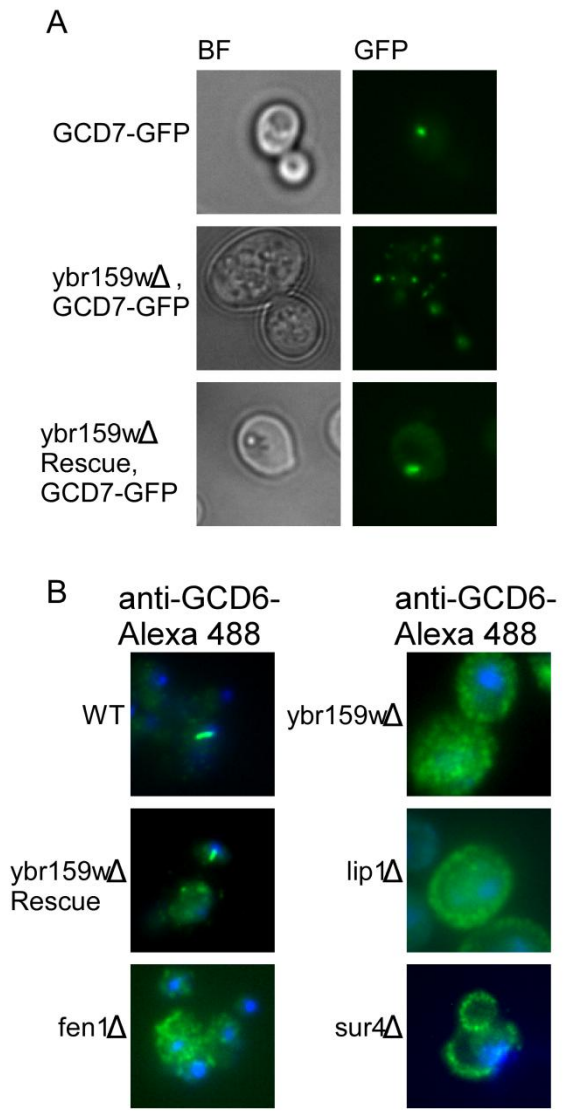

Figure 3-2 eIF2B localization in the ybr159wΔ background. (A) Live cell fluorescence microscopy of endogenously tagged eIF2B subunit *GCD7-GFP*. Brightfield (BF) images are included for clarity. (B) Immunofluorescence microscopy of formaldehyde fixed yeast cells. A polyclonal antibody against yeast eIF2B subunit Gcd6 was used along with an Alexa Fluor 488 tagged secondary. Nuclei are stained with DAPI for clarity.

Table 3-1 Statistics for eIF2B localization phenotypes. (A) Live Yeast. Statistics for eIF2B localization phenotypes in live yeast cells are given. The strains are described in Fig 3-3A. (B) Fixed Yeast. Shown are statistics for eIF2B localization phenotypes via immunofluorescence of fixed yeast cells. The strains are described in Fig 3-3B.

Strains	Cell #	Single 2B body (%)	Multi-Foci (%)	No Foci (%)
A. Live Yeast				
WT	173	50.9	0.0	49.1
ybr159wΔ	122	3.3	71.3	24.6
Rescue	72	44.4	0.0	55.6
B. Fixed Yeast				
WT	105	63.8	7.6	28.6
ybr159wΔ	59	1.7	83.1	15.3
Rescue	111	35.1	15.3	49.5
lip1Δ	29	6.9	93.1	0.0
fen1Δ	96	4.2	63.5	32.3
sur4Δ	122	1.6	58.2	40.2

Previous work has shown that disruption of VLCFA utilization in yeast causes abnormal formation of lipid membranes (Schneiter et al. 2004). The compound 3,3'-dihexyloxacarbocyanine iodide ($DiOC_6(3)$) is a lipophilic dye used to label a variety of lipid membranes (Terasaki et al. 1984). We used $DiOC_6(3)$ to stain membranes of wild type strain AL400, *ybr159wΔ* strain AL401, and the VLCFA mutant strains AL413 (*fen1Δ*), and AL414 (*sur4Δ*), and the ceramide synthase mutant strain RH5994 (*lip1Δ*). The *ybr159wΔ*, *fen1Δ*, *sur4Δ*, and *lip1Δ* null strains all displayed disrupted lipid membranes using epifluorescence imaging (Fig. 3-3). This supported previous work showing that VLCFAs are important for proper membrane formation (Schneiter et al. 2004).

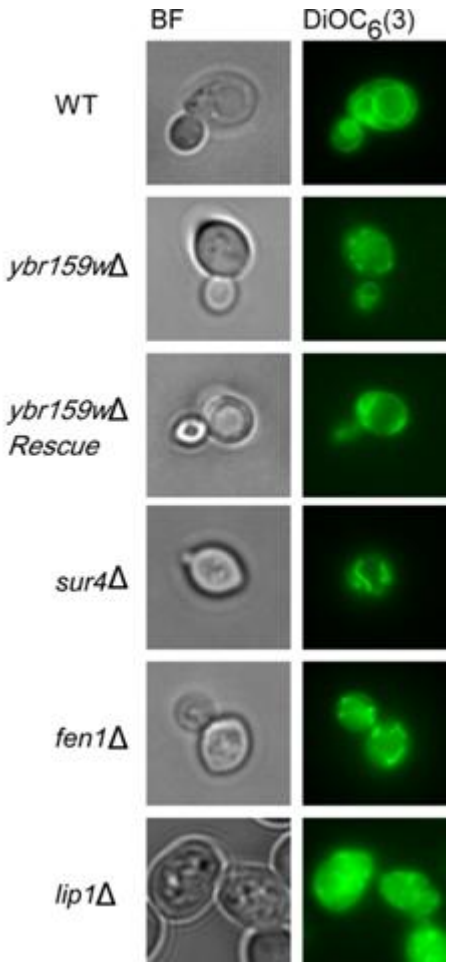

Figure 3-3 Null mutations of genes in the VLCFA pathway disrupt lipid membranes. The lipophilic dye $DiOC_6(3)$ was used to label membranes in live yeast cells. Dye was applied to cells in suspension 10 min before plating on a microscope slide and imaging. Included are the VLCFA and ceramide synthase mutants *fen1Δ, sur4Δ*, and *lip1Δ* as controls. 100% of these mutants showed abnormal membranes (N=246) versus 1.1% for WT (N=89) and 9.7% for the rescue (N=93).

Because eIF2B is thought to be a soluble cytoplasmic protein and YBR159W has been shown to be an integral membrane protein in the endoplasmic reticulum (Han et al. 2002; Klein 1957), we performed membrane float experiments to determine if a population of eIF2B complexes physically interacted with lipid membranes. The lack of signal from the Western blot for the control yeast GAPDH analogs *TDH1, 2,* and *3* in the membrane fraction showed the fractionation was efficient at separating cytoplasmic proteins from membrane-associated proteins (Fig. 3-4A). A significant lipid membrane signal was seen for the ER proteins YBR159W and Dpm1. A portion of the YBR159W and control ER membrane protein Dpm1 signals was still present in the soluble fraction indicating the membrane-associated proteins do not appear to completely separate from the soluble fraction. The membrane float experiments showed that in WT AL400 cells, a significant fraction of the eIF2B subunit *GCD6* localized to the lipid membrane fractions (Fig. 3-4A). The Western blot profiles of the membrane and soluble fractions for *GCD6* showed the same pattern as the known ER membrane proteins YBR159W and Dpm1 (Fig. 3-4A). Interestingly, the *SUI2* component of eIF2 also showed a similar membrane association pattern. The data indicates a fraction of eIF2 complexes are associated with membranes in yeast cells.

To validate our observation that eIF2B is membrane-associated, we used whole cell extracts prepared from TAP-tagged eIF2B and control strains and the membrane float separation experiment to collect fractions from the membrane-associated and soluble protein region of the density gradients. Next, we performed a modified TAP purification on each fraction and analyzed the affinity purified complexes using LC-MS/MS. Our data showed that the interaction between eIF2B and YBR159W was still present in both the membrane-associated and soluble protein fractions (Fig. 3-4B). Because of the incomplete separation of membrane proteins in the assay, it is not known if both soluble and membrane-associated eIF2B interact with YBR159W or if only membrane-associated eIF2B interacts with YBR159W. To see if YBR159W was required for the membrane association of eIF2B, we performed the membrane floatation assay and Western blots using the *ybr159wΔ* strain AL401. We found that eIF2B associated with the membrane fraction in the *ybr159wΔ* strain at similar levels as seen in the control strain (Fig. 3-4C). Overall, the membrane float experiments showed a fraction of yeast eIF2B is associated with membranes but the interaction is independent of YBR159W.

To determine if the membrane association seen for eIF2B is possibly mediated by rough ER-bound ribosomes, we performed a sub-cellular fractionation experiment to isolate smooth membranes. Cell lysates from WT strain AL400 were treated with either elevated levels of EDTA or the ribosome releasing antibiotic puromycin (Adelman et al. 1973). Following fractionation and Western blotting, ribosomal protein signal in the insoluble membrane fraction was significantly reduced in both the EDTA and puromycin treated cell extracts compared to untreated control extracts. However, the eIF2B signal in the rough or smooth membrane fraction did not noticeably change (Fig. 3-4D). The data indicates that the eIF2B-membrane association is independent of ribosomes.

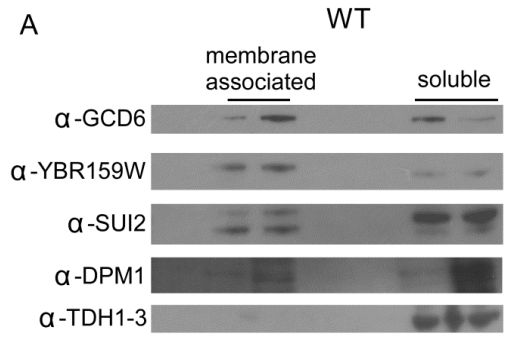

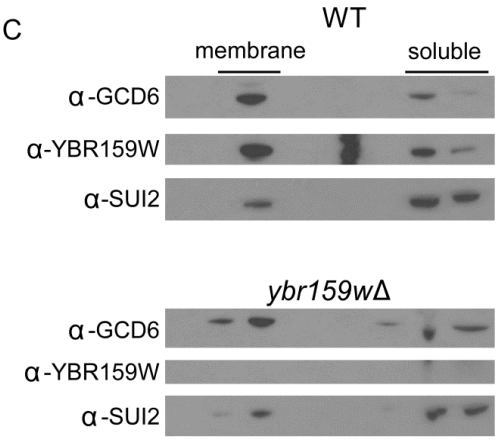

B

Gene	TAP-YBR Membrane	TAP-YBR-Soluble	TAP-GCD7 Membrane	TAP-GCD7 Soluble	TAP-GCD2 Membrane	TAP-GCD2 Soluble
YBR159W	16(57.06)	12(48.41)	2(8.36)	3(17.58)	4(20.75)	3(18.16)
GCD1	3(10.38)	2(7.09)	7(20.59)	12(35.29)	1(3.11)	1(3.11)
GCD2	2(5.07)	2(4.3)	9(13.82)	5(9.68)	1(2.15)	2.(4.3)
GCN3	1(7.54)	-	5(24.26)	6(34.43)	1(5.9)	2(16.07)
GCD6	8(16.57)	5(12.92)	13(27.81)	11(21.63)	6(14.47)	2(4.21)
GCD7	1(2.89)	1(7.35)	7(15.49)	6(22.83)	3(11.55)	1(2.89)

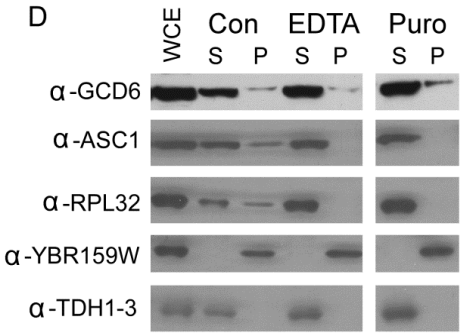

Figure 3-4 eIF2B and YBR159W localization using membrane floatation assays. (A) Western blot of membrane floatation assay fractions using protein extracts from WT yeast showing the localization of the eIF2B subunit *GCD6* and YBR159W. Controls include the eIF2 subunit *SUI2*, ER integral membrane protein *DPM1*, and the cytosolic protein GAPDH. *TDH1-3* are the three GAPDH genes in yeast. The lanes represent 20% of fractions from the membrane floatation gradients. Labels show the location of the membrane-associated and soluble protein fractions. (B) Mass spectrometry analysis of affinity purified TAP complexes from the membrane and soluble fractions of membrane floatation experiments. Unique peptides, percent coverage and "-" are described in Fig 2-2A. (C) Western blot of membrane floatation assay fractions comparing WT and *ybr159wΔ* strains. Conditions are the same as in "A". (D) Western blot of crude fractionation following EDTA or puromycin treatment. Abbreviations are WCE = whole cell extract, Con = non-treated control, EDTA = EDTA treatment, Puro = puromycin treatment, S = supernatant, P = pellet. *ASC1* is a component of the small ribosomal subunit and *RPL32* is a large ribosomal subunit protein. Lanes represent 15 µL of WCE following fractionation, pellets were resuspended in starting volume.

Discussion

Membrane floatation and subcellular fractionation assays show eIF2B interacts with lipid membranes. Our data and previous studies showed YBR159W is an integral membrane protein that co-localizes with the ER membrane (Abraham et al. 1961; Han et al. 2002; Klein 1957). We interpret these findings to mean that the membranes eIF2B is interacting with are ER membranes. It is unknown if ER-associated eIF2B is actively engaged in guanine nucleotide exchange. A number of conclusions can be made about this ER membrane-interacting eIF2B. First, the eIF2B-membrane interaction is not mediated by rough ER-bound ribosomes. Treatment of cell extracts with EDTA or puromycin greatly reduces the amount of ribosomes that fractionate with lipid membranes but does not reduce the portion of eIF2B that fractionates with membranes. This fits the prevailing theory that the role of eIF2B in translation is independent of the ribosome (Merrick W. C.). Second, YBR159W is not required for the interaction. The *ybr159wΔ* null strain does not affect the interaction of eIF2B with the membrane showing that the interaction of eIF2B with ER membranes is YBR159W independent. This indicates that other factor(s) are possibly required.

This new data modifies the models to explain the interaction between eIF2B and YBR159W presented in the previous chapter (Fig. 2-7). Model A, which states that eIF2B and YBR159W interact directly and independently of other factors can be ruled out based on the fact that eIF2B still associates with membranes in the *ybr159wΔ* null strain. Model C, where an as yet unidentified soluble factor binds directly to YBR159W and mediates the interaction with eIF2B can also be ruled out based on the same data. This leaves models B and D. Model B posits that eIF2B is palmitoylated for its membrane association and interaction with YBR159W. Model D states eIF2B is interacting with another unknown membrane-associated protein, this membrane protein then is interacting with YBR159W. This unknown factor could be an intergral membrane protein like YBR159W or a soluble factor that is peripherally anchored to the membrane by a lipid modification. Figure 3-5 presents modified models for the eIF2B-YBR159W interaction (Fig. 3-5). The possibility that a number of these possibilities all happen simultaneously is also available. In Figure 3-5, model D1is very similar to model C in Figure 2-7 from the previous chapter. An unknown soluble protein is mediating the observed interaction between eIF2B and YBR159W. By lipid

modifying the factor in model D1, the membrane association of eIF2B no longer becomes YBR159W-dependent. As before, no new data is available for identification of an unknown membrane-associated interactor with eIF2B.

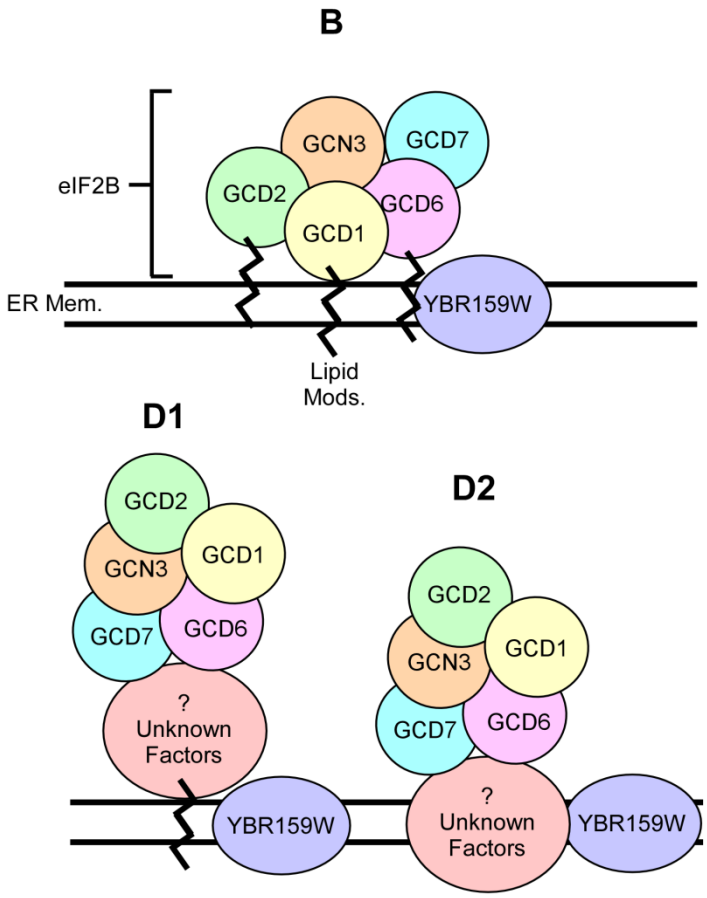

Figure 3-5 Modified Models for the interaction of eIF2B and YBR159W. Parts B and D are taken from Figure 2-7. (B) Model for direct lipid modification of eIF2B subunits *GCD1*, *GCD2*, and *GCD6*. (D1) Model for peripheral membrane-association of an unknown factor interacting with both eIF2B and YBR159W. (D2) Model for an unknown integral membrane protein interacting with eIF2B and YBR159W.

Possibilities for palmitoylation of either eIF2B itself or an unkown factor need to be considered. In Table 2-1 the palmitoylation site predictor CSS-Palm predicted possible palmitoylation sites on eIF2B subunits *GCD1*, *GCD2*, and *GCD6* (Table 2-1). Unfortunately, no structures are available for *GCD1* or *GCD2* in yeast. A structure for the catalytic domain of yeast eIF2Bε gene *GCD6* is available but the structure does not include the cysteine 342 residue predicted to be palmitoylated on *GCD6* (Boesen et al. 2004). This makes it impossible to determine whether the predicted sites are exposed and able to be palmitoylated and interact with the membrane. A global analysis of yeast palmitoylated proteins did not identify any subunits of eIF2B as containing a palmitoyl modification (Roth et al. 2006). Interestingly, this study did find some evidence that eIF2 subunit *GCD11* is potentially palmitoyl modified. From Table 2-1, the CSS-Palm generated CSS score for the predicted palmitoylation site on *GCD11* is actually lower than the score for a predicted site on eIF2B subunit *GCD2* (Table 2-1). It is quite possible a subpopulation of palmitoylated eIF2B could have been missed in the study. Direct examination of eIF2B palmitoylation is required. Sensitive, non-radioactive methods can be used to determine the palmitoylation of proteins (Kostiuk et al. 2009).

Confocal microscopy shows that the majority of eIF2B bodies are in close proximity to YBR159Wp and ER membranes, supporting the model that eIF2B bodies and the ER interact. This could indicate that the eIF2B shown to interact with ER membranes resides in eIF2B bodies. A possible conflicting interpretation of the data is that YBR159W-RFP is being overexpressed and its localization is an artifact. The co-localization experiment used a RFP-tagged YBR159W allele expressed from a GPD promoter on a centromeric plasmid. Global protein expression analysis shows that the target protein of the GPD promoter, tdh3p, is expressed at roughly 4 times that of YBR159W (Ghaemmaghami et al. 2003). The fact that the RFP-tagged YBR159W localization agrees with endogenously expressed YBR159W-GFP localization leads us to believe that artifacts caused by the RFP tagged construct are not disrupting the localization of YBR159W. In addition, the RFP-tagged allele complements a *ybr159wΔ* null strain. How and why eIF2B might be interacting with the ER membrane is unknown. A population of membrane-interacting eIF2B bodies might possibly explain recent findings that eIF2B bodies can exist in a mobile or static state with mobile eIF2B bodies free in the cytoplasm and static eIF2B bodies being associated with membranes (Taylor et al. 2010). Further work is needed to prove this hypothesis.

Figure 3-6 displays several models for the eIF2B-ER membrane association in the cell (Fig. 3-6). Model A depicts the interaction occurring between diffuse, cytoplasmic eIF2B not in eIF2B bodies with the entire surface of the ER membrane. If the interaction is weak, it may not be detected by co-localization in microscopy. The large surface area of the ER in the cell gives the most opportunity for the interaction to occur in this model. In yeast cells, eIF2B bodies often appear as a line or thread about a half to a third the diameter of the cell. Figure 3-6D displays several examples of the linearity of eIF2B bodies in the cell (Fig. 3-6D). As the linear bodies have numerous 3-dimensional orientations in the cell, the Z-slice of a single confocal microscope image often shows the bodies as points instead of lines. Model B posits that the entire length of the linear eIF2B body interacts with a cortical ER tubule membrane. Because of the relative intensity of eIF2B body signal this interaction should show a large amount of co-localization under microscopy if this model were true. The lack of co-localization makes this model unlikely to be the case. Model C posits that the eIF2B body is only anchored to the ER membrane and the majority of the body is free in the cytoplasm. Co-localization between the eIF2B body and the ER membrane would be small under this model. Figure 3-6C shows only one anchor point for the eIF2B body with the ER, though nothing precludes multiple anchor points with the membrane. Confocal microscopy showing a high proportion of eIF2B bodies having some amount of co-localization with ER membrane-bound YBR159W supports this model. One way to test between models A and C is to find a way to completely disrupt eIF2B body formation. Evidence suggests that treatment of cells with cycloheximide as being able to disrupt eIF2B body formation (Campbell et al. 2005). This finding would need to be confirmed. If eIF2B membrane association is not greatly affected after cycloheximide treatment, the model that non-eIF2B body-bound eIF2B is interacting with membranes is favored (Fig. 3-6A). If the membrane association of eIF2B is reduced after cycloheximide treatment and subsequent loss of eIF2B bodies then the model that eIF2B bodies are anchored to the membrane would be favored (Fig. 3-6C). To test model C directly, strains containing mutations in eIF2B subunits could be constructed that abolish the membrane association of eIF2B. If the percentage of eIF2B bodies showing preferential localization with the cortical ER membrane goes down in the eIF2B mutants, then the bodies may be membrane anchored. If the percentage stays the same it would be assumed the proximity of eIF2B bodies with the ER membrane is a coincidence and not representative of an actual interaction with ER membranes. This set of experiments assumes the mechanism

of eIF2B membrane association can be readily determined and abolished through mutations without affecting any other property of the eIF2B complex.

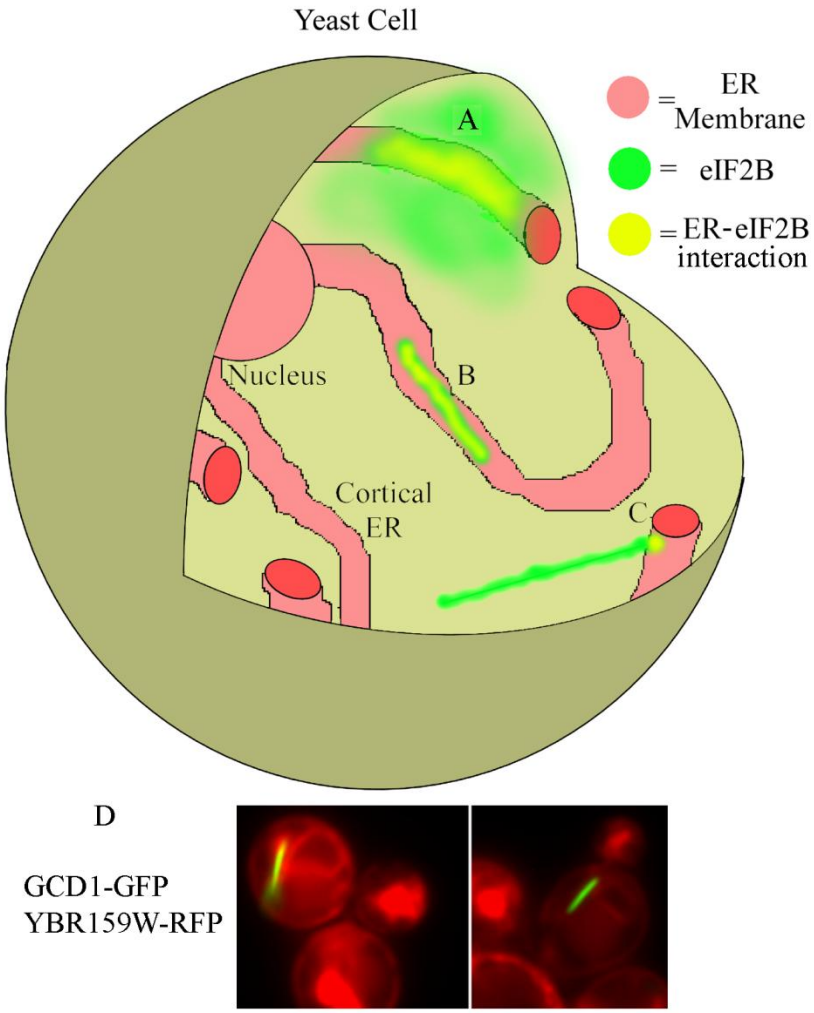

Figure 3-6 Models for the ER membrane association of eIF2B. (A) Diffuse cytoplasmic eIF2B interacts with ER membranes. The interaction would occur across the entire ER membrane. (B) eIF2B bodies interact with ER membranes across their entire lengths. (C) eIF2B bodies are anchored to ER membranes. The eIF2B-ER membrane interaction would occur only at the anchor point. (D) Examples of eIF2B bodies showing their linearity. *GCD1-GFP* is endogenously expressed while YBR159W-RFP is overexpressed from a plasmid.

The observation that the *ybr159wΔ* null strain leads to multiple eIF2B foci is intriguing. This phenotype is also seen in other VLCFA mutants. The fact that these mutants all display disrupted lipid membranes lends itself to the theory that properly formed membranes are required for the integrity of eIF2B bodies. Figure 3-7 depicts this model for eIF2B body disruption via membrane disruption (Fig. 3-7). An interesting question is whether the membrane disruption prevents the eIF2B bodies from forming properly or whether the eIF2B bodies are unable to be maintained once formed? For the first model, an as yet unknown factor in membranes required for eIF2B body formation could be scattered by membrane disruption and cause eIF2B bodies to form throughout the cell. We speculate that this membrane-associated factor could serve as a nucleating site for the formation of eIF2B bodies. The second model would predict that membrane disruption is affecting a factor needed for eIF2B body stability. Loss of this factor leads to eIF2B bodies dissociating into multiple smaller foci. A previous study showed VLCFAs were important for lipid raft formation (Gaigg et al. 2006). It is possible that lipid raft disruption in the VLCFA mutants causes the multiple eIF2B foci phenotype. Translation assays using the *ybr159wΔ* strain suggested the disruption of eIF2B bodies into multiple foci does not affect translation. The translation activity of yeast cells does not appear to be affected by the change from a single eIF2B body to multiple eIF2B foci. The model in Figure 3-7 predicts that the continued membrane association of eIF2B in elongase mutants is the cause of the multiple eIF2B foci. This could be tested if the mediator of the membrane association of eIF2B can be found. If eIF2B bodies form normally after disruption of the membrane association of eIF2B even in an elongase mutant background, it would suggest the model is correct.

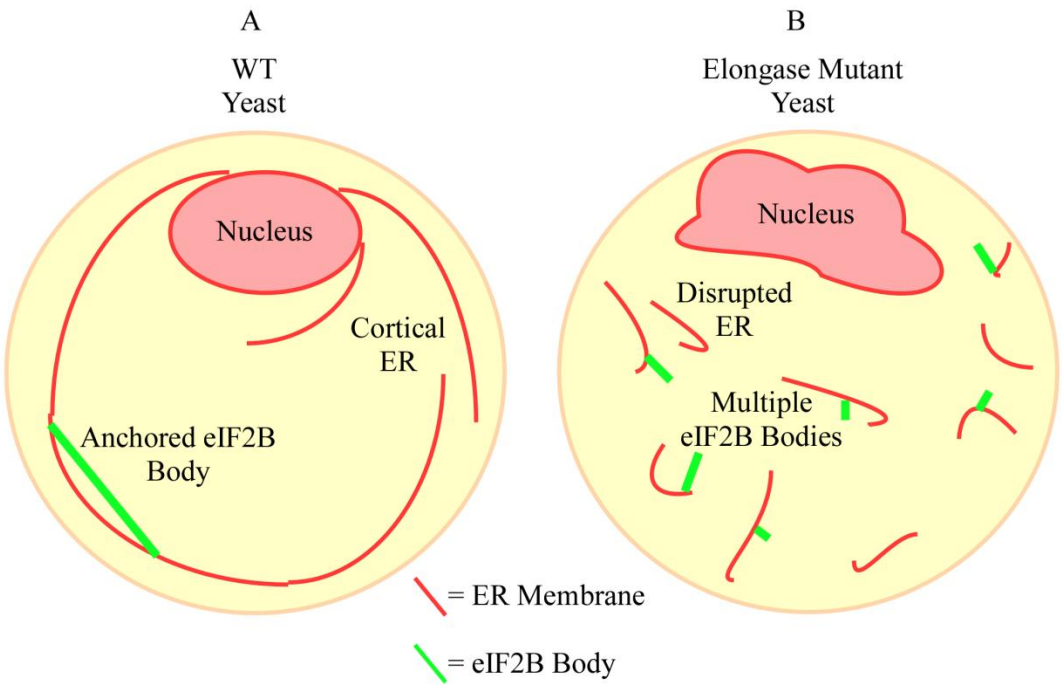

Figure 3-7 Model of multiple eIF2B body phenotypes seen in yeast elongase mutants. (A) Wild-type yeast showing a eIF2B body anchored at multiple points to the ER membrane as presented in Fig. 3-6C. (B) Mutations in elongase genes lead to disruption of lipid membranes in the cell. The disrupted ER membranes causes anchor points for eIF2B bodies to be scattered throughout the cell, leading to the multiple eIF2B body phenotype.

Our work sheds light on the recently discovered eIF2B body. The data show a relationship between eIF2B localization and an ER membrane bound protein. We discovered the membrane co-localization of eIF2B while examining its interaction with YBR159W. This membrane association has not been described previously and opens up new possibilities for eIF2B function. A possible function of the membrane association of eIF2B is to increase translation efficiency of membrane proteins and secreted proteins. Faster guanine nucleotide exchange at the ER could increase the efficiency of rough ER-bound ribosomes. If a means of disabling the membrane association of eIF2B can be found this hypothesis could be readily tested using quantitative proteomics. By examining membrane and secreted proteins with and without membrane-associated eIF2B it could be seen if there is increased expression of the levels of these proteins. Our data suggest that YBR159W is not necessary for the co-localization of eIF2B with the membrane. This data supports the model that YBR159W is not directly mediating the membrane association of eIF2B. The primary mediator of the membrane association of eIF2B is unknown. Future work will need to determine if eIF2B itself is interacting with the membrane via palmitoylation or if an unknown factor is responsible.

Acknowledgements

CB was supported by NIH training grant T32 AI007611. PS and AL were supported by NIH grant GM64779**.** We thank Dr. Tom Dever, Dr. Allan Hinnebusch, Dr. Howard Riezman, and Dr. Jonathan Warner for reagents and yeast strains. Experiments, data analysis, and presentation of fluorescent microscope images were performed in part through the use of the VUMC Cell Imaging Shared Resource, which is supported by NIH grants CA68485, DK20593, DK58404, HD15052, DK59637.

CHAPTER IV

CONCLUSIONS AND FUTURE DIRECTIONS

The purpose of this dissertation was the biochemical and genetic investigation of novel functions for yeast genes in the process of protein translation. In this chapter, I will analyze the significance of my findings and discuss its relevance to the study of protein translation and molecular biology as a whole. I will discuss how my research has advanced our scientific understanding of protein synthesis and will propose additional experiments to further the work I have done and answer new questions that have arisen due to my research.

The Translation Initiation Factor eIF2B and Its Interaction with the Elongase Enzyme YBR159W

The translation initiation factor eIF2B is an essential regulator of protein synthesis (Pavitt 2005). Numerous studies during the last several decades have shown eIF2B to be a key component of the cell's response to stress (Bushman et al. 1993; Hinnebusch 1985; Pavitt et al. 1998; Rowlands et al. 1988; Taylor et al. 2010). The very-long-chain fatty acid (VLCFA) ketoacyl reductase YBR159W is an ER membrane bound enzyme important for VLCFA synthesis and eventually sphingolipid synthesis in yeast cells (Beaudoin et al. 2002). My laboratory discovered a novel protein-protein interaction in yeast between eIF2B and YBR159W. As part of my dissertation research, I set out to biochemically characterize this interaction and determine the reason for its existence in the cell. This work led to a publication detailing not only the interaction between eIF2B and YBR159W, but also the previously uncharacterized membrane association of eIF2B (Browne et al. 2012). This report indicates that eIF2B associates with ER membranes and that VLCFA synthesis and the elongase pathway that controls it is important for proper localization of eIF2B complexes in the cell. My work presents a never before seen interaction for eIF2B and further solidifies the importance of very-long-chain fatty acids in the cell.

My work strongly suggests that eIF2B interacts with YBR159W alone. Initiation factor eIF2 is not found to co-purify with YBR159W, and other members of the elongase complex do no co-purify with

eIF2B. The latter observation could be explained by the fact that the elongase enzymes do not seem to strongly co-purify with each other. This would lend itself to the presiding model that each member of the pathway binds its substrate in the lipid bilayer, conducts its enzyme activity, and then releases the product back into the bilayer (Beaudoin et al. 2002; Han et al. 2002; Jakobsson et al. 2006; Kihara 2012). In this way members of the pathway do not have to physically interact with each other for their enzymatic function. The lack of interaction between eIF2 and YBR159W is more intriguing. The confocal microscopy that I conducted looking at the colocalization of eIF2B bodies and the ER suggests that the bodies show some preference for close proximity to the cortical ER. Previous work showed that eIF2B bodies also contain eIF2 (Campbell and Ashe 2006; Campbell et al. 2005). Though I did not look at co-localization of eIF2 and YBR159W, this could imply that either the eIF2B bodies near the ER do not contain eIF2 or that the bodies near the ER are not interacting with YBR159W. There is no evidence that a population of eIF2B bodies does not also contain eIF2 so this option is unlikely. Of course, the only evidence that eIF2B bodies and the ER are interacting is from statistical analysis of confocal microscopy so it is always possible the proximity between the two is just coincidence. This would mean a fraction of eIF2B not in 2B bodies is interacting with YBR159W and is not detected using immunofluorescence microscopy. A third possibility is that eIF2 and eIF2B in the eIF2B bodies does not strongly interact and eIF2 is dissociating during the affinity purification of YBR159W. A simple way to prove this hypothesis would be to gently cross-link proteins in a YBR159W TAP-tagged strain. If YBR159W now copurifies with both eIF2B and eIF2 this would again open the possibility for eIF2B bodies interacting with YBR159W and the ER membrane. In the event that eIF2 is still not identified in a YBR159W-TAP affinity purification, it would have to be assumed that eIF2B bodies do not interact with YBR159W and that the eIF2B-YBR159W interaction is truly eIF2-free.

Regardless of whether eIF2B bodies interact with ER membranes, fractionation experiments that I performed unquestionably show that eIF2B complexes themselves associate with lipid membranes. I was able to show that this membrane association is ribosome-independent. This fits with the current model of translation initiation where eIF2B performs it GEF exchange separate from the ribosome (Merrick W. C. ; Pavitt 2005). Intriguingly, I also found eIF2B associates with membranes independently from YBR159W. To attempt to explain this one can think of two explanations. A complex explanation is that eIF2B

associates with membranes in at least two separate ways, one association is with the ER membrane and is mediated by YBR159W while the second is through an as yet unknown mechanism and is with an as yet undetermined lipid membrane. In this model, only the YBR159W interaction can be identified by affinity purification and mass spectrometry. Assays that I performed using wild-type and *ybr159wΔ* null strains did not show a noticeable change in the amount of eIF2B that associates with lipid membranes between the two strains. This would tend to discredit the first explanation that eIF2B is interacting with two sets of membranes. The second and simpler explanation is that eIF2B is associating with only one set of lipid membranes and that the protein-protein interaction we see with YBR159W is a consequence of the association. This theory would be supported by future research examining whether eIF2B subunits are palmitoylated in yeast or eIF2B interacts with another unidentified membrane protein.

The yeast 2-hybrid analysis I performed suggested that eIF2B subunits *GCD6* and *GCD7* are mediating the interaction with YBR159W. *GCD6* is the primary catalytic subunit of eIF2B and is part of a separate subcomplex from the regulatory subunit *GCD7* (Pavitt et al. 1998). This finding represents a new functionality for eIF2B. If YBR159W is acting as a regulator of eIF2B function, this would be a completely new regulatory activity in yeast. Only a handful of factors have been found to regulate translation by direct interaction with eIF2B outside of the canonical eIF2 and phospho-eIF2 pathways (Pavitt 2005). Direct regulation of eIF2B by various protein kinases and butanol has been identified (Taylor et al. 2010; Woods et al. 2001). Phosphorylation of eIF2B has only been shown in mammals and is mediated by the dual-specificity tyrosine-phosphorylated and regulated kinase (DYRK) and glycogen synthase kinase 3(GSK3) (Woods et al. 2001). YBR159W interacting with Gcd6 and Gcd7 to regulate eIF2B would be the first protein shown outside of eIF2α to directly regulate eIF2B function in yeast. Alternatively, if eIF2B was serving to regulate YBR159W and the elongase pathway, this would represent a totally new role for eIF2B in the cell.

Taken together, this data suggests several models for the eIF2B-YBR159W interaction. At least one theory can be disregarded; the membrane-association of eIF2B is not dependent on it interaction with YBR159W, either direct or indirect. The existence of membrane-associated eIF2B in a *ybr159wΔ* null strains shows this in Chapter 3, Fig. 3-4C. Because of this result, either eIF2B is interacting with another membrane protein or eIF2B can independently associate with membranes. I have no evidence to support

another membrane protein interaction but that does not mean it does not exist. Software prediction fits with the direct association of eIF2B with lipid membranes via palmitoylation. This theory is intriguing and straightforward to test. Mass spectrometry methods are available to identify palmitoylated proteins. In addition, biochemistry methods exit to directly identify palmitoylated proteins (Drisdel and Green 2004). The existence of palmitoylated eIF2B would definitely put a new twist on the function of eIF2B in the cell. It supports the idea that eIF2B is needed at the ER membrane for more efficient translation of integral membrane and secreted proteins. If eIF2B subunits were found to be palmitoylated, it would be fairly straightforward to mutate the modified cysteine residues from the proteins and observe the effects it has on the cell. An interesting idea is if it leads to a slow growth rate similar to the *ybr159wΔ* deletion mutant. This would give additional evidence to the theory that the growth defect of the *ybr159wΔ* strain is not caused by reduced VLCFA synthesis.

The eIF2B body is one of several translation-associated foci in yeast only observable under fluorescence-microscopy (Buchan and Parker 2009; Campbell et al. 2005; Parker and Sheth 2007). At the time they were discovered, 2B bodies were implicated as important sites of eIF2B-GEF exchange (Campbell et al. 2005). Fluorescence recovery after photobleaching (FRAP) suggested that eIF2 shuttles slower in and out of the bodies during stress events compared to logarithmic growth (Campbell et al. 2005). The reduced shuttling of eIF2 correlated with reduced eIF2B activity. The authors hypothesized that eIF2 enters the eIF2B body for the purpose of nucleotide exchange (Campbell et al. 2005). When I examined eIF2B localization in a *ybr159wΔ* null strain as well as other elongase enzyme null strains, I found that eIF2B bodies are forming into dozens of individual foci in the cells. Although I have immunofluorescence data showing that other elongase pathway mutants in the also display the multiple eIF2B body phenotype, I will refer only to the *ybr159wΔ* strain when discussing the foci. My live-cell microscopy of the *ybr159wΔ* strain shows this multiple, small foci phenotype (Chapter 3, Fig. 3-2). Morphologically, the multiple eIF2B foci are distinct from eIF2B bodies. In wide-field microscopy, the eIF2B bodies are linear in shape and take up one half to one third of the diameter of the cell (Chapter 3, Fig. 3-6D). The multiple foci in the *ybr159wΔ* strains are each single points. Furthermore, a population of eIF2B bodies can be seen vibrating and moving in the cell. The vibrations cause the bodies to move in place. While vibrations are occurring, the 2B bodies will also transit across the length of the cell in the span of 15 to 30 seconds. The movement

of the bodies causes them to constantly move in and out of the focal plane of the microscope. The foci seen in the *ybr159wΔ* null strain do not appear to move within the cell nor do they vibrate in place. Colocalization between the eIF2B in the multiple foci and eIF2 in the *ybr159wΔ* null strain has not been performed. If it were found that eIF2 is not present in the foci, it would be difficult to call the foci eIF2B bodies. They may represent some new microscopic body or granule only seen in specific mutant strains. Until more evidence is available supporting the naming of a new body/granule separate from the already known examples (eIF2B bodies, P-bodies, and stress granules), eIF2B foci will serve as an accurate and adequate description. Other studies have so far not described the multiple foci phenotype for eIF2B that I see in the *ybr159wΔ* strain. Mark Ashe's laboratory, who discovered eIF2B bodies, has observed a similar phenotype in strains with mutations in the eIF2B subunit *GCN3* (M. Ashe, personal communication). The fact a similar phenotype is seen in eIF2B mutants suggests the interaction between eIF2B and YBR159W and the ER membrane is significant.

Previous to my work, little evidence existed suggesting that eIF2B interacted with an ER membrane protein. Work had shown several other translation factors interact with membranes, including eIF4E and eIF4GI interacting with the Golgi (Willett et al. 2011). There is proteomics data suggesting that the eIF2 subunit Gcd11p is palmitoylated (Roth et al. 2006; Willett et al. 2011). In eukaryotic organisms, the rough ER has translating ribosomes- interacting on the cytosolic face (Merrick W. C.). These examples suggest that the interaction between eIF2B and YBR159W is feasible. The rough ER synthesizes both the integral-membrane and secreted proteins in the cell. The existence of a mechanism to increase the efficiency of translation at the rough ER is possible. The interaction of eIF2B and the ER protein YBR159W might be such a mechanism.

The Consequences of the Interaction of eIF2B and YBR159W on Protein Translation and the Elongase Pathway

My first assumption concerning the interaction between eIF2B and YBR159W was that it represented a new form of translation regulation. As my training mainly focuses on protein translation, I will attest that there may have been some bias in this hypothesis. My tests were based on the assumption

that a *ybr159wΔ* strain would have deficiencies in protein synthesis. Right away, issues arose in analyzing the translation efficiency of the *ybr159wΔ* mutant strain. Although translation is reduced in the mutant, the growth rate of the strains was also slow. A slow growing *lip1Δ* null strain was employed to see if it also had translation defects. Evidence showed a very similar translation phenotype between the two strains, lending itself to the possibility that the slowed translation rate of the *ybr159wΔ* strain could be explained by its slow growth rate. The wild-type growth rate *fen1Δ* and *sur4Δ* strains have similar VLCFA synthesis defects to the *ybr159wΔ* strain so a VLCFA defect was considered unlikely to account for the translation defects. Later immunofluorescence microscopy of the *lip1Δ* strain revealed that it possessed the same multiple eIF2B foci seen in the *ybr159wΔ* strain. However, the VLCFA mutant *fen1Δ* and *sur4Δ* strains has the multiple eIF2B foci phenotype but wild-type growth-rates. Translation assays using the *fen1Δ* and *sur4Δ* strains did not show any defects in protein translation. Whether the slow growth of the *ybr159wΔ* strain was caused by VLCFA synthesis defects or something else would need to be considered

Two theories could explain the translation defects and slow growth in the *ybr159wΔ* strain. The first theory is that disruptions in VLCFA synthesis in the *ybr159wΔ* mutant are causing slow growth. While examining and quantifying sphingolipid defects in elongase mutants, I observed the consequence of *ybr159wΔ* deletion on sphingolipid content. My data show that the effects of *ybr159wΔ* deletion on sphingolipids are rather modest when compared to other elongase and ceramide synthase mutants. Compared to wild-type, the *ybr159wΔ* strain has reduced IPC 46:0;4 sphingolipid species, about 10% of the wild-type IPC 44:0;4, and about 6 times the levels of IPC 42:0;4 (Chapter 2, Fig. 2-6). The *ybr159wΔ* strain also has increased levels of the IPC 38:0;4 species which is not found in wild-type cells. The *sur4Δ* strain had almost no detectable IPC 46:0;4 or IPC 44:0;4, 12 times the IPC 42:0;4 as wild-type, and large amounts of the non-wild-type sphingolipid species IPC 40:0;4 and IPC 38:0;4. When comparing *ybr159wΔ* and *sur4Δ* sphingolipids, the sphingolipids from *ybr159wΔ* are similar to wild-type levels. The *sur4Δ* strain did not have a translation defect. Given this evidence, it is not unreasonable to think that the slow growth of the *ybr159wΔ* strain is not caused by defects in VLCFA synthesis. A new theory is needed to explain the slow growth and translation defect seen in the *ybr159wΔ* mutant. One theory could be that the interaction of YBR159W with eIF2B is disrupted and causing the translation defect. The translation defect is then causing slow growth in the strain. It is currently impossible to rescue elongase mutants with supplemental

VLCFAs. Thus, one option to determine the cause of slow growth in the *ybr159wΔ* deletion mutant is to rescue VLCFA synthesis with an exogenous VLCFA ketoacyl reductase. One candidate for rescue is the human homologue of YBR159W, HSD17B12 (Moon and Horton 2003). If sphingolipid analysis shows that the rescue strain has sphingolipids similar to wild-type and is still slow growing, the theory that the slow growth seen in the *ybr159wΔ* strain is unrelated to VLCFA synthesis would be supported. Affinity purifications of *ybr159wΔ* deletion strains with tagged eIF2B subunits that express HSD17B12 from a plasmid followed by mass spectrometry analysis of the purified complexes would confirm whether eIF2B also interacts with the human homolog of YBR159W.

An important point that needs to be tested is whether YBR159W plays a role in translation by regulating eIF2B during stress. If YBR159W was important during a specific cellular stress, it would follow that the *ybr159wΔ* strain would be susceptible to that same stress. The *ybr159wΔ* null strain has been shown to be temperature sensitive at 37 ˚C (Beaudoin et al. 2002). This sensitivity could be caused by the cell's inability to regulate translation following an increase in temperature. If this were the case, it would be predicted that there would be upregulation of genes involved in the unfolded protein response (UPR). In yeast, the serine-threonine kinase and endoribonuclease *IRE1* mediates the UPR via the cleavage of the mRNA of transcription factor *HAC1* (Cox et al. 1993; Mori et al. 1996). UPR activation can be easily tested by looking at expression of *HAC1*. A recent study shows that activation of the UPR in yeast and rats leads to increased levels of ceramide in the cell (Epstein et al. 2012). The study shows that one of the genes activated by the UPR is a ceramide synthase which is able to rescue the deletion of the ceramide synthase *LCB1*. This illustrates the importance of ceramides and sphingolipids and may be a model for the function of the interaction between eIF2B and YBR159W in the cell. It is possible eIF2B is regulating the activity of YBR159W enzyme activity and VLCFA synthesis.

Another question is the unexplained phenomenon of eIF2B being regulated by $NADP^+$/NADPH in mammals (Dholakia et al. 1986; Oldfield and Proud 1992; Wang et al. 2012). My model presented in Figure 2-8 of Chapter II details possible mechanisms for YBR159W regulating eIF2B activity through interactions with the $NADP^+$/NADPH bound to YBR159W. Obviously, the regulation via dinucleotide would first need to be observed in yeast. This could be done with *in vitro* GEF exchange assays using eIF2B containing cell extracts with and without $NADP^+$ and NADPH. If yeast eIF2B was under the same

regulation, then addition of $NADP^+$ should inhibition GEF exchange. Addition of equimolar concentrations of NADPH should rescue eIF2B activity if the effect is identical to that in mammals. If this could be shown in yeast, testing whether YBR159W is a mediator of the effect would be the next step. For the model to be correct, $NADP^+$-bound YBR159Wp would need to be able to inhibit eIF2B activity at $NADP^+$ concentrations lower than those used in the previous studies (Dholakia et al. 1986; Oldfield and Proud 1992). An *in vitro* assay would use purified eIF2B, YBR159W, and low concentrations of $NADP^+$ and test if eIF2B GEF activity is lowered. The model would predict that $NADP^+$ concentrations closer to physiological levels would be sufficient to inhibit eIF2B GEF activity in the presence of YBR159W. NADPH would be expected to reverse the inhibition. This would present a very interesting explanation for an effect on eIF2B that until now has been unexplainable.

Though the possibility that YBR159W played a role in translation regulation is still an open question, I wanted to examine whether eIF2B had an effect on VLCFA synthesis. The importance of eIF2B in protein translation proved to be problematic for these experiments since only the *GCN3* subunit of eIF2B is nonessential. Regardless, I used the *gcn3Δ* null strain for examination of sphingolipid levels. My results showed that this mutant strain did possess less VLCFA containing sphingolipids when compared to wild-type (Chapter 2, Fig. 2-6). However, the strain did not have shorter-chain fatty acid-containing sphingolipids that would be indicative of an attempt by the cell to compensate for a lack of sphingolipids. I interpreted this result to mean the levels of VLCFA containing sphingolipids in the *gcn3Δ* null strain were not indicative of a defect in VLCFA synthesis.

Originally, I wanted to use temperature-sensitive degron alleles of the essential eIF2B subunits to see if they possessed VLCFA synthesis defects. Analysis of degron-tagged *GCD2*, *GCD6*, and *GCD7* yeast strains did not show any sphingolipid defects. To complicate the matter, a degron-tagged YBR159W strain also did not show sphingolipid defects. Western blots of the YBR159W degron-tagged strain confirmed that YBR159Wp protein was being depleted in as little as 30 min after shifting to the non-permissive temperature. For the sphingolipid analysis, cells were grown for up to 8 h at the non-permissive temperature. This apparently was not long enough for defects in VLCFA synthesis to affect sphingolipids in the YBR159W degron-tagged strain. A longer time course at the non-permissive temperature would be needed to determine the amount of time required for VLCFA defects to start to manifest. This time would

be used to verify that the *GCD2*, *GCD6*, and *GCD7* subunits do not play a role in VLCFA synthesis. Growth assays showed the *GCD2*, *GCD6*, and *GCD7* degron-tagged strains were unable to grow at the non-permissive temperature. This is an understandable consequence of depleting essential genes but it confounds the analysis of the cells for VLCFA synthesis defects. If the cells are not growing, it is unknown if there would be any turnover of sphingolipids. A genuine VLCFA synthesis defect could thus be masked in the non-growing cells. One of the essential elongase genes such as *PHS1* or *TSC13* would need to be degron-tagged and examined to account for this possibility. With the *gcn3Δ* null strain not showing a VLCFA synthesis defect, I chose not to continue this line of investigation.

Functional analysis of the eIF2B-YBR159W interaction revealed evidence that translation is negatively affected in a *ybr159wΔ* mutant. My data points to slow growth being a major factor in the translation defect. What is not known is the exact mechanism for the slow growth in the null strain. In the following section I will discuss the future of research into the interaction between eIF2B and YBR159W.

The Future of eIF2B-YBR159W Research

A number of experiments are still required to develop a proper understanding of the mechanism and function of the eIF2B-YBR159W interaction. For determining the mechanism of the interaction, crosslinking followed by affinity purification might reveal other components interacting with eIF2B and YBR159W that are transiently associated and fail to be purified by the standard TAP protocol. This could also provide evidence that eIF2B is interacting with eIF2 and YBR159W at the same time and would lend support to the theory that eIF2B bodies are interacting with YBR159W and the ER membrane.

Examination of whether eIF2B subunits are palmitoylated in yeast needs to be performed. The results would open up a whole new line of questions about the function of eIF2B on the membrane. Is eIF2B on the membrane aiding in translation of membrane and secreted proteins? Is its membrane-association regulated during stress or other cellular events? If so, which palmitoylating and depalmitoylating enzymes are responsible? I'm excited by the results of these future experiments. Palmitoylation requires specific cysteine residues so mutation of these cysteines could be used to disrupt eIF2B membrane association. Quantitative proteomics of yeast membranes from these eIF2B

palmitoylation mutants could be used to determine if rough ER associated protein translation is upregulated because of eIF2B membrane association. Microarrays or RNA-seq of mRNA present in rough ER bound ribosomes would show if there is a change in the proteins being translated at the membrane in the eIF2B palmitoylation mutants.

I have shown that eIF2B in a *ybr159wΔ* null background forms multiple eIF2B foci. Are these foci compositionally identical to eIF2B bodies? Dual labeling colocalization of eIF2 and eIF2B would prove this model. FRAP experiments would show if eIF2 is shuttling in and out of individual foci in the same manner as eIF2B bodies. Additionally, what other mutations cause the phenotype? My research showed that mutants in the elongase pathway cause the phenotype. Do other sphingolipid synthesis mutants cause it as well? Does growth rate play a role in the effect? These questions will need to be answered before the cause and consequences of the multiple eIF2B foci phenotype can be truly understood.

Further assays looking at whether the *ybr159wΔ* null strain has disrupted translation during stress are needed. Heat stress starting at 37 ˚C is the most straightforward and promising from a phenotypic standpoint. The null mutants already stop growing at this temperature. Translation assays of cells shifted to higher temperatures could answer whether the lack of growth is caused by eIF2B and if protein synthesis is being inhibited in the mutant. Another set of experiments that may reveal the function for the eIF2B-YBR159W interaction would be toexamine the effects of $NADP^+$/NADPH on eIF2B in the presence of YBR159W. My model predicts that $NADP^+$ bound YBR159Wp inhibits eIF2B activity at much lower concentrations than the concentrations used in previous studies (Dholakia et al. 1986; Oldfield and Proud 1992). This would implicate that YBR159W has a regulatory function on eIF2B during oxidative stress.

Finally, examination of whether possible homologs of YBR159W like human HSD17B12 can rescue the VLCFA synthesis defects of a *ybr159wΔ* null strain would allow us to examine the effects of *ybr159wΔ* deletion without VLCFA defects interfering. The first experiment that would need to be performed is the successful rescue of wild-type VLCFA synthesis by HSD17B12 in a *ybr159wΔ* null strain. Following a demonstration that HSD17B12 is capable of rescuing the *ybr159wΔ* VLCFA phenotype, affinity purification of mammalian eIF2B complexes followed by mass spectrometry analysis would determine if eIF2B-HSD17B12 physically interact. With only 32% sequence identity, I find it unlikely that the two would interact. A lack of interaction would then allow us to examine the eIF2B-YBR159W

interaction independent of the role of YBR159W in VLCFA synthesis. Translation assays on this HSD17B12 rescued *ybr159wΔ* strain could definitively show YBR159W is affecting protein translation. Microscopy of the strain would show if the multiple eIF2B foci phenotype seen in a *ybr159wΔ* strain is due to a defect in VLCFA synthesis or some other cause.

My research has revealed an intriguing interaction between the translation initiation factor eIF2B and the ER membrane bound fatty acid synthesis enzyme YBR159W. I have shown a novel requirement for members of the elongase pathway in eIF2B localization. My work has identified a previously unknown membrane association for eIF2B that may represent a new form of regulation of protein synthesis of integral membrane proteins and secreted proteins. My work has only scratched the surface of the mechanism and role of the eIF2B-YBR159W interaction. Many more experiments are needed to gain a full understanding of what is truly taking place during this protein-protein interaction.

APPENDIX

MOLECULAR AND CELLULAR BIOLOGY MANUSCRIPT

The yeast eIF2B translation initiation complex interacts with the fatty acid synthesis enzyme YBR159W and ER membranes

Christopher M. Browne[1], Parimal Samir[1], J. Scott Fites[2], Seth A. Villarreal[2,†] and Andrew J. Link[3,*]

Vanderbilt University School of Medicine, [1]Department of Biochemistry, [2]Interdisciplinary Graduate Program in the Biomedical and Biological Sciences, [3]Department of Pathology, Microbiology, and Immunology, Nashville, TN 37232

[†]Present address: Case Western Reserve University School of Medicine, Dept of Pharmacology and Cleveland Center for Membrane and Structural Biology, Cleveland, OH 44106

Running title: Yeast eIF2B interactions with YBR159W and membranes

Accepted Dec 21, 2012 (Browne et al. 2012)

*Corresponding author

Andrew J. Link, Ph.D

Vanderbilt University School of Medicine

Department of Pathology, Microbiology, and Immunology

1161 21st Ave South

Nashville, TN 37232

Tel: 615-343-6823

Fax: 615-343-7392

andrew.link@vanderbilt.edu

Abstract

Using affinity purifications coupled with mass spectrometry and yeast-2-hybrid assays, we show the *Saccharomyces cerevisiae* translation initiation factor complex eIF2B and the very-long-chain-fatty acid (VLCFA) synthesis keto-reductase enzyme YBR159W physically interact. The data show the interaction is specifically between YBR159W and eIF2B and not between other members of the translation initiation or VLCFA pathways. A *ybr159wΔ* null strain has a slow growth phenotype and reduced translation rate but a normal GCN4 response to amino acid starvation. While YBR159W localizes to the ER membrane, subcellular fractionation experiments show that a fraction of eIF2B co-fractionates with lipid membranes in a YBR159W-independent manner. We show that a *ybr159wΔ* yeast strain and other strains with null mutations in the VLCFA pathway cause eIF2B to appear as numerous foci throughout the cytoplasm.

Introduction

In eukaryotic translation initiation, the initiation factor eIF2 bound with GTP is required to interact with the initiator Met-tRNA to form a ternary complex. Following start codon recognition, eIF2-GTP is hydrolyzed to GDP and eIF2 dissociates from the translation initiation complex (Preiss and M 2003; Sonenberg 2000). eIF2-GDP must exchange GDP with GTP before it can initiate another round of translation (Fig. 1A). The initiation factor eIF2B is an essential guanine nucleotide exchange factor (GEF) responsible for exchanging GDP for GTP on eIF2 (Pavitt 2005). It is the only known target of eIF2B. This exchange reaction is one of the rate limiting steps in translation initiation and is the target of numerous signaling pathways in yeast as well as higher eukaryotes (Harding et al. 1999; Olsen et al. 1998; Rowlands et al. 1988; Schneider and Mohr 2003; Sood et al. 2000; Wek et al. 1990; Zhan et al. 2004). While the majority of eukaryotic GEFs are monomeric, eIF2B is unique among GEFs in that it is composed of multiple subunits. In *S. cerevisiae*, eIF2B is composed of the five subunits GCD1, GCD2, GCN3, GCD6, and GCD7. The GCD6 subset is necessary and sufficient for catalytic activity, although at a significantly reduced rate compared to the eIF2B complex (Fabian et al. 1997; Gomez and Pavitt 2000; Pavitt et al. 1998). Co-expression of GCD6 with GCD1 yields similar GEF activity as the eIF2B holoenzyme (Pavitt et al. 1998). Of the other 3 subunits, previous studies show GCD2 and GCD7 to be involved in the stability of the complex and regulatory activity (Bushman et al. 1993; Pavitt et al. 1998; Pavitt et al. 1997). GCN3 is required for eIF2B's role in the GCN4 stress response pathway (Hinnebusch 1985; Kubica et al. 2006). With the exception of *GCN3*, all of the yeast eIF2B genes are essential (Pavitt 2005).

Recent studies show that a significant fraction of yeast eIF2B resides in distinct foci in the cytoplasm known as "2B bodies" (Campbell and Ashe 2006; Campbell et al. 2005). GFP fluorescence microscopy shows the bodies contain both eIF2B and eIF2. The initiation factor eIF2 appears to shuttle in and out of the 2B bodies (Campbell et al. 2005). The shuttling occurs quickly during logarithmic growth and slower following disruptions of translation initiation. The 2B bodies are thought to be sites of eIF2B's GEF activity.

In eukaryotes two distinct complexes are responsible for the synthesis of fatty acids (Rossler et al. 2003; Stoops and Wakil 1978). The cytoplasmic fatty acid synthase complex (FAS) elongates fatty acids

from 2 to 18 carbons in length in a four reaction cycle. A second fatty acid synthesis complex, the elongase complex, is responsible for the elongation of fatty acids from 18-26 carbons (Fig. 1B) (2). The longer chain fatty acids are known as very-long-chain fatty acids (VLCFA). In *S. cerevisiae*, VLCFAs make up 1-5% of total fatty acids (Dittrich et al. 1998; Welch and Burlingame 1973) and the predominant VLCFA is 26 carbons long (Dickson et al. 2006). The VLCFAs are crucial for the formation of lipid rafts in yeast (Gaigg et al. 2006). Although the FAS and elongase complexes share very similar catalytic steps, different sets of enzymes catalyze the elongation reactions in the two pathways (Fig. 1B). The elongase complex's enzymes localize to the endoplasmic reticulum membrane (ER) (Abraham et al. 1961; Klein 1957). The complex receives fatty acids from the cytoplasmic FAS complex and elongates them to VLCFAs (Tehlivets et al. 2007). Previous studies show YBR159W, also known as IFA38, is a keto-acyl reductase required for the second step in the yeast elongase's pathway (Fig. 1B) (Beaudoin et al. 2002; Han et al. 2002). A *ybr159wΔ* null yeast strain has a slow growth phenotype and altered VLCFA lipid composition (Han et al. 2002). Though both FEN1 and SUR4 catalyze the first enzymatic step in the elongase pathway, they are not redundant and are responsible for different chain-length precursor fatty acids. FEN1 prefers 20 carbon long precursors while SUR4 has a broader range of chain-length specificity but is required to convert 24 carbon long VLCFAs to their final 26 carbon long form (Oh et al. 1997). The elongase enzymes TSC13 and PHS1 are both essential (Schuldiner et al. 2005; Tuller et al. 1999). In yeast, newly synthesized VLCFAs are predominately incorporated first into ceramide and eventually into sphingolipids (Dickson et al. 2006). LIP1 is a component of the ceramide synthase complex required for the formation of ceramide from a VLCFA and a sphingoid base (Vallee and Riezman 2005). Each sphingolipid contains one 24-26 carbon long VLCFA in addition to the long-chain base and head group (Dickson 2008).

The ER in budding yeast is composed of the classical membrane network connected to the nuclear envelope as well as a network of tubules known as the cortical ER that extend throughout the cell and encase the inner face of the entire plasma membrane (Preuss et al. 1991). In microscopy, the cortical ER can often be mistaken as the plasma membrane itself (Preuss et al. 1991). While the bulk of yeast's cortical ER lies under the plasma membrane, in most metazoan cells, including mammalian cells, the ER is continuous with the nuclear envelope and forms a network of tubules throughout the cytoplasm that closely align with microtubules (Lowe and Barr 2007).

Using protein affinity purifications coupled with mass spectrometry and yeast 2-hybrid analysis, we provide direct evidence for an interaction between the *S. cerevisiae* eIF2B complex and YBR159W. We find that in wild-type cells eIF2B co-localizes with lipid membranes and that this membrane co-localization is not altered in a *ybr159wΔ* strain. Our experiments show that a *ybr159wΔ* mutation causes eIF2B to appear as numerous foci. While *ybr159wΔ* null cells have a lower rate of translation, the appearance of numerous eIF2B foci does not appear to correlate with the cell's translation rate. Other VLCFA mutant strains showing multiple eIF2B foci have WT translation rates. Overall, this work shows a novel interaction between the essential yeast translation initiation factor and the fatty acid synthesis enzyme YBR159W.

MATERIALS AND METHODS

Strains and Media

All yeast media, growth, and genetic manipulation was done using standard techniques (David C. Amberg 2005). To create the *ybr159wΔ* strain AL401, the kanamycin resistance cassette from plasmid pFa6a-kanmx6 was first amplified with primers CGTACGCTGCAGGTCGAC and ATCGATGAATTCGAGCTCG. Using the PCR double fusion approach (David C. Amberg 2005), the primers CGGATTTGGAAGTCCTTTATAG, GTCGACCTGCAGCGTACGCATTTCTTAAGCTGCACCG, CGAGCTCGAATTCATCGATTAGAATTATCGTTCTCG, and GGACTTGGTCCTTCCACC were used to expand the YBR159W genomics flanking the kanmx6 cassette. The YBR159W disruption cassette was transformed into strain BY4741 and transformants were selected on YPD + 300 mM G418 plates and screened using Western blotting and α-YBR159W polyclonal antibodies. Candidate BY4741 *ybr159wΔ* strains were crossed with the HIS+ strain H1511 and sporulated to create the *ybr159wΔ* null strain AL401. An isogenic wild type HIS+ control strain AL400 was selected from the same sporulation. The *lip1Δ* strain RH5994 was kindly provided by the Howard Riezman Laboratory (Vallee and Riezman 2005). The *gcn3Δ, fen1Δ, and sur4Δ* deletion strains were obtained from the MATa yeast deletion collection (Winzeler et al. 1999). The *fen1Δ* and *sur4Δ* deletion strains from the MATa yeast deletion collection were mated with the HIS+ strain H1511 and sporulated to create the *fen1Δ* and *sur4Δ* strains, AL413 and AL414 respectively. The TAP tagged strains were obtained from the yeast TAP-tagged library (Ghaemmaghami et al. 2003).

The GFP tagged strains were obtained from a GFP-tagged yeast library (Huh et al. 2003). To make the *ybr159wΔ*, GCD7-GFP strain, we mated the *ybr159wΔ* strain AL401 with the GCD7-GFP strain AL429 from the GFP-tagged yeast library and sporulated the diploids to obtain the *ybr159wΔ*, GCD7-GFP strain AL403. The yeast 2-hybrid activation-domain strains derived from parent strain pJ69 Ra, the binding-domain parent strain pJ69-4alpha, and yeast 2-hybrid plasmids were obtained from the Yeast Resource Center (University of Washington) (James et al. 1996). Using the protocol previously described by the Yeast Resource Center (30), the AL408 (YBR159W-BD), AL409 (GCD1-BD), AL410 (GCD2-BD), AL411 (GCD6-BD), and AL412 (GCD7-BD) strains expressing yeast 2-hybrid binding-domain tagged alleles were generated from parent strain pJ69-4alpha. Briefly, initial forward and reverse primers were used to PCR the target gene from yeast genomic DNA. The PCR product and the common forward and reverse 2-hybrid primers were used for a second round of PCR to extend the flanking sequences. The 2nd PCR product and the *PvuII* and *NcoI* linearized pOBD2 plasmid were co-transformed into yeast strain PJ69-4alpha and plated on SC-trp to select for recombinants fusing the target gene to the GAL4 binding domain. Tables 1, 2, and 3 list all strains, plasmids, and primers used in this study.

Plasmids

The plasmid pOBD2 used in generating yeast 2-hybrd binding-domain strains has been previously described (Hudson et al. 1997). To create a plasmid expressing endogenous level of YBR159W, we used PCR to amplify the YBR159W gene along with 600 bp of the genomic region upstream of the gene's start codon and the YBR159's stop codon using the primers CACCATGGTTTTTGTGACTTTACCTATAAATAGTACACAAC and CTATTCCTTTTTAACCTGTCTTGCGGCTTTTTTTAAGGC. The PCR product was cloned into the pENTR entry vector using Directional TOPO Cloning (Invitrogen) to create pENTR-YBR159W 5' UTR-YBR159W. The YBR159W cassette was transferred to the pAG415GAL-ccdB yeast destination vector using LR Clonase recombination (Invitrogen) (Alberti et al. 2007) . To eliminate possible promoter interference, the vector's endogenous GAL promoter was deleted using the restriction enzymes *SacI* and *SpeI* and replaced with the primer insert GGGAGCTCCATACTGATTAGTACACTAGTGG and CCACTAGTGTACTAATCAGTATGGAGCTCCC to create the YBR159W expression plasmid YCp-

YBR159W. To create a plasmid expressing RFP-tagged YBR159W, the YBR159W ORF without the stop codon was amplified by PCR and cloned into the pENTR vector creating pENTR-YBR159W. The YBR159W ORF insert was transferred by recombinational cloning into the pAG415GPD-ccdB-dsRed vector (Addgene) to create the final expression plasmid YCp-YBR159W-dsRed. All plasmids used in this study are listed in Table 2.

Antibodies

The α-YBR159W polyclonal antibodies were generated by inoculation of a rabbit with the synthetic peptide CETVKAENKKSGTRG (Covance). The peptide was covalently bound to cyanogen bromide beads (Sigma-Aldrich) to affinity purify α-YBR159W from rabbit whole blood. Polyclonal antibodies to yeast SUI2 were kindly provided by Dr. Tom Dever. Polyclonal antibodies to yeast GCD6 and GCD1 were kindly provided by Dr. Allan Hinnebusch. The mouse α-DPM1 was obtained from Molecular Probes. Antibodies to yeast TDH1, 2, 3 were obtained from Millipore. The antibody to yeast RPL32 was kindly provided by Dr. Jonathan Warner.

Mass Spectrometry-Proteomics

For yeast TAP experiments, TAP-tagged protein complexes were purified as previously described (Powell et al. 2004; Sanders et al. 2002). For each TAP strain, a 2 L culture was grown to OD_{600} 1-2 in YPD. The purified TAP complexes were reduced with 1/10 volume of 50 mM DTT at 65 °C for 5 min, and cysteines were alkylated with 1/10 volume of 100 mM iodoacetamide at 30 °C for 30 min. The proteins were digested overnight at 37 °C with modified sequencing grade trypsin at ~25:1 subtrate:enzyme ratio (Promega, Madison, WI). Proteins were identified using Multidimensional Protein Identification Technology (MudPIT) and a LTQ linear ion trap mass spectrometer (ThermoFisher) (Link et al. 1999; Link et al. 2005). A fritless, microcapillary (100 μm-inner diameter) column was packed sequentially with 12 cm of 5 μm C_{18}reverse-phase packing material (Synergi 4 μ Hydro RP80a, Phenomenex) and 3 cm of 5 μm strong cation exchange packing material (Partisphere SCX, Whatman). The entire trypsin-digested samples were loaded onto the biphasic column equilibrated in 0.1% formic acid, 2% acetonitrile, which was then placed in-line with an LTQ linear ion trap mass spectrometer. An automated six-cycle multidimensional

chromatographic separation was performed using buffer A (0.1% formic acid, 5% acetonitrile), buffer B (0.1% formic acid, 80% acetonitrile) and buffer C (0.1% formic acid, 5% acetonitrile, 500 mM ammonium acetate) at a flow rate of 300 nL/min. Cycles 1−6 consisted of 3 min of buffer A, 2 min of 0−100% buffer C, 5 min of buffer A, followed by a 60-min linear gradient to 60% buffer B. In cycles 1−6, the percent of buffer C was increased incrementally from 0, 15, 30, 50, 70, and 100% in each cycle. During the linear gradient, the eluting peptides were analyzed by one full MS scan (200−2000 *m*/*z*), followed by five MS/MS scans on the five most abundant ions detected in the full MS scan while operating under dynamic exclusion.

For proteomic analysis of membrane float experiment's membrane and cytoplasmic fractions, a modified MudPIT protocol was utilized. Purified yeast protein and subcellular complexes were processed and analyzed essentially as described above except a 12 step MuDPIT experiments was used with the salt pulses of 0mM, 25mM, 50mM, 75mM, 100mM, 150mM, 200mM, 250mM, 300mM, 500mM, 750mM and 1M ammonium acetate. Eluting peptides were analyzed using an LTQ-OrbitrapXL mass spectrometer with preview mode and monoisotopic precursor selection enabled. The top 10 precursors ions based on intensity were fragmented using CID in the ion trap using 35% normalized collision energy. Dynamic exclusion was enabled for 180s with repeat count of 1 at 30 s duration, list size of 500, mass tolerance of 10 ppm. Mass spectrometry data was analyzed as previously described (McAfee et al. 2006).

GFP Affinity Purification

Two liters of the GCD7-GFP, *ybr159wΔ* strain AL403,GCD7-GFP strain AL429, and untagged *ybr159wΔ* strain AL401 were grown to OD_{600} 1-2 in YPD. Yeast cells were harvested by centrifuging at 1500 xg for 5 min, and resuspended in 10 mL ice-cold NP-40 lysis buffer (6 mM Na_2HPO_4, 4 mM NaH_2PO_4, 1% NP-40, 150 mM NaCl, 2 mM EDTA, 50 mM NaF, 4 µg/mL leupeptin, 0.1 mM Na_3VO_4). Cells were lysed for 10 min with glass beads in NP-40 lysis buffer. The lysates were centrifuged at 500 xg for 5 min. The cleared supernatant was brought up to 25 mL with ice-cold lysis buffer. Five hundred µL bed volume of protein A/G agarose beads (Thermo Scientific) and 50 µg of anti-GFP antibody (ThermoFisher) were added simultaneously and allowed to incubate for 1 h at RT. The beads were centrifuged at 300 xg for 5 min, transferred to a Poly Prep Chromatography Column (Bio Rad) and washed at 4^{o}C with 50 column volumes

of wash buffer (10 mM Tris pH 8.0, 150 mM NaCl, 0.1% NP-40). Protein digestion was carried out directly on the agarose beads. The beads were suspended in 1 mL of digestion buffer (10 mM Tris pH 8.0, 150 mM NaCl, 0.5 mM EDTA, 1 mM DTT) and transferred to a 1.5 mL microcentrifuge tube. The resuspended beads were trypsin digested as described for yeast TAP complexes. After digestion the beads were centrifuged at 13,000 xg for 1 min and the supernatant was transferred to a fresh microcentrifuge tube. MudPIT was performed identical as described for the TAP purifications. Mass spectrometry data was analyzed as previously described using C_n scoring filters of 1.5 (+1), 3.5 (+2) and 3.5 (+3) (McAfee et al. 2006).

Fatty Acid Profiling

The protocol for extracting lipids from yeast cells was adapted from Ejsing *et al.* 2008 (Ejsing et al. 2009). Each yeast strain was grown to OD_{660} 1.0-1.5 in YPD media at 30 ^{o}C. Fifty mg of wet weight yeast cells was incubated in 200 µL PBS with 100µg/mL lyticase (Sigma) for 1 h at 37°C. Next, 990 µL of chloroform/methanol (17:1 V/V) was added and incubated for 2 h at 37°C. The lower organic layer was collected and vacuum evaporated. Next, 990 µL of chloroform/methanol (2:1 V/V) was added to the upper aqueous layer and incubated for 2 h at 37°C. The lower layer was collected and pooled with the evaporated fraction taken from the first extraction and vacuum evaporated. The sample was solubilized with 100µL chloroform/methanol (1:2 V/V) and mixed 1:1 with 0.4 mM methylamine in methanol. Samples were directly injected into an ESI-LTQ OrbitrapXL at 2 µL/min and precursor ions were scanned using the Orbitrap analyzer at a resolution of 30,000 in negative ion mode. Using published inositolphosphoceramide (IPC) precursor *m/z* values, precursor ion peaks were identified using a mass tolerance of 10 ppm (Ejsing et al. 2006; Sud et al. 2007). Using inositolphosphoceramide (IPC) structure data at the LIPID MAPS Lipidomics Gateway (Sud et al. 2007), the following theoretical precursor $[M-H]^-$ ion *m/z* values were used to identify the IPC ions in the high resolution scan: IPC 46:0;4 (980.717), IPC 44:0;4 (952.686), IPC 42:0;4 (924.655), IPC 40:0;4 (896.623), IPC 38:0;4 (868.592). To validate the identity of these IPC ions, the IPC precursor ions were fragmented by CID in the linear ion trap. The observed *m/z* values of the MS/MS fragment ions for each IPC precursor was compared to predicted $[\text{ceramide phosphate} - H_2O]^-$ and $[\text{ceramide phosphate}]^-$ *m/z* values at a mass tolerance of 0.1 Da. The following theoretical *m/z* [ceramide

phosphate – $H_2O]^-$ and [ceramide phosphate]$^-$ fragment ions were used to validate the IPC lipids: IPC 38:0;4 (688.53, 706.54), IPC 40:0;4 (716.56, 734.57), IPC 42:0;4 (744.59, 762.60), and IPC 46:0;4 (800.65, 818.66). In addition, to validate the identification of IPC 44:0;4, the fragmentation spectrum of precursor *m/z* 952.68 at a mass tolerance of 0.1 Da was compared to the previously published fragment ions [ceramide phosphate – $H_2O]^-$, *m/z* 772.62 and [ceramide phosphate]$^-$, *m/z* 790.63 values (Ejsing et al. 2006). To compare the observed abundance for each IPC species between strains, the precursor ion signal intensity for each identified IPC species was normalized to the signal intensity of the *m/z* 835.53 base peak corresponding to the phosphatidyl inositol (PI) species PI 16:1-18:0 and PI 16:0-18:1.

Growth Rate Analysis

Yeast strains were grown overnight at 30 ^oC in YPD. Relative cell number was measured at OD_{660} using a Beckman DU 530 Spectrophotometer. Cells were diluted in 50 mL of fresh YPD to ~0.05 OD_{660} units/mL. Individual strains were grown at 30 ^oC and an OD_{660} measurement was taken every 2 h. The formula for used for converting OD_{660} readings to cell numbers was $y = 1.1564x^3 - 0.6815x^2 + 1.3996x$ with y = cell number/mL and x = OD_{660} value (David C. Amberg 2005). Cell doubling time was determined by plotting the growth curve for each strain and measuring the maximum rate of cell growth during logarithmic growth.

Yeast 2-Hybrid

Mating type A strains containing AD tagged alleles and mating type α strains containing BD tagged alleles have been previously described (Fields and Song 1989). The A and α strains were allowed to mate in liquid YPD at 30^oC overnight. Relative cell number was determined by measuring OD_{660} and 4 μL of a $1x10^7$ cells/mL solution was plated onto SC -leu, -trp, -his, 1.5 mM 3-AT agar plates. Plates were scanned after 48 h.

Membrane Flotation

Membrane flotation of yeast extracts was performed as previously described (Bergmann and Fusco 1988). Fifty mL of each yeast strain was grown to OD_{660} 1.0-1.5 in YPD media at 30 ^oC. The cells were lysed with

glass beads in ice-cold breaking buffer (30 mM Tris pH 7.0, 1 mM EDTA). The lysate was cleared by centrifugation at 500 xg for 3 min. Lysate corresponding to 10 OD_{660} units of cells in 222 µL was mixed with 1778 µL of ice-cold 90% sucrose (wt/vol), 10 mM Tris pH 7.0 solution. The 2 mL of lysate/sucrose solution was transferred to the bottom of a 14 x 89 mm ultracentrifuge tube (Beckman, cat. # 344059) and layered with 6 mL of 65% sucrose, 10mM Tris pH7.0 and then 3 mL of 10% sucrose, 10mM Tris pH 7.0. The tubes were centrifuged in a Beckman SW-41 rotor at 24,000 rpm for 18 h. Individual 1.5 mL fractions were collected from the top of the gradient and the proteins TCA precipitated. Ten percent of each fraction was used for SDS-PAGE and Western blotting.

Membrane Flotation Fractions Affinity Purifications

For each TAP strain, a 1 L culture was grown to OD_{600} ~1 in YPD and the cells were split into 6 fractions. Each cell fraction was separated using the membrane flotation gradients as described above. The 10%-65% sucrose interface layer and 80% sucrose layer from each gradient were collected and pooled. TAP purification was performed as previously described up to TEV protease cleavage (Powell et al. 2004; Sanders et al. 2002).

GCN4-LacZ Induction

The yeast reporter plasmid p180 containing the GCN4 5′ untranslated region (UTR) coupled to a -*lacZ* reporter has been previously described (Hinnebusch 1985). Yeast strains transformed with p180 were grown overnight at 30 ^{o}C in SC-ura. Cultures were diluted 1:10 and allowed to continue growing for 2 h in SC -ura, -his. Cells were spun down and split into two tubes containing 10 mL of SC -ura, -his media. A 1 M 3-AT solution was added to the starvation tube to a final concentration of 10 mM. The cells continued to grow for 4 h at 30 ^{o}C. β-galactosidase assays were performed as previously described (Rose and Botstein 1983). Cells were centrifuged at 1500 xg for 5 min and lysed with glass beads in 1 mL of ice-cold breaking buffer (100mM Tris pH 8.0, 1mM DTT, 20% glycerol). Twenty microliters of whole cell extract was added to 900 µL of Z buffer (16.1 g/L Na_2HPO_4-$7H_2O$, 5.5 g/L NaH_2PO_4-H_2O, 0.75 g/L KCl, 0.246 g/L $MgSO_4$-$7H_2O$, 2.7 mL/L βME, pH 7.0) and incubated at 28 ^{o}C for 5 min. The reaction was initiated by adding 200 µL of 4 mg/mL ONPG in Z buffer and incubated at 28 ^{o}C. After the reaction turned a pale yellow color, 0.5

mL of 1 M Na_2CO_3 was added. LacZ expression was determined by measuring the absorbance at 420 nm using a Beckman DU 530 Spectrophotometer. Protein concentration of the extracts was determined using the BioRad Dc protein assay. LacZ specific activity was determined using the equation: (OD_{420} x 1.7)/(0.0045 x protein conc. (mg/mL) x extract volume(mL) x time (min)) (David C. Amberg 2005). Values were normalized to wild type.

^{35}S-Met Incorporation

Overnight cultures of yeast grown in YPD were diluted 1:10 in 10 mL of SC-Met and grown for 3 h at 30 ^{o}C. The OD_{660} of the culture was measured to determine cell numbers. For labeling, ^{35}S-methionine (MP Biomedicals) was added to 5 mL of the cell culture to a final concentration of 10 μCi/mL. Samples were incubated with shaking for 30 min at 30 ^{o}C. Labeling was stopped by the addition of 1/10 volume 100% TCA and heating to 100 ^{o}C for 30 min. TCA precipitates were collected on GFC filters (Whatman) then washed sequentially with 5 mL each of 10% TCA and 95% ethanol. Filters were then placed in 5 mL EcoLume scintillation fluid (MP Biomedicals) and ^{35}S-Met incorporation was measured using a Beckman LS 6500 scintillation counter. Values were reported as (Counts per minute) / (OD_{660} unit).

Microscopy

Epifluorescent microscopy was performed using live yeast cells grown in SC media to an OD_{660} 1.0-1.5 at 30 ^{o}C. Cells were mounted on slides and visualized using a Zeiss Axiophot brightfield microscope with a 63x / 1.40 Plan-Apochromat oil DIC lense. Images were analyzed with MetaMorph imaging software (Molecular Devices). Live yeast cells imaged using confocal microscopy were grown in SC media to an OD_{660} 1.0-1.5 at 30 ^{o}C., Cells were visualized with a Zeiss LSM 510 META inverted confocal microscope using a 63x / 1.40 Plan Apochromat oil immersion lens. Microscopic images used for quantitative analysis were analyzed using ImageJ imaging software (Schneider et al. 2012). To quantify the percentage of 2B bodies that co-localized with the ER, a 2B body was judged to be co-localized with the ER only if the 2B body signal overlapped with an area of YBR159W at least half as bright as the brightest YBR159W signal seen in the cell. Cells were pooled into groups of approximately 25 cells to calculate a standard deviation for the percentage of 2B bodies co-localized with the ER. The bright regions of the ER were subtracted

from the total area of the cell minus the nuclear area to determine the fraction of the cell taken up by the ER. The compound 3,3'-dihexyloxacarbocyanine iodide ($DiOC_6(3)$) was used to stain and image the membranes of wild type strain AL400, and *ybr159wΔ* strain AL401 as previously described (Terasaki et al. 1984). Yeast cells were incubated in media containg 2.5 µg/mL DiOC6(3) for 10 min before imaging.

Polysome Profiling

Polysome analysis was performed as previously described (Gerbasi et al. 2004). Yeast strains were grown in YPD to an OD_{660} of ~1. Cells were lysed with glass beads in ice-cold breaking buffer (10 mM Tris pH 7.0, 100 mM NaCl, 30 mM $MgCl_2$, 50 µg/mL cycloheximide, 200 µg/mL heparin). The crude lysate was cleared by centrifugation at 500 xg for 3 min and 20 OD_{660} units of cells was loaded on top of a 7 to 47% continuous sucrose gradient (wt/vol) cast in 50 mM Tris pH 7.0, 50 mM NH_4Cl, 12 mM $MgCl_2$, 50 µg/mL cycloheximide in a 14 x 89 mm ultracentrifuge tube (Beckman). Gradients were centrifuged in a Beckman SW-41 rotor at 14,000 rpm for 18 h at 4 ^oC. Absorbance profile at 254 nm was collected from the gradients as previously described (16). One mL fractions were used for Western blotting. Monosome and polysome peak areas were determined using ImageJ software (Schneider et al. 2012). A moving baseline for each profile was established by connecting the minima between each peak and the area under each peak above this line was calculated. The polysome peak areas were summed and compared to the monosome peak area.

Subcellular Fractionation

WT yeast strain AL400 was grown to OD_{660} 1.0-1.5 in YPD media at 30 ^oC. To isolate subcellular fractions, 45 OD_{660} units of cells were split into three samples: control, puromycin treatment, and EDTA treatment. The control sample was lysed using glass beads in 750 µL of ice-cold control buffer (10 mM Tris pH 8.0, 100 mM NaCl, 1 mM EDTA, 10 mM KCl, 30 mM $MgCl_2$). The puromycin and EDTA treatment samples were lysed using glass beads in 750 µL of ice-cold ribosome dissociation buffer (10 mM Tris pH 8.0, 100 mM NaCl, 1 mM EDTA). The control sample was diluted in 750 µL of control buffer. The puromycin treated sample was diluted with750 µL of ribosome dissociation buffer containing 2 mM puromycin to a final concentration of 1 mM. The EDTA-treated sample was diluted in Ribosome

dissociation buffer (20mM EDTA) to a final concentration of 10 mM EDTA. Lysates were gently mixed at RT for 30 min to facilitate dissociation of ribosomes from the ER. Lysates were centrifuged at 900 xg for 5 min, and the supernatant was centrifuged at 11,000 xg for 20 min. The soluble fraction was recovered from the supernatant. The pellets was resuspended in either control buffer (1 mM puromycin, 10 mM Tris pH 8.0, 100 mM NaCl, 1 mM EDTA) or EDTA solution (10mM EDTA, 10 mM Tris pH 8.0, 100 mM NaCl, 1 mM EDTA) and centrifuged at 11,000 xg for 20 min. The pellets were resuspended in 1.5 mL of resuspension buffer (1 mM puromycin, 10 mM Tris pH 8.0, 100 mM NaCl, 1 mM EDTA, 1% SDS) and 15 µL of each fraction was used for Western blotting.

RESULTS

In a tandem affinity purification proteomics screen of *S. cerevisiae* translation initiation factors followed by liquid mass spectrometry analysis, we discovered that all five subunits of eIF2B co-purified with the VLCFA enzyme YBR159W (Link et al, in preparation; and Fig. 2A). Subsequent LC-MS/MS analysis of TAP-YBR159W affinity purification showed YBR159W co-purified with all five subunits of the eIF2B complex and several members of the VLCFA synthesis pathway. In this study, additional TAP experiments examined whether other members of the VLCFA synthesis pathway also interact with eIF2B subunits. With the exception of YBR159W, our data showed that other members of the VLCFA synthesis pathway did not interact with eIF2B (Fig. 2A). To rule out the possibility that the YBR159W-eIF2B interaction was due to an artifact of the TAP-tagged strains, we performed a GFP affinity purification using the GCD7-GFP strain AL429. LC-MS/MS analysis identified YBR159W co-purifying with all five subunits of eIF2B (Fig. 5E). Next, we utilized yeast 2-hybrid to identify interactions between eIF2B subunits and YBR159W. The activation-domain tagged strains pOAD(YBR159W), pOAD(GCD1), pOAD(GCD2), pOAD(GCN3), pOAD(GCD6), pOAD(GCD7), pOAD(SUI2), and pOAD(TDH1) were mated with binding-domain tagged strains AL408 (YBR159W), AL409 (GCD1), AL410 (GCD2), AL411 (GCD6) and AL412 (GCD7). The positive interactions between different subunits of the eIF2B complex validated the experiment's ability to detect previously described interactions (Fig. 2B). The 2-hybrid analysis showed that YBR159W positively interacted with both the GCD6 and GCD7 subunits of eIF2B (Fig. 2B).

The GFP-tagged YBR159W strain AL425 showed the YBR159W protein localizes to the ER membrane using epifluorescence microscopy (Fig. 3A). DPM1 encodes the enzyme dolichol phosphate mannose synthase which adds a mannose moiety to dolichyl phosphate on the cytosolic side of the endoplasmic reticulum (Orlean 1990; Orlean et al. 1988). DPM1 is an ER membrane protein unrelated to VLCFA synthesis or utilization (Orlean et al. 1988). Confocal microscopy using the FEN1-GFP, YBR159W-RFP strain AL422 and the DPM1-GFP, YBR159W-RFP strain AL423 confirmed that RFP-tagged YBR159W expressed from a low-copy plasmid co-localizes with the VLCFA protein FEN1 and ER protein DPM1 (Fig. 3B).

We constructed a *ybr159wΔ* yeast strain AL401 to examine the null phenotype. The mutant strain had a slow growth phenotype (Fig. 3C) and was temperature sensitive at 37^{o} C (data not shown). To show the slow growth phenotype was due to the deletion of *ybr159wΔ* and not a second site mutation in the strain, the *ybr159wΔ* null yeast strain was complemented in strain AL402 expressing YBR159W from the low-copy plasmid YCp-YBR159W (Fig. 3C). Our results agreed with previous studies using an unrelated *ybr159wΔ* null strain (Beaudoin et al. 2002).

Previous work has shown that disruption of VLCFA utilization in yeast causes abnormal formation of lipid membranes (Schneiter et al. 2004). The compound 3,3'-dihexyloxacarbocyanine iodide ($DiOC_6(3)$) is a lipophilic dye used to label a variety of lipid membranes (Terasaki et al. 1984). We used $DiOC_6(3)$ to stain membranes of wild type strain AL400, *ybr159wΔ* strain AL401, and the VLCFA mutant strains AL413 (*fen1Δ*), and AL414 (*sur4Δ*), and the ceramide synthase mutant strain RH5994 (*lip1Δ*). The *ybr159wΔ*, *fen1Δ*, *sur4Δ*, and *lip1Δ* null strains all displayed disrupted lipid membranes using epifluorescence imaging (Fig. 4). This supported previous work showing that VLCFAs are important for proper membrane formation (Schneiter et al. 2004).

To determine if YBR159W has a role in translation, we examined if the *ybr159wΔ* strain AL401 causes a defect in protein synthesis. We used ^{35}S-methionine incorporation to quantify the global translation rate. The ^{35}S-methionine incorporation experiments showed that the *ybr159wΔ* strain has a reduced translation rate (Fig. 5A). The ceramide synthase mutant *lip1Δ* strain RH5994 also showed a reduction in the rate of translation. The *lip1Δ* strain had a similar slow growth rate as the *ybr159wΔ* strain.

However, the VLCFA mutant strains AL413 (*fen1Δ)* and AL414 (*sur4Δ)* showed no reduction in translation or growth rates (Fig. 5A).

Next, we performed polyribosome profiling to examine the distribution of 40S, 60S, 80S, and polyribosomes in the *ybr159wΔ* strain AL401. Compared to the WT strain, we observed the polysome profiles for the *ybr159wΔ* strain showed an increase in the 80S monosome peak and a decrease in polysome peaks (Fig. 5B). As expected, the complemented *ybr159wΔ* strain AL402 showed a similar polysome profile to WT. To normalize and quantify the observed differences in the peak areas, the ratio of the 80S monosome to polysome peak areas was calculated. The monosome:polysome ratio significantly increased for the *ybr159wΔ* strain compared to the WT and complemented strains (Fig 5D). Polysome profiles of the *lip1Δ* strain RH5994 showed similar defects to the *ybr159wΔ* strain (Fig. 5B and 5D). Polysome profiling of the *fen1Δ* strain AL413 and *sur4Δ* strain AL414 showed no noticeable differences from wild type strain AL400 (Fig. 5B and 5D). These polysome distributions were consistent with the reduced global translation rates seen previously in the ^{35}S-methionine labeling experiments.

We next examined *ybr159wΔ*'s effect on eIF2B's activity. We used a GCN4-lacZ expression assay to examine GCN4 expression during the starvation response (Hinnebusch 1994). Strains AL400 (HIS+ control strain), AL401 (*ybr159wΔ)*, AL402 (*ybr159wΔ* +YCp-YBR159W), AL413 (*fen1Δ)*, AL414 (*sur4Δ)*, RH5994 (*lip1Δ)*, H2557 (*gcn2Δ*) and F98 (*gcd1*) were transformed with the GCN4-lacZ reporter plasmid p180. Our results showed that the *ybr159wΔ*, *fen1Δ*, *sur4Δ*, and *lip1Δ* null strains did not affect the induction of GCN4 during amino acid starvation (Fig. 5C). This suggested that eIF2B's role in the regulation of GCN4 response is not affected by the *ybr159wΔ* null or other VLCFA pathway mutation.

We next tested if the *ybr159wΔ* mutation affected the composition of the eIF2B complex. Using the *ybr159wΔ*, GCD7-GFP tagged strain AL403, the untagged *ybr159wΔ* strain AL401, and the GCD7-GFP strain AL429, we performed GFP affinity purifications and LC-MS/MS mass spectrometry analysis of the affinity purified complexes. All five subunits of eIF2B were identified in the *ybr159wΔ,* GCD7-GFP strain and the GCD7-GFP strain (Fig. 5E). No subunits of eIF2B were identified in the untagged *ybr159wΔ* control strain AL401. These results suggested that the composition of eIF2B is not dependent upon presence of YBR159W.

While the composition of eIF2B appeared to be independent of YBR159W, the consistently lower number of identified peptides for each eIF2B subunit from the mass spectrometry data for the GCD7-GFP, *ybr159wΔ* null strain compared to the GCD7-GFP strain suggested that the cellular abundance of eIF2B was lower in the *ybr159wΔ* null background (Fig. 5E). To determine if the cellular abundance of eIF2B is lower in a *ybr159wΔ* null strain, Western analysis was performed on the yeast strains used in the GCD7-GFP affinity purification of eIF2B complexes. Lack of signal for YBR159W in the *ybr159wΔ* strains confirmed the expected null genotype (Fig. 5F). In concordance with the mass spectrometry results, the GFP7-YFP, *ybr159wΔ* strain had a lower abundance of eIF2B compared to GCD7-GFP strain (Fig. 5E). To validate this observation in untagged strains, Western analysis was also performed using the WT strain AL400 and the untagged *ybr159wΔ* null strain AL401. The *ybr159wΔ* null strain again showed lower abundance of eIF2B compared to the WT strain (Fig. 5F)

We next tested whether eIF2B played a role in VLCFA synthesis. Previous studies had shown a *ybr159wΔ* null strain had an altered VLCFA lipid composition (Han et al. 2002). Since four of the five subunits of eIF2B are essential, we used a *gcn3Δ* strain AL424 to test for VLCFA defects. WT strain AL400, *ybr159wΔ* strain AL401, *ybr159wΔ* rescue strain AL402, *sur4Δ* strain AL414, and *lip1Δ* strain RH5994 were used as positive and negative controls. To profile the VLCFAs, lipids were extracted from yeast cells and directly infused into an ESI-LTQ-Orbitrap mass spectrometer while scanning at high resolution in negative ion mode. Several inositolphosphoceramides (IPC), a class of VLCFA-containing sphingolipid, were identified using previously published *m/z* values at 10 ppm mass accuracy (Ejsing et al. 2009; Sud et al. 2007). We validated the identification of the IPC species using either previously observed fragmentation spectrum or expected *m/z* values for the IPC's [ceramide phosphate – H_2O]$^-$ and [ceramide phosphate]$^-$ fragment ions (Fig. 6) (Ejsing et al. 2006). The IPC 44:0;4 and IPC 46:0;4 sphingolipids contain full-length VLCFAs and are the most abundant yeast sphingolipid species (Dickson et al. 2006). Compared to WT, the *gcn3Δ*, *ybr159wΔ,* and other VLCFA and ceramide synthase mutant strains all showed a reduction in the IPC 44:0;4 and IPC 46:0;4 sphingolipids containing full-length VLCFAs (Fig. 7A). The IPC sphingolipid species IPC 38:0;4, IPC 40:0;4, and IPC 42:0;4 contain shorter-chain fatty acids and are typically only detected in VLCFA biosynthesis mutant strains (Dickson et al. 2006). As previously observed, the *sur4Δ* strain had elevated shorter-chain fatty acid-containing IPC species 38:0;4, 40:0;4, and

42:0;4 (36). We observed IPC 38:0;4 and IPC 42:0;4 were also elevated in the *ybr159wΔ* strain. The *gcn3Δ* strain showed no significant changes in the shorter-chain fatty acid sphinglipid's IPC 38:0;4, 40:0;4, and 42:0;4 levels (Fig. 7B). The *lip1Δ* strain contained barely perceptible levels of any IPC, supporting its requirement for ceramide synthesis (Vallee and Riezman 2005).

We next looked at cellular localization of eIF2B and YBR159W using strains with subunits of eIF2B endogenously tagged with GFP and the YBR159W-RFP expression plasmid YCp-YBR159W-dsRed. To show the RFP-tagged YBR159W allele was functional, the plasmid YCp-YBR159W-dsRed complemented the ybr159w*Δ* null strain AL401 (data not shown). Confocal microscopy of the dual-fluorescently-labeled strains was used to look for co-localization between eIF2B and YBR159W (Fig. 8). As observed in previous studies and Fig. 2, YBR159W localized to membranes corresponding to the endoplasmic reticulum (Fig. 8). Using strains with different eIF2B subunits tagged with GFP, we observed eIF2B localized as 1-2 large foci (Fig. 8). In addition, GFP-tagged eIF2B is seen dispersed throughout the cytoplasm (data not shown). Surprisingly, the confocal microscopy images did not convincingly show the majority of YBR159W signal co-localizing with eIF2B subunits. Because we observed that the 2B body localizing near the ER membrane-bound YBR159W, we performed a statistical analysis to test if eIF2B and YBR159W co-localize. We examined 221 individual 2B bodies from 140 dual labeled cells by pooling results from the YCp-YBR159W-dsRed transformed GCD1-GFP, GCD6-GFP, and GCD7-GFP strains (AL405, AL406, and AL407). We found 60.1% ±6.6% of 2B bodies examined showed partial co-localization with a bright area of YBR159W signal. Based on the area of the cell taken up by bright areas of YBR159W signal, it would be expected that only 30.7% ±6.9% of 2B bodies would co-localize with YBR159W signal if the two signals were independent of each other. A Student's *t*-test ($P=2.9x10^{-8}$) shows this difference to be significant.

To observe the effects of the *ybr159wΔ* deletion on eIF2B localization, we performed live cell imaging using epifluorescence microscopy on the yeast strains *ybr159wΔ*, GCD7-GFP (AL403), GCD7-GFP (AL429), and *ybr159wΔ*, GCD7-GFP, [YCp-YBR159W] (AL404) . Cells from the GCD7-GFP control strain were found to contain 1 to 2 large 2B bodies (Fig. 9A). In the *ybr159wΔ* strain AL403, eIF2B appeared as multiple foci (Fig. 9A). The *ybr159wΔ* phenotype of AL403 was rescued by expression of plasmid YCp-YBR159W in strain AL404 (Fig. 9A). Using these strains, we counted the number of cells

containing 1 to 2 large 2B bodies compared to the number of cells having the multiple eIF2B foci or diffuse cytoplasmic localization. We found that the majority of *ybr159wΔ* cells had multiple eIF2B foci phenotype (Table 4A). For the GCD7-GFP WT control strain, no cells had the multiple eIF2B foci phenotype and a majority of cells had either 1 or 2 2B bodies. The rescued *ybr159wΔ*, GCD7-GFP, [YCp-YBR159W] strain AL404 did not have multiple eIF2B foci (Table 4A). To show the 2B body phenotype was independent of the GFP-tagged alleles, we performed immunofluorescence microscopy on untagged yeast strains using polyclonal antibody against the eIF2B subunit GCD6 (Fig. 9B). We observed the 1 to 2 large 2B body foci phenotype for the majority of the WT control AL400 cells while the majority of the *ybr159wΔ* cells (AL401) displayed multiple eIF2B foci (Table 4B). The *ybr159wΔ*, [YCp-YBR159W] rescue strain AL402 showed a majority of cells had eIF2B present as either a single 2B foci or no detectable foci (Table 4B). The VLCFA and ceramide synthase mutants AL413 (*fen1Δ)*, AL414 (*sur4Δ)*, and RH5994 (*lip1Δ)* were all found to have the multiple eIF2B foci phenotype (Table 4B).

Because eIF2B is thought to be a soluble cytoplasmic protein and YBR159W has been shown to be an integral membrane protein in the endoplasmic reticulum (Klein 1957), we performed membrane float experiments to determine if a population of eIF2B complexes physically interacted with lipid membranes. The lack of signal from the Western blot for the control yeast GAPDH analogs TDH1, 2, and 3 in the membrane fraction showed the fractionation was efficient at separating cytoplasmic proteins from membrane-associated proteins (Fig. 10A). A significant lipid membrane signal was seen for the ER proteins YBR159W and DPM1. A portion of the YBR159W and control ER membrane protein DPM1 signals was still present in the soluble fraction indicating the membrane-associated proteins do not appear to completely separate from the soluble fraction. The membrane float experiments showed that in WT AL400 cells, a significant fraction of the eIF2B subunit GCD6 localized to the lipid membrane fractions (Fig. 10A). The Western blot profiles of the membrane and soluble fractions for GCD6 showed the same pattern as the known ER membrane proteins YBR159W and DPM1 (Fig. 10A). Interestingly, the SUI2 component of eIF2 also showed a similar membrane association pattern. The data indicates a fraction of eIF2 complexes are associated with membranes in yeast cells.

To validate our observation that eIF2B is membrane-associated, we used whole cell extracts prepared from TAP-tagged eIF2B and control strains and the membrane float separation experiment to

collect fractions from the membrane-associated and soluble protein region of the density gradients. Next, we performed a modified TAP purification on each fraction and analyzed the affinity purified complexes using LC-MS/MS. Our data showed that the interaction between eIF2B and YBR159W was still present in both the membrane-associated and soluble protein fractions (Fig. 10B). Because of the incomplete separation of membrane proteins in the assay, it is not known if both soluble and membrane-associated eIF2B interact with YBR159W or if only membrane-associated eIF2B interacts with YBR159W. To see if YBR159W was required for eIF2B's membrane association, we performed the membrane floatation assay and Western blots using the *ybr159wΔ* strain AL401. We found that eIF2B associated with the membrane fraction in the *ybr159wΔ* strain at similar levels as seen in the control strain (Fig. 10C). Overall, the membrane float experiments showed a fraction of yeast eIF2B is associated with membranes but the interaction is independent of YBR159W.

To determine if the membrane association seen for eIF2B is possibly mediated by rough ER-bound ribosomes, we performed a sub-cellular fractionation experiment to isolate smooth membranes. Cell lysates from WT strain AL400 were treated with either elevated levels of EDTA or the ribosome releasing antibiotic puromycin (Adelman et al. 1973). Following fractionation and Western blotting, ribosomal protein signal in the insoluble membrane fraction was significantly reduced in both the EDTA and puromycin treated cell extracts compared to untreated control extracts. However, the eIF2B signal in the rough or smooth membrane fraction did not noticeably change (Fig. 10D). The data indicates that the eIF2B-membrane association is independent of ribosomes.

DISCUSSION

Previous large-scale yeast interactions studies failed to show eIF2B interacting with the VLCFA pathway (Gavin et al. 2002; Krogan et al. 2006; Miller et al. 2005). We show using TAP-tagged and GFP-tagged affinity purifications as well as yeast-2-hybrid that the VLCFA keto-reductase YBR159W interacts with the translation initiation factor complex eIF2B. Because our unpublished proteomic screen of translation factor interactions identified YBR159W interacting with eIF2B, we named the *S. cerevisiae* locus Initiation Factor Associated protein of 38 kD or IPA38 (Link et al., unpublished). Affinity purification and LC-MS/MS experiments show that YBR159W co-purifies with all five subunits of eIF2B

and not in controls. No other member of the VLCFA pathway co-purifies in the eIF2B affinity purifications. Interestingly, the TAP-tagged members of the VLCFA pathway do not seem to strongly interact with each other. Our Y2H data suggest the eIF2B subunits GCD6 and GCD7 physically interact with YBR159W.

The interaction between the VLCFA synthesis pathway and the eIF2B translation initiation pathway presents a number of possibilities. Is one pathway regulating the other or vice versa? It can be hypothesized that the cell might need to regulate VLCFA synthesis if translation is disrupted. Alternatively, it might be advantageous to reduce translational activity if VLCFAs are being down regulated. Finally, the YBR159W-eIF2B complex could be involved in a novel function. A link between a translation initiation factor and lipid membranes is not totally unique. Experiments in human cells have shown an interaction between the translation initiation factor eIF4E and the Golgi apparatus (Willett et al. 2011).

To test the hypothesis that YBR159W and VLCFA synthesis play a role in translation, we used ^{35}S-methionine incorporation and polysome profiling to assay translation activity in mutant strains. Both experiments show a reduction in the translation rate for the *ybr159wΔ* strain. However, a similar phenotype is seen for the slow growing *lip1Δ* strain. The VLFCA mutant *fen1Δ* and *sur4Δ* strains have wild type growth rates and do not share a translation defect with the slower growing members of the pathway. It is not known if the cause of the translation defect seen in the *ybr159wΔ* strain is directly related to its interaction with eIF2B or is an indirect consequence of slow growth or a VLCFA defect.

When GCN4 expression is examined using the GCN4-LacZ assay, the *ybr159wΔ* strain has WT levels of GCN4 induction. The GCN4-LacZ assay was normalized to protein concentration so the slow growth rate of *ybr159wΔ* should not affect the results. The data indicates that the *ybr159wΔ* strain does not have a defect in the GCN4 pathway. We cannot rule out the possibility that the slow growth of *ybr159wΔ* may be masking a subtle defect in eIF2B's GEF activity unrelated to the GCN4 pathway. Our affinity purification experiments of eIF2B in a *ybr159wΔ* deletion background showed that the eIF2B complex is intact. A Western blot of *ybr159wΔ* strains showed that the overall abundance of eIF2B was lower in the deletion background compared to WT. It is not clear if the lower level of eIF2B is caused by the slow growth phenotype of the *ybr159wΔ* null background or some other factor.

To test the hypothesis that eIF2B plays a role in VLCFA synthesis, several limitations arose that made answering the question problematic. Of the 5 yeast eIF2B subunits, only GCN3 is nonessential. The *gcn3Δ* strain did not show a defect in VLCFA production or utilization. While the *gcn3Δ* strain showed a reduction in the sphingolipid species IPC 44:0;4 and IPC 46:0;4, it did not show a concomitant rise in shorter-chain fatty acid-containing IPC species indicative of a defect in VLCFA production. The presence of shorter-chain sphingolipids would indicate the cell is trying to compensate for a lack of VLCFAs. Therefore, we postulate the lower levels of IPC 44:0;4 and IPC 46:0;4 seen in the *gcn3Δ* strain are unrelated to a defect in VLCFA production. The VLCFA defect in *ybr159wΔ* is modest; with only a small rise in the shorter-chain fatty acid-containing sphingolipids. The loss of IPC 46:0;4 is the strain's most striking characteristic. Previous work suggests that Ayr1p is able to perform 3-ketoacyl activity in the absence of YBR159W (Han et al. 2002). The same study showed *ayr1* and *ybr159w* are synthetically lethal (Han et al. 2002).

A *gcn3Δ* null strain is unable to fully derepress GCN4 expression during amino acid starvation (Hannig and Hinnebusch 1988). GCN4 is a transcription factor involved in the expression of several hundred genes during a wide variety of cellular stresses (Natarajan et al. 2001). Though growth conditions for the *gcn3Δ* strain should not have activated a stress response, we suspected analysis of the lipid content of the *gcn3Δ* strain could prove problematic if the VLCFA pathway was a downstream target of the GCN4 transcription factor. We examined the effects of loss of GCN4 using expression data for *gcn4Δ* strains from the Gene Expression Omnibus (GEO) Database (Barrett et al. 2011). Two separate datasets showed no significant changes in the expression of various VLCFA genes (data not shown, GEO Accession GSE24057 (Fendt et al. 2010) and GSE25582). We concluded that under the conditions used for the analysis of sphingolipids, loss of GCN4 did not significantly alter VLCFA gene expression. We concluded our *gcn3Δ* strain was not experiencing alterations in VLCFA gene expression due to repression of GCN4. The lack of a direct translation defect in the *ybr159wΔ* strain and the lack of a VLCFA defect in the *gcn3Δ* strain suggest there is no significant cross-talk between the GEF and VLCFA pathways.

Membrane floatation and subcellular fractionation assays show eIF2B interacts with lipid membranes. Our data and previous studies showed YBR159W is an integral membrane protein that co-localizes with the ER membrane (Abraham et al. 1961; Klein 1957). We interpret these findings to mean

that the membranes eIF2B is interacting with are ER membranes. It is unknown if ER-associated eIF2B is actively engaged in guanine nucleotide exchange. A number of conclusions can be made about this ER membrane-interacting eIF2B. First, the eIF2B-membrane interaction is not mediated by rough ER-bound ribosomes. Treatment of cell extracts with EDTA or puromycin greatly reduces the amount of ribosomes that fractionate with lipid membranes but does not reduce the portion of eIF2B that fractionates with membranes. This fits the prevailing theory that eIF2B's role in translation is independent of the ribosome (Merrick W. C.). Second, YBR159W is not required for the interaction. The *ybr159wΔ* null strain does not affect eIF2B's interaction with the membrane showing that the interaction of eIF2B with ER membranes is YBR159W independent. This indicates that other factor(s) are possibly required.

Confocal microscopy shows that the majority of 2B bodies are in close proximity to YBR159Wp and ER membranes, supporting the model that 2B bodies and the ER interact. This could be taken to indicate that the eIF2B shown to interact with ER membranes resides in 2B bodies. A possible conflicting interpretation of the data is that YBR159W-RFP is being overexpressed and its localization is an artifact. The co-localization experiment used a RFP-tagged YBR159W allele expressed from a GPD promoter on a centromeric plasmid. Global protein expression analysis shows that the GPD promoter's target protein, TDH3, is expressed at roughly 4 times that of YBR159W (Ghaemmaghami et al. 2003). The fact that the RFP-tagged YBR159W localization agrees with endogenously expressed YBR159W-GFP localization leads us to believe that artifacts caused by the RFP tagged construct are not disrupting YBR159W's localization. In addition, the RFP-tagged allele complements a *ybr159wΔ* null strain. How and why eIF2B might be interacting with the ER membrane is unknown. A population of membrane-interacting 2B bodies might possibly explain recent findings that 2B bodies can exist in a mobile or static state with mobile 2B bodies free in the cytoplasm and static 2B bodies being associated with membranes (Taylor et al. 2010). Further work is needed to prove this hypothesis.

The observation that the *ybr159wΔ* null strain leads to multiple eIF2B foci is intriguing. This phenotype is also seen in other VLCFA mutants. The fact that these mutants all display disrupted lipid membranes lends itself to the theory that properly formed membranes are required for the integrity of 2B bodies. An intriguing question is whether the membrane disruption prevents the 2B bodies from forming properly or whether the 2B bodies are unable to be maintained once formed? For the first model, an as yet

unknown factor in membranes required for 2B body formation could be disrupted and cause 2B bodies to form throughout the cell. We speculate that this membrane-associated factor could serve as a nucleating site for the formation of 2B bodies. The second model would predict that membrane disruption is affecting a factor needed for 2B body stability. Loss of this factor leads to 2B bodies dissociating into multiple smaller foci. A previous study showed VLCFAs were important for lipid raft formation (Gaigg et al. 2006). It is possible that lipid raft disruption in the VLCFA mutants causes the multiple eIF2B foci phenotype. Translation assays using the *ybr159wΔ* strain suggested the disruption of 2B bodies into multiple foci does not affect translation. The translation activity of yeast cells does not appear to be affected by the change from a single 2B body to multiple eIF2B foci.

Our work sheds light on the recently discovered 2B body. The data show a relationship between eIF2B localization and an ER membrane bound protein. We discovered the membrane co-localization of eIF2B while examining its interaction with YBR159W. Our data show that YBR159W is not necessary for the co-localization of eIF2B with the membrane. The primary mediator of the membrane association of eIF2B is unknown. It remains to be determined if the translation defect seen in the *ybr159wΔ* strain is the cause of the slow growth of the strain or vice versa. Further experiments are required to determine the functional role of YBR159W interacting with eIF2B.

Acknowledgements

CB was supported by NIH training grant T32 AI007611. PS and AL were supported by NIH grant GM64779**.** We thank Dr. Tom Dever, Dr. Allan Hinnebusch, Dr. Howard Riezman, and Dr. Jonathan Warner for reagents and yeast strains. Experiments, data analysis, and presentation of fluorescent microscope images were performed in part through the use of the VUMC Cell Imaging Shared Resource, which is supported by NIH grants CA68485, DK20593, DK58404, HD15052, DK59637.

Table 1. Strains used in this study

Strain	Source	Genotype
AL400	This study	*MATa, ura3, leu2, HIS$^+$*
AL401	This study	*MATa, ura3, leu2, HIS$^+$, YBR159W::KanR*
AL402	This study	*MATa, ura3, leu2, HIS$^+$, YBR159W::KanR, [YCp-YBR159W]*
AL403	This study	*MATa, ura3, leu2, HIS$^+$, YBR159W::KanR, GCD7-GFP*
AL404	This study	*MATa, ura3, leu2, HIS$^+$, YBR159W::KanR, GCD7-GFP, [YCp-YBR159W]*
AL405	This study	*MATa, leu2, ura3, met15, GCD1-GFP, [YCp-YBR159W-dsRed]*
AL406	This study	*MATa, leu2, ura3, met15, GCD6-GFP, [YCp-YBR159W-dsRed]*
AL407	This study	*MATa, leu2, ura3, met15, GCD7-GFP, [YCp-YBR159W-dsRed]*
AL408	This study	*MATalpha, trp1-901, leu2-3,112, ura3-52, his3-200, gal4Δ, gal80Δ, LYS2::GAL1-HIS3, GAL2-ADE2, met2::GAL7-lacZ, [YBR159W-GAL4DBD]*
AL409	This study	*MATalpha, trp1-901, leu2-3,112, ura3-52, his3-200, gal4Δ, gal80Δ, LYS2::GAL1-HIS3, GAL2-ADE2, met2::GAL7-lacZ, [GCD1-GAL4DBD]*
AL410	This study	*MATalpha, trp1-901, leu2-3,112, ura3-52, his3-200, gal4Δ, gal80Δ, LYS2::GAL1-HIS3, GAL2-ADE2, met2::GAL7-lacZ, [GCD2-GAL4DBD]*
AL411	This study	*MATalpha, trp1-901, leu2-3,112, ura3-52, his3-200, gal4Δ, gal80Δ, LYS2::GAL1-HIS3, GAL2-ADE2, met2::GAL7-lacZ, [GCD6-GAL4DBD]*
AL412	This study	*MATalpha, trp1-901, leu2-3,112, ura3-52, his3-200, gal4Δ, gal80Δ, LYS2::GAL1-HIS3, GAL2-ADE2, met2::GAL7-lacZ, [GCD7-GAL4DBD]*
AL413	This study	*MATa, leu2, ura3, met15, HIS$^+$, FEN1::KanR*
AL414	This study	*MATa, leu2, ura3, met15, HIS$^+$, SUR4::KanR*
AL415	This study	*MATa, ura3, leu2, HIS$^+$ [p180]*
AL416	This study	*MATa, ura3, leu2, HIS$^+$, YBR159W::KanR, [p180]*
AL417	This study	*MATa, ura3, leu2, HIS$^+$, YBR159W::KanR, [YCp-YBR159W], [p180]*
AL418	This study	*MATa, leu2, ura3, met15, FEN1::KanR, [p180]*
AL419	This study	*MATa, leu2, ura3, met15, SUR4::KanR, [p180]*
AL420	This study	*MATalpha, ura3-52, gcd1-101, [p180]*
AL421	This study	*MATalpha, ura3-52, trp1-63, leu2-3, leu2-112, GAL2$^+$, gcn2Δ, [p180]*
AL422	This study	*MATa, leu2, ura3, met15, FEN1-GFP, [YCp-YBR159W-dsRed]*
AL423	This study	*MATa, leu2, ura3, met15, DPM1-GFP, [YCp-YBR159W-dsRed]*
AL424	Deletion library	*MATa, leu2, ura3, met15, his3, GCN3::KanR*
AL425	GFP library	*MATa, leu2, ura3, met15, YBR159W-GFP*
AL426	GFP library	*MATa, leu2, ura3, met15, FEN1-GFP*
AL427	GFP library	*MATa, leu2, ura3, met15, GCD1-GFP*
AL428	GFP library	*MATa, leu2, ura3, met15, GCD6-GFP*
AL429	GFP library	*MATa, leu2, ura3, met15, GCD7-GFP*
AL430	TAP library	*MATa, leu2, ura3, met15, GCD2-TAP*
AL431	TAP library	*MATa, leu2, ura3, met15, GCD7-TAP*
AL432	TAP library	*MATa, leu2, ura3, met15, YBR159W-TAP*
AL433	TAP library	*MATa, leu2, ura3, met15, FEN1-TAP*
AL434	TAP library	*MATa, leu2, ura3, met15, SUR4-TAP*
AL435	TAP library	*MATa, leu2, ura3, met15, TSC13-TAP*
AL436	Deletion library	*MATa, leu2, ura3, met15, his3, FEN1::KanR*

AL436	GFP library	*MATa, leu2, ura3, met15, DPM1-GFP*
AL437	Deletion library	*MATa, leu2, ura3, met15, his3, SUR4::KanR*
F98	A. Hinnebusch	*MATalpha, ura3-52, gcd1-101*
H1511	A. Hinnebusch	*MATalpha, ura3-52, trp1-63, leu2-3, leu2-112, GAL2^{+}*
H2557	A. Hinnebusch	*MATalpha, ura3-52, trp1-63, leu2-3, leu2-112, GAL2^{+}, gcn2Δ*
pAD(GCD7)	Yeast Resource Center	*MATa, trp1-901, leu2-3,112, ura3-52, his3-200, gal4Δ, gal80Δ, LYS2::GAL1-HIS3, GAL2-ADE2, met2::GAL7-lacZ, [GCD7-AD]*
PJ69-4a	Yeast Resource Center	*MATa, trp1-901, leu2-3,112, ura3-52, his3-200, gal4Δ, gal80Δ, LYS2::GAL1-HIS3, GAL2-ADE2, met2::GAL7-lacZ*
PJ69-4alpha	Yeast Resource Center	*MATalpha, trp1-901, leu2-3,112, ura3-52, his3-200, gal4Δ, gal80Δ, LYS2::GAL1-HIS3, GAL2-ADE2, met2::GAL7-lacZ*
pOAD(GCD1)	Yeast Resource Center	*MATa, trp1-901, leu2-3,112, ura3-52, his3-200, gal4Δ, gal80Δ, LYS2::GAL1-HIS3, GAL2-ADE2, met2::GAL7-lacZ, [GCD1-AD]*
pOAD(GCD2)	Yeast Resource Center	*MATa, trp1-901, leu2-3,112, ura3-52, his3-200, gal4Δ, gal80Δ, LYS2::GAL1-HIS3, GAL2-ADE2, met2::GAL7-lacZ, [GCD2-AD]*
pOAD(GCD6)	Yeast Resource Center	*MATa, trp1-901, leu2-3,112, ura3-52, his3-200, gal4Δ, gal80Δ, LYS2::GAL1-HIS3, GAL2-ADE2, met2::GAL7-lacZ, [GCD6-AD]*
pOAD(GCN3)	Yeast Resource Center	*MATa, trp1-901, leu2-3,112, ura3-52, his3-200, gal4Δ, gal80Δ, LYS2::GAL1-HIS3, GAL2-ADE2, met2::GAL7-lacZ, [GCN3-AD]*
pOAD(SUI2)	Yeast Resource Center	*MATa, trp1-901, leu2-3,112, ura3-52, his3-200, gal4Δ, gal80Δ, LYS2::GAL1-HIS3, GAL2-ADE2, met2::GAL7-lacZ, [SUI2-AD]*
pOAD(TDH1)	Yeast Resource Center	*MATa, trp1-901, leu2-3,112, ura3-52, his3-200, gal4Δ, gal80Δ, LYS2::GAL1-HIS3, GAL2-ADE2, met2::GAL7-lacZ, [TDH1-AD]*
pOAD(YBR159W)	Yeast Resource Center	*MATa, trp1-901, leu2-3,112, ura3-52, his3-200, gal4Δ, gal80Δ, LYS2::GAL1-HIS3, GAL2-ADE2, met2::GAL7-lacZ, [YBR159W-AD]*
RH5994	H. Riezman	*MATalpha, leu2, ura3, trp1, bar1, LIP1::HIS3*

Table 2. Plasmids used in this study.

Name	backbone	Source	Notes
pOBD2	pOBD2	Yeast Resource Center	ampR, TRP1, CEN4 ORI, GAL4-DBD
YCp-YBR159W	pAG415GAL-ccdB	This study	ampR, LEU2, CEN ORI, YBR159W 5' UTR-YBR159W
YCp-YBR159W-dsRed	pAG415GPD-ccdB-dsRed	This study	ampR, LEU2, CEN ORI, P_{GPD}-YBR159W-dsRed
p180	YCp50	A. Hinnebusch	ampR, URA3, CEN ORI, GCN4 5' UTR-LacZ
pFa6a-kanmx6	pFa6a-kanmx6	Addgene	ampR, KanR2
pENTR	pENTR	Invitrogen	KanR
pENTR-YBR159W 5' UTR-YBR159W	pENTR	this study	KanR, YBR159W 5' UTR-YBR159W
pENTR-YBR159W	pENTR	this study	KanR, YBR159W
pAG415GAL-ccdB	pAG415GAL-ccdB	Addgene	ampR, LEU2, CEN ORI ccdB
pAG415GPD-ccdB-dsRed	pAG415GPD-ccdB-dsRed	Addgene	ampR, LEU2, CEN ORI ccdB-dsRed

Table 3. Primers used in this study.

Genomic YBR159W Deletion primers	Primer Sequence (5'-3')
for del primer	CGTACGCTGCAGGTCGAC
rev del primer	ATCGATGAATTCGAGCTCG
for 5' extension	CGGATTTGGAAGTCCTTTATAG
rev 5' extension	GTCGACCTGCAGCGTACGCATTTCTTAAGCTGCACCG
for 3' extension	CGAGCTCGAATTCATCGATTAGAATTATCGTTCTCG
rev 3' extension	GGACTTGGTCCTTCCACC
Yeast 2-Hybrid primers	
for common primer	CTATCTATTCGATGATGAAGATACCCCACCAAACCCAAAAAAAGAGATCGAATT CCAGCTGACCACCATG
rev common primer	GTACCGTTAAGGGCCCCTAGGCAGCTGGACGTCTCTAGATACTTAGCATCTATGA CTTTTTGGGGCGTTC
for YBR159W	AATTCCAGCTGACCACCATGACTTTTATGCAACAGCTTCAAGAGGCTGG
rev YBR159W	GATCCCCGGGAATTGCCATGCTATTCCTTTTTAACCTGTCTTGCGGCTTTTTTTAAGG
for GCD1	AATTCCAGCTGACCACCATGTCAATTCAGGCTTTTGTCTTTTGCGGTAAAGG
rev GCD1	GATCCCCGGGAATTGCCATGTTAACGCTCAAATAATCCGTCATCTTCGTACTCGTAC
for GCD2	AATTCCAGCTGACCACCATGAGCGAATCGGAAGCCAAATCTAGGTCG
rev GCD2	GATCCCCGGGAATTGCCATGTTATGCGGAACCTTTGTACTCTCTTAAAATAACAGGGAC
for GCD6	AATTCCAGCTGACCACCATGGCTGGAAAAAAGGGACAAAAGAAAAGTGGACTAG
rev GCD6	GATCCCCGGGAATTGCCATGTTATTCCTCTTCTGAGGAAGATTCTTCGTCAGCATTC
for GCD7	AATTCCAGCTGACCACCATGTCCTCTCAAGCATTCACTTCAGTACATCCG
rev GCD7	GATCCCCGGGAATTGCCATGTCACGCCTTATTTTTATCCAAATGCACATCAATTTGC
YBR159W ORF + 600 bp upstream primers	
for primer	CACCATGGTTTTTGTGACTTTACCTATAAATAGTACACAAC
rev primer	CTATTCCTTTTTAACCTGTCTTGCGGCTTTTTTTAAGGC
prom remove 1	GGGAGCTCCATACTGATTAGTACACTAGTGG
prom remove 2	CCACTAGTGTACTAATCAGTATGGAGCTCCC

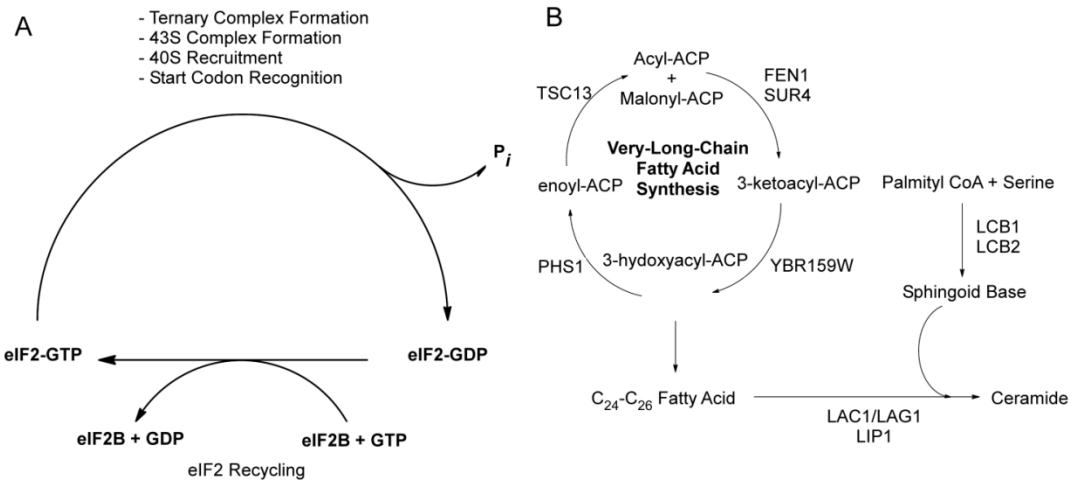

Figure 1. eIF2B and the VLCFA functional pathways. (A) Diagram showing the GEF pathway of eIF2B that is required for recharging eIF2 with GTP to begin a new round of translation initiation. (B) Diagram showing the cyclical VLCFA elongase pathway and the genes required for the catalytic steps. Also depicted is the pathway utilizing VLCFAs by the ceramide synthase complex LAC1/LAG1 and LIP1 to make ceramide. Ceramide is later modified to generate various sphingolipids.

A

Gene	TAP-GCD2	TAP-YBR159W	TAP-FEN1	TAP-SUR4	TAP-TSC13
GCD1	10(28.72)	10(23.49)	-	-	-
GCD2	7(20.58)	10(21.47)	-	-	-
GCN3	7(47.54)	4(17.97)	-	-	-
GCD6	13(30.34)	16(30.58)	-	-	-
GCD7	8(34.91)	6(21.47)	-	-	-
YBR159W	6(23.92)	10(27.59)	-	-	-
FEN1	-	-	2(6.63)	-	-
SUR4	-	-	-	2(5.20)	1(5.49)
TSC13	-	1(2.89)	-	1(3.22)	2(5.79)

B

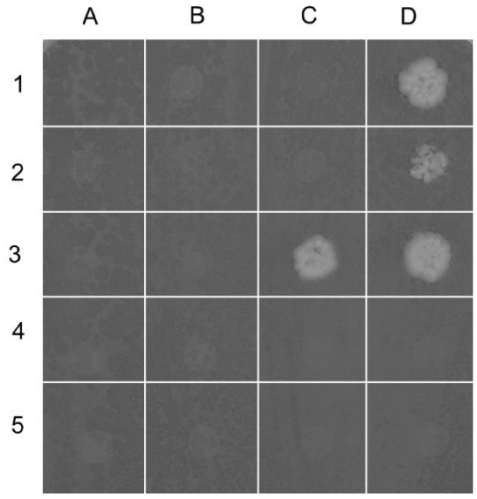

	A	B	C	D
1	YBR : GCD1	YBR : GCD2	YBR : GCD6	YBR : GCD7
2	GCD1 : YBR	GCD2 : YBR	GCN3 : YBR	GCD6 : YBR
3	GCD7 : YBR	GCD6 : GCD1	GCD6 : GCD7	GCD1 : GCD7
4	GCD1 : GCD6	GCD2 : GCD6	GCN3 : GCD6	GCD7 : GCD6
5	SUI2 : GCD1	SUI2 : YBR	TDH1 : GCD1	TDH1 : YBR

KEY
BAIT : PREY
YBR = YBR159W
Positive interaction

Figure 2. YBR159W's interaction with eIF2B is unique among VLCFA genes. (A) Mass spectrometry analysis of the affinity-purified TAP-GCD2, TAP-YBR159W, and other TAP-tagged VLCFA protein complexes. Listed are unique peptide identifications with the percent coverage of identified peptides in the protein in parentheses. A "-" indicates no peptides were detected for the gene. (B) Yeast 2-hybrid (Y2H) analysis of interactions between YBR159W and eIF2B subunits GCD6 and GCD7. Shown is both the assay plate used for scoring the Y2H interactions and a table of the interactions tested at each spot. Shading on the table corresponds to a positive interaction on the plate.

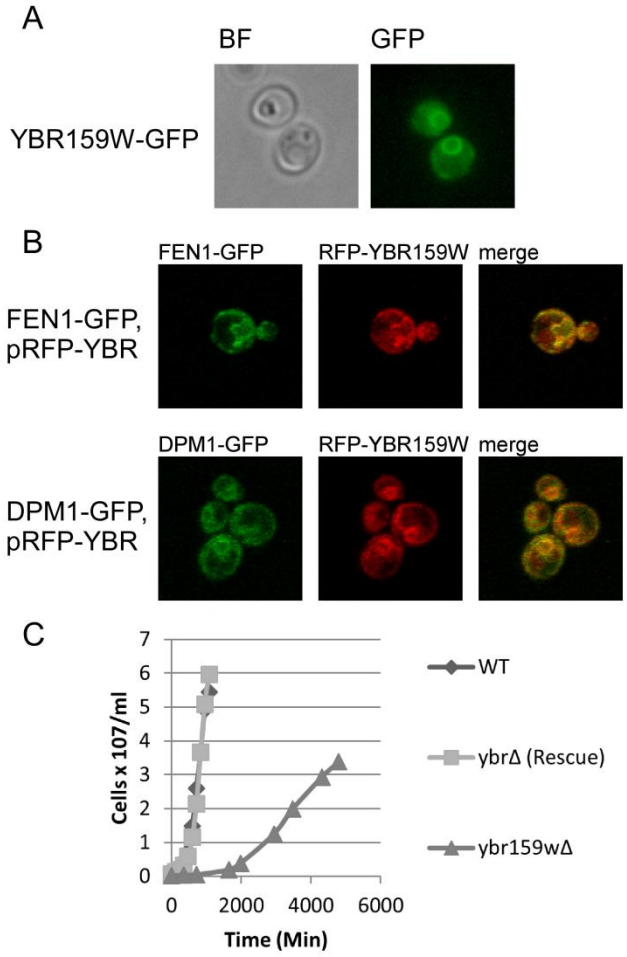

Figure 3. Cellular analysis of YBR159W. (A) Live cell epifluorescence imaging of endogenously tagged YBR159W-GFP indicates YBR159W localizes mainly to the ER membrane. (B) Live cell confocal microscopy showing the co-localization of YBR159W with the VLCFA pathway enzyme FEN1 and ER membrane protein DPM1. YBR159W is expressed on a low-copy plasmid and tagged with dsRed. FEN1 and DPM1 are endogenously expressed and tagged with GFP. (C) Deletion of YBR159W results in a very slow growth rate.

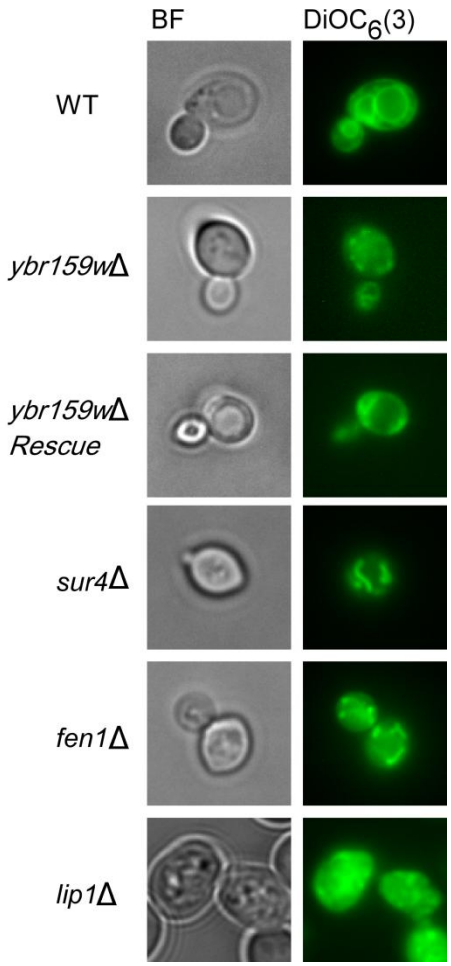

Figure 4. Null mutations of genes in the VLCFA pathway disrupt lipid membranes. The lipophilic dye $DiOC_6(3)$ was used to label membranes in live yeast cells. Dye was applied to cells in suspension 10 min before plating on a microscope slide and imaging. Included are the VLCFA and ceramide synthase mutants *fen1Δ, sur4Δ*, and *lip1Δ* as controls. 100% of these mutants showed abnormal membranes (N=246) versus 1.1% for WT (N=89) and 9.7% for the rescue (N=93).

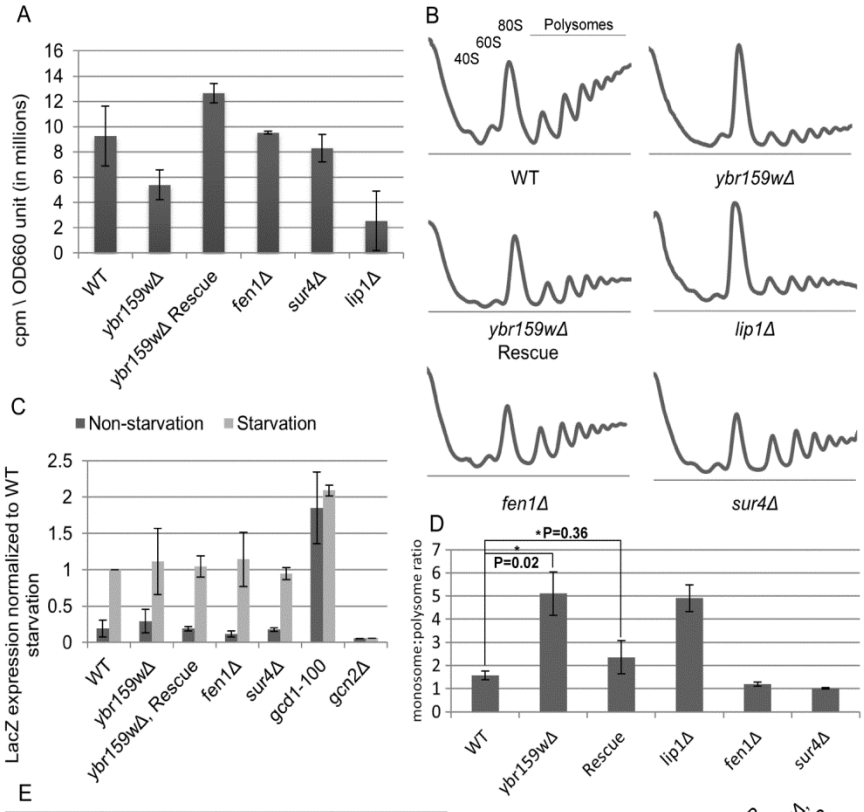

Gene	*ybr159wΔ*	GCD7-GFP	GCD7-GFP, *ybr159wΔ*
YBR159W	-	15(47.55)	-
GCD1	-	33(60.21)	13(33.39)
GCD2	-	30(36.41)	10(25.96)
GCN3	-	13(58.36)	8(50.49)
GCD6	-	34(54.63)	16(30.76)
GCD7	-	21(55.12)	11(38.58)

Figure 5. Translation assays on the *ybr159wΔ* strain. (A) Translation efficiency as measured by ^{35}S-methionine incorporation. Values are counts per minute per OD_{660} unit of cells. Results shown are from at least three replicates. (B) Polysome profiling of *ybr159wΔ* and other VLCFA null strains. At least three replicates were performed for each strain. Though the example *ybr159wΔ* plot does not show a 40S ribosome peak, all other replicates of the strain showed a 40S peak similar to WT. (C) Assay for GCN4 pathway competence by GCN4-LacZ induction. Results are LacZ expression per mg of protein per min normalized to the WT starvation condition. Starvation conditions were induced by 100 mM 3-AT in synthetic complete minus histidine media for 4 h. The gcd1-100 strain has a constitutively derepressed GCN4 pathway and constant GCN4 protein translation while the *gcn2Δ* strain is incapable of derepression of GCN4 and cannot produce significant amounts of GCN4 protein. (D) Ratio of monosome:polysome peak areas for the polysome profiles. P values were generated using a Student's *t*-test from at least 3 individual replicates. (E) GFP pull-down of eIF2B complexes in a *ybr159wΔ* background. Following pull-down LC-MS/MS was performed to identify the proteins. An untagged *ybr159wΔ* strain and GCD7-GFP tagged strain were used as controls. Displayed are unique peptide hits and percentage coverage as described in Figure 2A. (F) Western blot analysis of WT, *ybr159wΔ*, and GFP-GCD7 strains. Yeast strains in Fig. 5D and WT strain AL400 were used. Equivalent

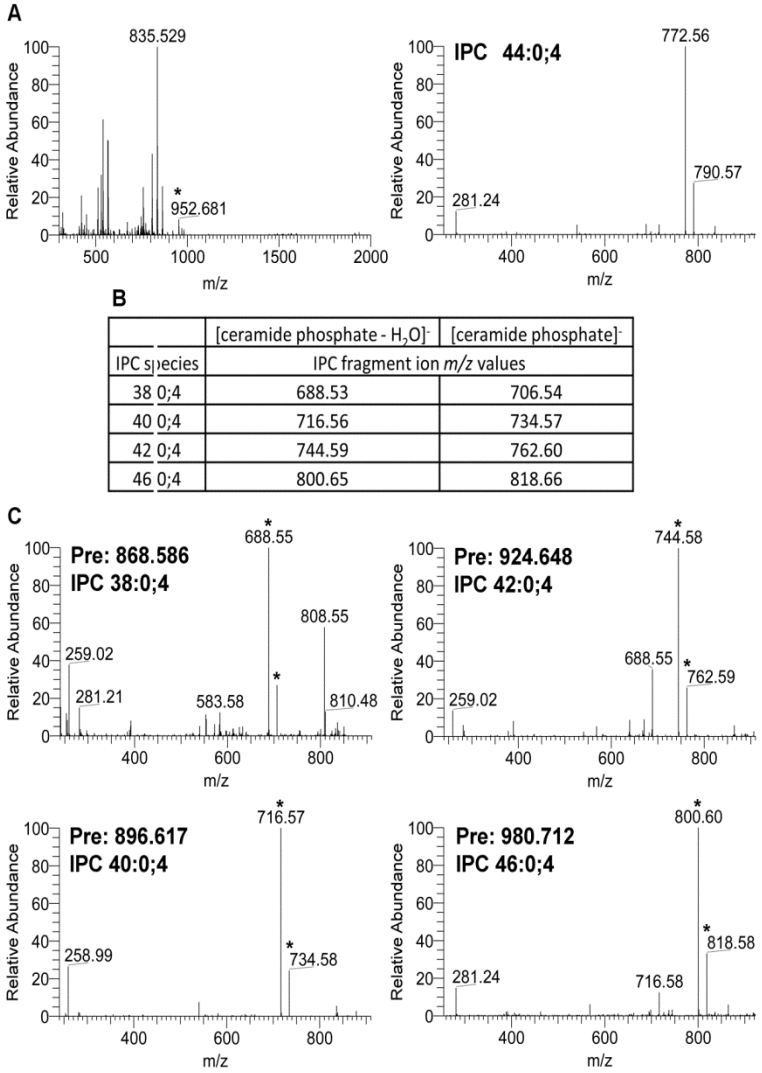

	[ceramide phosphate - H_2O]$^-$	[ceramide phosphate]$^-$
IPC species	IPC fragment ion *m/z* values	
38 0;4	688.53	706.54
40 0;4	716.56	734.57
42 0;4	744.59	762.60
46 0;4	800.65	818.66

Figure 6. Validation and Identification of IPCs. (A) Mass spectrometry precursor and MS/MS fragmentation spectrum for IPC 44:0;4 from WT yeast. The observed precursor ion *m/z* 952.681 represents the expected ion IPC 44:0;4 (952.686). The observed *m/z* 835.529 corresponds to the phosphotidyl inositols PI 16:0-18:1 and PI 16:1-18:0 used to normalize the relative abundance of each IPC species. In the lower MS/MS spectra of the 952.681 precursor ion, the first and second most abundant peaks correspond to the expected IPC 44:0;4 fragment ions [Ceramide Phosphate – H_2O]$^-$, *m/z* 772.62 and [Ceramide Phosphate]$^-$, *m/z* 790.63. (B) Theoretical fragmentation database for IPCs 38:0;4, 40:0;4, 42:0;4, and 46:0;4. Shown are the theoretical *m/z* values for fragment ions [ceramide phosphate – H_2O]$^-$ and [ceramide phosphate]$^-$ for IPCs 38:0;4, 40:0;4, 42:0;4, and 46:0;4. (C) MS/MS fragmentation spectra for IPCs 38:0;4, 40:0;4, 42:0;4, and 46:0;4. The observed precursor *m/z* values "Pre" of 868.586, 896.617, 924.648, and 980.712 correspond to the expected *m/z* values of IPC 38:0;4 (868.592), IPC 40:0;4 (896.623), IPC 42:0;4 (924.655), and IPC 46:0;4 (980.717) respectively. In the MS/MS spectra, the peaks corresponding to the expected theoretical IPC fragment ions [Ceramide Phosphate – H_2O]$^-$ and [Ceramide Phosphate]$^-$ are mark with a "*". In each case, the peak corresponding to the expected [Ceramide Phosphate – H_2O]$^-$ fragment ion was the most intense ion in the MS/MS spectrum.

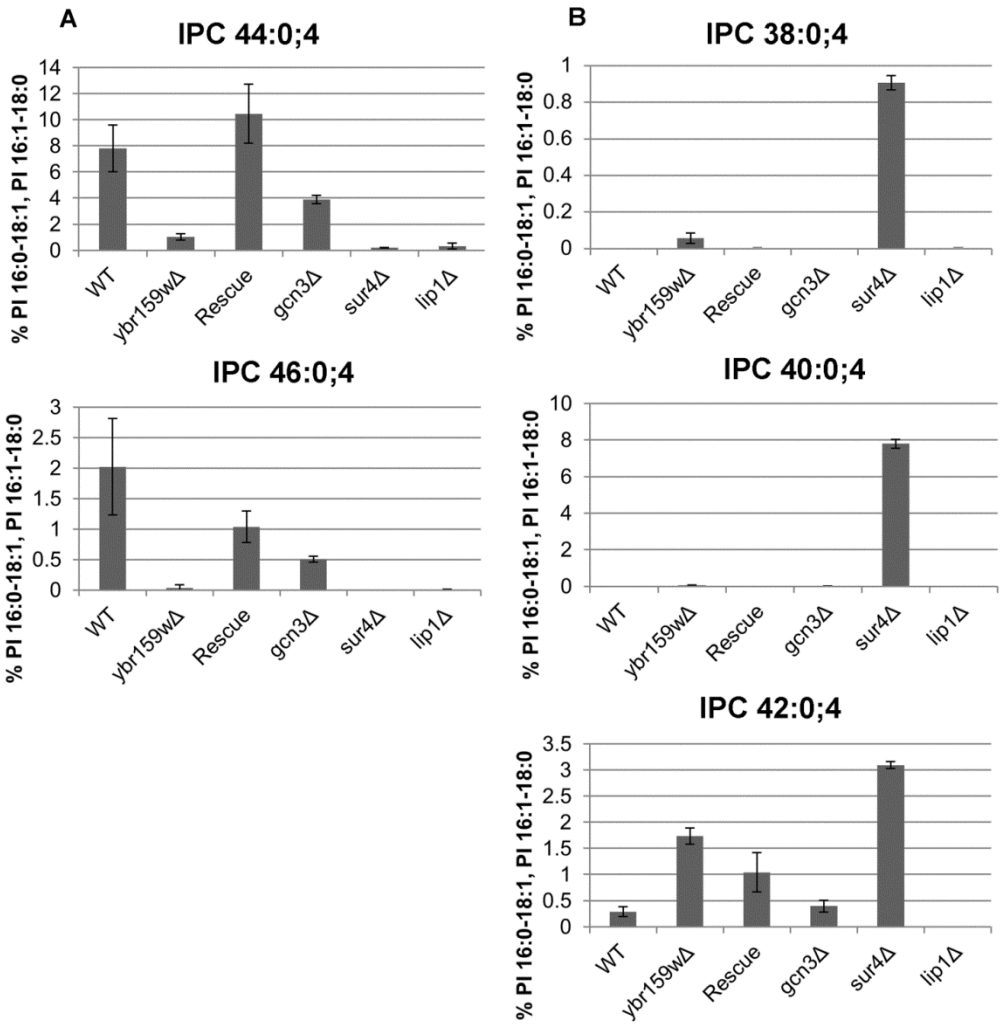

Figure 7. Fatty Acid profiling of WT and mutant yeast strains. (A) Longer-chain fatty acid-containing sphingolipid species. IPC species with 44 and 46 carbon-long acyl chains are shown. The VLCFA and ceramide synthase mutants *sur4Δ* and *lip1Δ* are included as controls. (B) Shorter-chain fatty acid-containing sphingolipid species. Three IPC species with 38, 40, and 42 carbon-containing acyl chains are shown. For both A and B, data represents percentage of signal of each lipid species normalized to the signal of the PI 16:0-18:1 and PI 16:1-18:0 ion.

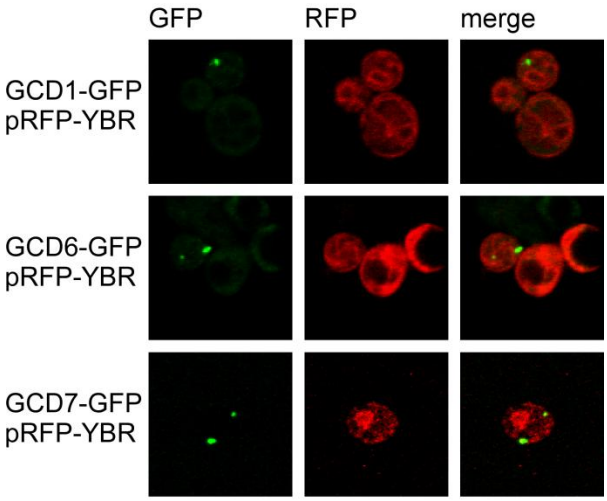

Figure 8. eIF2B and YBR159W localization in live cells. Confocal microscopy of live yeast cells showing localization of eIF2B subunits in relation to the localization of YBR159W. eIF2B subunits are endogenously tagged with GFP while YBR159W-RFP is expressed on a centromeric plasmid.

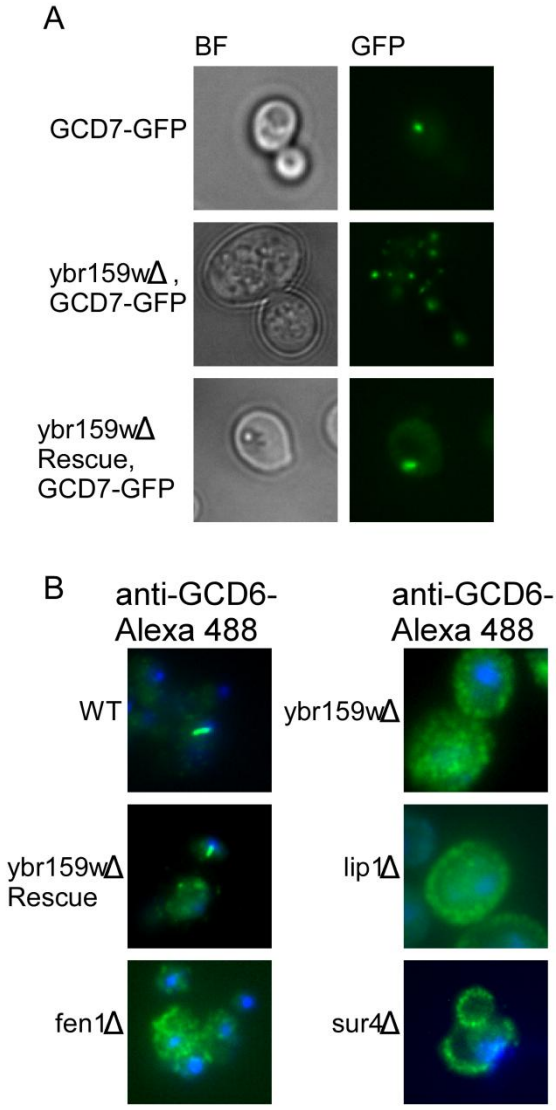

Figure 9. eIF2B localization in the *ybr159wΔ* background. (A) Live cell fluorescence microscopy of endogenously tagged eIF2B subunit GCD7-GFP. Brightfield (BF) images are included for clarity. (B) Immunofluorescence microscopy of formaldehyde fixed yeast cells. A polyclonal antibody against yeast eIF2B subunit GCD6 was used along with an Alexa Fluor 488 tagged secondary. Nuclei are stained with DAPI for clarity.

A

Strain	Cell #	Single 2B body (%)	Multi-Foci (%)	No Foci (%)
WT	173	50.9	0.0	49.1
*ybr159w*Δ	122	3.3	71.3	24.6
Rescue	72	44.4	0.0	55.6

B

Strain	Cell #	Single 2B body (%)	Multi-Foci (%)	No Foci (%)
WT	105	63.8	7.6	28.6
*ybr159w*Δ	59	1.7	83.1	15.3
Rescue	111	35.1	15.3	49.5
*lip1*Δ	29	6.9	93.1	0.0
*fen1*Δ	96	4.2	63.5	32.3
*sur4*Δ	122	1.6	58.2	40.2

Table 4. Statistics for eIF2B localization phenotypes. (A) Statistics of eIF2B localization phenotypes in live yeast cells. The strains are described in Fig 8A. (B) Statistics of eIF2B localization phenotypes via immunofluorescence of fixed yeast cells. The strains are described in Fig 8B.

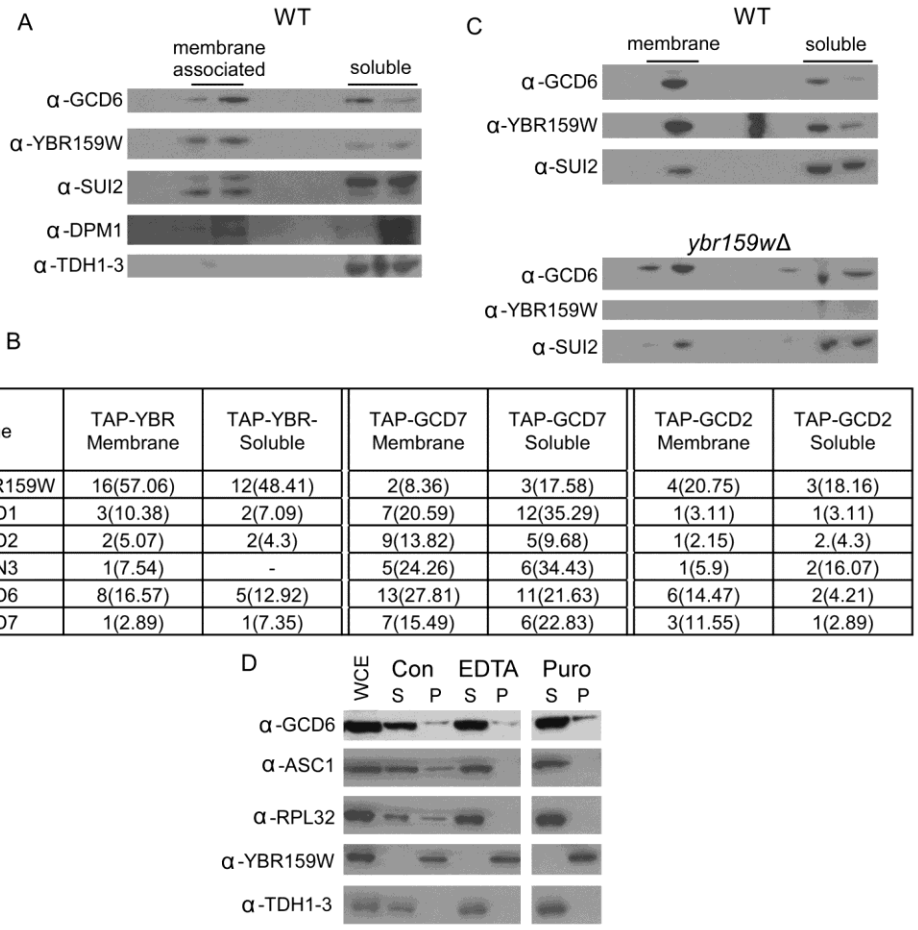

Gene	TAP-YBR Membrane	TAP-YBR-Soluble	TAP-GCD7 Membrane	TAP-GCD7 Soluble	TAP-GCD2 Membrane	TAP-GCD2 Soluble
YBR159W	16(57.06)	12(48.41)	2(8.36)	3(17.58)	4(20.75)	3(18.16)
GCD1	3(10.38)	2(7.09)	7(20.59)	12(35.29)	1(3.11)	1(3.11)
GCD2	2(5.07)	2(4.3)	9(13.82)	5(9.68)	1(2.15)	2.(4.3)
GCN3	1(7.54)	-	5(24.26)	6(34.43)	1(5.9)	2(16.07)
GCD6	8(16.57)	5(12.92)	13(27.81)	11(21.63)	6(14.47)	2(4.21)
GCD7	1(2.89)	1(7.35)	7(15.49)	6(22.83)	3(11.55)	1(2.89)

Figure 10. eIF2B and YBR159W localization using membrane floatation assays. (A) Western blot of membrane floatation assay fractions using protein extracts from WT yeast showing the localization of the eIF2B subunit GCD6 and YBR159W. Controls include the eIF2 subunit SUI2, ER integral membrane protein DPM1, and the cytosolic protein GAPDH. TDH1-3 are the three GAPDH genes in yeast. The lanes represent 20% of fractions from the membrane floatation gradients. Labels show the location of the membrane-associated and soluble protein fractions. (B) Mass spectrometry analysis of affinity purified TAP complexes from the membrane and soluble fractions of membrane floatation experiments. Unique peptides, percent coverage and "-" are described in Fig 2A. (C) Western blot of membrane floatation assay fractions comparing WT and *ybr159wΔ* strains. Conditions are the same as in "A". (D) Western blot of crude fractionation following EDTA or puromycin treatment. Abbreviations are WCE = whole cell extract, Con = non-treated control, EDTA = EDTA treatment, Puro = puromycin treatment, S = supernatant, P = pellet. ASC1 is a component of the small ribosomal subunit and RPL32 is a large ribosomal subunit protein. Lanes represent 15 µL of WCE following fractionation, pellets were resuspended in starting volume.

REFERENCES

Abraham, S., I. L. Chaikoff, et al. (1961). "Particle involvement in fatty acid synthesis in liver and yeast systems." Nature **192**: 1287-1288.

Adelman, M. R., D. D. Sabatini, et al. (1973). "Ribosome-membrane interaction. Nondestructive disassembly of rat liver rough microsomes into ribosomal and membranous components." J Cell Biol **56**(1): 206-229.

Agirrezabala, X. and J. Frank (2009). "Elongation in translation as a dynamic interaction among the ribosome, tRNA, and elongation factors EF-G and EF-Tu." Q Rev Biophys **42**(3): 159-200.

Alberti, S., A. D. Gitler, et al. (2007). "A suite of Gateway cloning vectors for high-throughput genetic analysis in Saccharomyces cerevisiae." Yeast **24**(10): 913-919.

Asano, K., T. Krishnamoorthy, et al. (1999). "Conserved bipartite motifs in yeast eIF5 and eIF2Bepsilon, GTPase-activating and GDP-GTP exchange factors in translation initiation, mediate binding to their common substrate eIF2." EMBO J **18**(6): 1673-1688.

Asano, K., L. Phan, et al. (2001). "A multifactor complex of eIF1, eIF2, eIF3, eIF5, and tRNA(i)Met promotes initiation complex assembly and couples GTP hydrolysis to AUG recognition." Cold Spring Harb Symp Quant Biol **66**: 403-415.

Asano, K., A. Shalev, et al. (2001). "Multiple roles for the C-terminal domain of eIF5 in translation initiation complex assembly and GTPase activation." EMBO J **20**(9): 2326-2337.

Ashe, M. P., J. W. Slaven, et al. (2001). "A novel eIF2B-dependent mechanism of translational control in yeast as a response to fusel alcohols." EMBO J **20**(22): 6464-6474.

Athenstaedt, K. and G. Daum (2000). "1-Acyldihydroxyacetone-phosphate reductase (Ayr1p) of the yeast Saccharomyces cerevisiae encoded by the open reading frame YIL124w is a major component of lipid particles." J Biol Chem **275**(1): 235-240.

Audet-Walsh, E., J. Bellemare, et al. (2012). "The impact of germline genetic variations in hydroxysteroid (17-beta) dehydrogenases on prostate cancer outcomes after prostatectomy." Eur Urol **62**(1): 88-96.

Barker, H. A., M. D. Kamen, et al. (1945). "The Synthesis of Butyric and Caproic Acids from Ethanol and Acetic Acid by Clostridium Kluyveri." Proc Natl Acad Sci U S A **31**(12): 373-381.

Barrett, T., D. B. Troup, et al. (2011). "NCBI GEO: archive for functional genomics data sets--10 years on." Nucleic Acids Res **39**(Database issue): D1005-1010.

Beaudoin, F., K. Gable, et al. (2002). "A Saccharomyces cerevisiae gene required for heterologous fatty acid elongase activity encodes a microsomal beta-keto-reductase." J Biol Chem **277**(13): 11481-11488.

Bedia, C., T. Levade, et al. (2011). "Regulation of autophagy by sphingolipids." Anticancer Agents Med Chem **11**(9): 844-853.

Belfield, G. P. and M. F. Tuite (1993). "Translation elongation factor 3: a fungus-specific translation factor?" Mol Microbiol **9**(3): 411-418.

Bergmann, J. E. and P. J. Fusco (1988). "The M protein of vesicular stomatitis virus associates specifically with the basolateral membranes of polarized epithelial cells independently of the G protein." J Cell Biol **107**(5): 1707-1715.

Bijlmakers, M. J. and M. Marsh (2003). "The on-off story of protein palmitoylation." Trends Cell Biol **13**(1): 32-42.

Boesen, T., S. S. Mohammad, et al. (2004). "Structure of the catalytic fragment of translation initiation factor 2B and identification of a critically important catalytic residue." J Biol Chem **279**(11): 10584-10592.

Boutin, J. A. (1997). "Myristoylation." Cell Signal **9**(1): 15-35.

Breslow, D. K., D. M. Cameron, et al. (2008). "A comprehensive strategy enabling high-resolution functional analysis of the yeast genome." Nat Methods **5**(8): 711-718.

Browne, C. M., P. Samir, et al. (2012). "The yeast eIF2B translation initiation complex interacts with the fatty acid synthesis enzyme YBR159W and ER membranes." Mol Cell Biol.

Buchan, J. R. and R. Parker (2009). "Eukaryotic stress granules: the ins and outs of translation." Mol Cell **36**(6): 932-941.

Bugiani, M., I. Boor, et al. (2010). "Leukoencephalopathy with vanishing white matter: a review." J Neuropathol Exp Neurol **69**(10): 987-996.

Bushman, J. L., A. I. Asuru, et al. (1993). "Evidence that GCD6 and GCD7, translational regulators of GCN4, are subunits of the guanine nucleotide exchange factor for eIF-2 in Saccharomyces cerevisiae." Mol Cell Biol **13**(3): 1920-1932.

Bushman, J. L., M. Foiani, et al. (1993). "Guanine nucleotide exchange factor for eukaryotic translation initiation factor 2 in Saccharomyces cerevisiae: interactions between the essential subunits GCD2, GCD6, and GCD7 and the regulatory subunit GCN3." Mol Cell Biol **13**(8): 4618-4631.

Calder, P. C. and P. Yaqoob (2009). "Omega-3 polyunsaturated fatty acids and human health outcomes." Biofactors **35**(3): 266-272.

Campbell, S. G. and M. P. Ashe (2006). "Localization of the translational guanine nucleotide exchange factor eIF2B: a common theme for GEFs?" Cell Cycle **5**(7): 678-680.

Campbell, S. G., N. P. Hoyle, et al. (2005). "Dynamic cycling of eIF2 through a large eIF2B-containing cytoplasmic body: implications for translation control." J Cell Biol **170**(6): 925-934.

Cassagne, C., D. Darriet, et al. (1978). "Biosynthesis of very long chain fatty acids by the sciatic nerve of the rabbit." FEBS Lett **90**(2): 336-340.

Cassagne, C., R. Lessire, et al. (1994). "Biosynthesis of very long chain fatty acids in higher plants." Prog Lipid Res **33**(1-2): 55-69.

Cerantola, V., C. Vionnet, et al. (2007). "Yeast sphingolipids do not need to contain very long chain fatty acids." Biochem J **401**(1): 205-216.

Chen, C. Y. and P. Sarnow (1995). "Initiation of protein synthesis by the eukaryotic translational apparatus on circular RNAs." Science **268**(5209): 415-417.

Cigan, A. M., J. L. Bushman, et al. (1993). "A protein complex of translational regulators of GCN4 mRNA is the guanine nucleotide-exchange factor for translation initiation factor 2 in yeast." Proc Natl Acad Sci U S A **90**(11): 5350-5354.

Claude, A. (1937). "Preparation of an Active Agent from Inactive Tumor Extracts." Science **85**(2203): 294-295.

Claude, A. (1938). "Concentration and Purification of Chicken Tumor I Agent." Science **87**(2264): 467-468.

Claude, A. (1940). "Particulate Components of Normal and Tumor Cells." Science **91**(2351): 77-78.

Clemens, M. J. (2001). "Initiation factor eIF2 alpha phosphorylation in stress responses and apoptosis." Prog Mol Subcell Biol **27**: 57-89.

Cox, J. S., C. E. Shamu, et al. (1993). "Transcriptional induction of genes encoding endoplasmic reticulum resident proteins requires a transmembrane protein kinase." Cell **73**(6): 1197-1206.

Das, S. and U. Maitra (2001). "Functional significance and mechanism of eIF5-promoted GTP hydrolysis in eukaryotic translation initiation." Prog Nucleic Acid Res Mol Biol **70**: 207-231.

David C. Amberg, D. J. B., Jeffrey N. Strathern (2005). Methods in Yeast Genetics. Cold Spring Harbor, Cold Spring Harbor Laboratory Press.

de Haro, C., R. Mendez, et al. (1996). "The eIF-2alpha kinases and the control of protein synthesis." FASEB J **10**(12): 1378-1387.

Denic, V. and J. S. Weissman (2007). "A molecular caliper mechanism for determining very long-chain fatty acid length." Cell **130**(4): 663-677.

Dever, T. E., A. Roll-Mecak, et al. (2001). "Universal translation initiation factor IF2/eIF5B." Cold Spring Harb Symp Quant Biol **66**: 417-424.

Dholakia, J. N., T. C. Mueser, et al. (1986). "The association of NADPH with the guanine nucleotide exchange factor from rabbit reticulocytes: a role of pyridine dinucleotides in eukaryotic polypeptide chain initiation." Proc Natl Acad Sci U S A **83**(18): 6746-6750.

Dickson, R. C. (2008). "Thematic review series: sphingolipids. New insights into sphingolipid metabolism and function in budding yeast." J Lipid Res **49**(5): 909-921.

Dickson, R. C., C. Sumanasekera, et al. (2006). "Functions and metabolism of sphingolipids in Saccharomyces cerevisiae." Prog Lipid Res **45**(6): 447-465.

Dietrich, L. E. and C. Ungermann (2004). "On the mechanism of protein palmitoylation." EMBO Rep **5**(11): 1053-1057.

Dittrich, F., D. Zajonc, et al. (1998). "Fatty acid elongation in yeast--biochemical characteristics of the enzyme system and isolation of elongation-defective mutants." Eur J Biochem **252**(3): 477-485.

Drisdel, R. C. and W. N. Green (2004). "Labeling and quantifying sites of protein palmitoylation." Biotechniques **36**(2): 276-285.

Ejsing, C. S., T. Moehring, et al. (2006). "Collision-induced dissociation pathways of yeast sphingolipids and their molecular profiling in total lipid extracts: a study by quadrupole TOF and linear ion trap-orbitrap mass spectrometry." J Mass Spectrom **41**(3): 372-389.

Ejsing, C. S., J. L. Sampaio, et al. (2009). "Global analysis of the yeast lipidome by quantitative shotgun mass spectrometry." Proc Natl Acad Sci U S A **106**(7): 2136-2141.

English, D. (1996). "Phosphatidic acid: a lipid messenger involved in intracellular and extracellular signalling." Cell Signal **8**(5): 341-347.

Epstein, S., C. L. Kirkpatrick, et al. (2012). "Activation of the unfolded protein response pathway causes ceramide accumulation in yeast and INS-1E insulinoma cells." J Lipid Res **53**(3): 412-420.

Fabian, J. R., S. R. Kimball, et al. (1997). "Subunit assembly and guanine nucleotide exchange activity of eukaryotic initiation factor-2B expressed in Sf9 cells." J Biol Chem **272**(19): 12359-12365.

Fendt, S. M., A. P. Oliveira, et al. (2010). "Unraveling condition-dependent networks of transcription factors that control metabolic pathway activity in yeast." Mol Syst Biol **6**: 432.

Fields, S. and O. Song (1989). "A novel genetic system to detect protein-protein interactions." Nature **340**(6230): 245-246.

Gable, K., G. Han, et al. (2002). "Mutations in the yeast LCB1 and LCB2 genes, including those corresponding to the hereditary sensory neuropathy type I mutations, dominantly inactivate serine palmitoyltransferase." J Biol Chem **277**(12): 10194-10200.

Gaigg, B., A. Toulmay, et al. (2006). "Very long-chain fatty acid-containing lipids rather than sphingolipids per se are required for raft association and stable surface transport of newly synthesized plasma membrane ATPase in yeast." J Biol Chem **281**(45): 34135-34145.

Gavin, A. C., M. Bosche, et al. (2002). "Functional organization of the yeast proteome by systematic analysis of protein complexes." Nature **415**(6868): 141-147.

Gerbasi, V. R., C. M. Weaver, et al. (2004). "Yeast Asc1p and mammalian RACK1 are functionally orthologous core 40S ribosomal proteins that repress gene expression." Mol Cell Biol **24**(18): 8276-8287.

Ghaemmaghami, S., W. K. Huh, et al. (2003). "Global analysis of protein expression in yeast." Nature **425**(6959): 737-741.

Giaever, G., A. M. Chu, et al. (2002). "Functional profiling of the Saccharomyces cerevisiae genome." Nature **418**(6896): 387-391.

Gingras, A. C., B. Raught, et al. (1999). "eIF4 initiation factors: effectors of mRNA recruitment to ribosomes and regulators of translation." Annu Rev Biochem **68**: 913-963.

Glover, E. I., B. R. Oates, et al. (2008). "Resistance exercise decreases eIF2Bepsilon phosphorylation and potentiates the feeding-induced stimulation of p70S6K1 and rpS6 in young men." Am J Physiol Regul Integr Comp Physiol **295**(2): R604-610.

Gomez, E., S. S. Mohammad, et al. (2002). "Characterization of the minimal catalytic domain within eIF2B: the guanine-nucleotide exchange factor for translation initiation." EMBO J **21**(19): 5292-5301.

Gomez, E. and G. D. Pavitt (2000). "Identification of domains and residues within the epsilon subunit of eukaryotic translation initiation factor 2B (eIF2Bepsilon) required for guanine nucleotide exchange reveals a novel activation function promoted by eIF2B complex formation." Mol Cell Biol **20**(11): 3965-3976.

Gongadze, G. M. (2011). "5S rRNA and ribosome." Biochemistry (Mosc) **76**(13): 1450-1464.

Grant, C. M. and A. G. Hinnebusch (1994). "Effect of sequence context at stop codons on efficiency of reinitiation in GCN4 translational control." Mol Cell Biol **14**(1): 606-618.

Han, G., K. Gable, et al. (2002). "The Saccharomyces cerevisiae YBR159w gene encodes the 3-ketoreductase of the microsomal fatty acid elongase." J Biol Chem **277**(38): 35440-35449.

Hannig, E. M. and A. G. Hinnebusch (1988). "Molecular analysis of GCN3, a translational activator of GCN4: evidence for posttranslational control of GCN3 regulatory function." Mol Cell Biol **8**(11): 4808-4820.

Hannun, Y. A. and R. M. Bell (1989). "Functions of sphingolipids and sphingolipid breakdown products in cellular regulation." Science **243**(4890): 500-507.

Harding, H. P., Y. Zhang, et al. (1999). "Protein translation and folding are coupled by an endoplasmic-reticulum-resident kinase." Nature **397**(6716): 271-274.

Hill, D. E. and K. Struhl (1988). "Molecular characterization of GCD1, a yeast gene required for general control of amino acid biosynthesis and cell-cycle initiation." Nucleic Acids Res **16**(19): 9253-9265.

Hinnebusch, A. G. (1985). "A hierarchy of trans-acting factors modulates translation of an activator of amino acid biosynthetic genes in Saccharomyces cerevisiae." Mol Cell Biol **5**(9): 2349-2360.

Hinnebusch, A. G. (1993). "Gene-specific translational control of the yeast GCN4 gene by phosphorylation of eukaryotic initiation factor 2." Mol Microbiol **10**(2): 215-223.

Hinnebusch, A. G. (1994). "Translational control of GCN4: an in vivo barometer of initiation-factor activity." Trends Biochem Sci **19**(10): 409-414.

Hinnebusch, A. G. (2005). "Translational regulation of GCN4 and the general amino acid control of yeast." Annu Rev Microbiol **59**: 407-450.

Hinnebusch, A. G. (2006). "eIF3: a versatile scaffold for translation initiation complexes." Trends Biochem Sci **31**(10): 553-562.

Hinnebusch, A. G. (2011). "Molecular mechanism of scanning and start codon selection in eukaryotes." Microbiol Mol Biol Rev **75**(3): 434-467, first page of table of contents.

Hinnebusch, A. G. and G. R. Fink (1983). "Positive regulation in the general amino acid control of Saccharomyces cerevisiae." Proc Natl Acad Sci U S A **80**(17): 5374-5378.

Hinnebusch, A. G., B. M. Jackson, et al. (1988). "Evidence for regulation of reinitiation in translational control of GCN4 mRNA." Proc Natl Acad Sci U S A **85**(19): 7279-7283.

Hiyama, T. B., T. Ito, et al. (2009). "Crystal structure of the alpha subunit of human translation initiation factor 2B." J Mol Biol **392**(4): 937-951.

Horzinski, L., L. Kantor, et al. (2010). "Evaluation of the endoplasmic reticulum-stress response in eIF2B-mutated lymphocytes and lymphoblasts from CACH/VWM patients." BMC Neurol **10**: 94.

Hudson, J. R., Jr., E. P. Dawson, et al. (1997). "The complete set of predicted genes from Saccharomyces cerevisiae in a readily usable form." Genome Res **7**(12): 1169-1173.

Huh, W. K., J. V. Falvo, et al. (2003). "Global analysis of protein localization in budding yeast." Nature **425**(6959): 686-691.

Ibba, M. and D. Soll (2000). "Aminoacyl-tRNA synthesis." Annu Rev Biochem **69**: 617-650.

Jackson, R. J., C. U. Hellen, et al. (2012). "Termination and post-termination events in eukaryotic translation." Adv Protein Chem Struct Biol **86**: 45-93.

Jakobsson, A., R. Westerberg, et al. (2006). "Fatty acid elongases in mammals: their regulation and roles in metabolism." Prog Lipid Res **45**(3): 237-249.

James, P., J. Halladay, et al. (1996). "Genomic libraries and a host strain designed for highly efficient two-hybrid selection in yeast." Genetics **144**(4): 1425-1436.

Jang, S. K., H. G. Krausslich, et al. (1988). "A segment of the 5' nontranslated region of encephalomyocarditis virus RNA directs internal entry of ribosomes during in vitro translation." J Virol **62**(8): 2636-2643.

Jenni, S., M. Leibundgut, et al. (2007). "Structure of fungal fatty acid synthase and implications for iterative substrate shuttling." Science **316**(5822): 254-261.

Kageyama-Yahara, N. and H. Riezman (2006). "Transmembrane topology of ceramide synthase in yeast." Biochem J **398**(3): 585-593.

Karbstein, K. (2011). "Inside the 40S ribosome assembly machinery." Curr Opin Chem Biol **15**(5): 657-663.

Keiper, B. D., W. Gan, et al. (1999). "Protein synthesis initiation factor 4G." Int J Biochem Cell Biol **31**(1): 37-41.

Kihara, A. (2012). "Very long-chain fatty acids: elongation, physiology and related disorders." J Biochem **152**(5): 387-395.

Kim, L. and A. R. Kimmel (2000). "GSK3, a master switch regulating cell-fate specification and tumorigenesis." Curr Opin Genet Dev **10**(5): 508-514.

Kimball, S. R. (1999). "Eukaryotic initiation factor eIF2." Int J Biochem Cell Biol **31**(1): 25-29.

Klein, H. P. (1957). "Some observations on a cell free lipid synthesizing system from Saccharomyces cerevisiae." J Bacteriol **73**(4): 530-543.

Klinge, S., F. Voigts-Hoffmann, et al. (2012). "Atomic structures of the eukaryotic ribosome." Trends Biochem Sci **37**(5): 189-198.

Kolesnick, R. N., A. Haimovitz-Friedman, et al. (1994). "The sphingomyelin signal transduction pathway mediates apoptosis for tumor necrosis factor, Fas, and ionizing radiation." Biochem Cell Biol **72**(11-12): 471-474.

Kolitz, S. E. and J. R. Lorsch (2010). "Eukaryotic initiator tRNA: finely tuned and ready for action." FEBS Lett **584**(2): 396-404.

Komar, A. A. and M. Hatzoglou (2011). "Cellular IRES-mediated translation: the war of ITAFs in pathophysiological states." Cell Cycle **10**(2): 229-240.

Kostiuk, M. A., B. O. Keller, et al. (2009). "Non-radioactive detection of palmitoylated mitochondrial proteins using an azido-palmitate analogue." Methods Enzymol **457**: 149-165.

Kozak, M. (1980). "Evaluation of the "scanning model" for initiation of protein synthesis in eucaryotes." Cell **22**(1 Pt 1): 7-8.

Kozak, M. (1987). "An analysis of 5'-noncoding sequences from 699 vertebrate messenger RNAs." Nucleic Acids Res **15**(20): 8125-8148.

Kozak, M. and A. J. Shatkin (1978). "Identification of features in 5' terminal fragments from reovirus mRNA which are important for ribosome binding." Cell **13**(1): 201-212.

Krogan, N. J., G. Cagney, et al. (2006). "Global landscape of protein complexes in the yeast Saccharomyces cerevisiae." Nature **440**(7084): 637-643.

Kubica, N., L. S. Jefferson, et al. (2006). "Eukaryotic initiation factor 2B and its role in alterations in mRNA translation that occur under a number of pathophysiological and physiological conditions." Prog Nucleic Acid Res Mol Biol **81**: 271-296.

Lamphear, B. J., R. Kirchweger, et al. (1995). "Mapping of functional domains in eukaryotic protein synthesis initiation factor 4G (eIF4G) with picornaviral proteases. Implications for cap-dependent and cap-independent translational initiation." J Biol Chem **270**(37): 21975-21983.

Leonard, A. E., S. L. Pereira, et al. (2004). "Elongation of long-chain fatty acids." Prog Lipid Res **43**(1): 36-54.

Li, W., X. Wang, et al. (2004). "Mutations linked to leukoencephalopathy with vanishing white matter impair the function of the eukaryotic initiation factor 2B complex in diverse ways." Mol Cell Biol **24**(8): 3295-3306.

Link, A. J., J. Eng, et al. (1999). "Direct analysis of protein complexes using mass spectrometry." Nat Biotechnol **17**(7): 676-682.

Link, A. J., T. C. Fleischer, et al. (2005). "Purifying protein complexes for mass spectrometry: applications to protein translation." Methods **35**(3): 274-290.

Liu, A. R., H. D. van der Lei, et al. (2011). "Severity of Vanishing White Matter disease does not correlate with deficits in eIF2B activity or the integrity of eIF2B complexes." Hum Mutat.

Lowe, M. and F. A. Barr (2007). "Inheritance and biogenesis of organelles in the secretory pathway." Nat Rev Mol Cell Biol **8**(6): 429-439.

Luu-The, V., P. Tremblay, et al. (2006). "Characterization of type 12 17beta-hydroxysteroid dehydrogenase, an isoform of type 3 17beta-hydroxysteroid dehydrogenase responsible for estradiol formation in women." Mol Endocrinol **20**(2): 437-443.

Maier, T., S. Jenni, et al. (2006). "Architecture of mammalian fatty acid synthase at 4.5 A resolution." Science **311**(5765): 1258-1262.

Maier, T., M. Leibundgut, et al. (2010). "Structure and function of eukaryotic fatty acid synthases." Q Rev Biophys **43**(3): 373-422.

McAfee, K. J., D. T. Duncan, et al. (2006). "Analyzing proteomes and protein function using graphical comparative analysis of tandem mass spectrometry results." Mol Cell Proteomics **5**(8): 1497-1513.

McKendrick, L., V. M. Pain, et al. (1999). "Translation initiation factor 4E." Int J Biochem Cell Biol **31**(1): 31-35.

Merrick W. C., H. J. W. B. Translation Control. M. M. B. Hershey J. W. B., Sonenber N. Cold Spring Harbor, NY, Cold Spring Harbor Laboratory**:** pp 31-69.

Methot, N., M. S. Song, et al. (1996). "A region rich in aspartic acid, arginine, tyrosine, and glycine (DRYG) mediates eukaryotic initiation factor 4B (eIF4B) self-association and interaction with eIF3." Mol Cell Biol **16**(10): 5328-5334.

Miller, J. P., R. S. Lo, et al. (2005). "Large-scale identification of yeast integral membrane protein interactions." Proc Natl Acad Sci U S A **102**(34): 12123-12128.

Mineo, C. and P. W. Shaul (2012). "Novel biological functions of high-density lipoprotein cholesterol." Circ Res **111**(8): 1079-1090.

Mitchell, S. F. and J. R. Lorsch (2008). "Should I stay or should I go? Eukaryotic translation initiation factors 1 and 1A control start codon recognition." J Biol Chem **283**(41): 27345-27349.

Mohammad-Qureshi, S. S., M. D. Jennings, et al. (2008). "Clues to the mechanism of action of eIF2B, the guanine-nucleotide-exchange factor for translation initiation." Biochem Soc Trans **36**(Pt 4): 658-664.

Moon, Y. A. and J. D. Horton (2003). "Identification of two mammalian reductases involved in the two-carbon fatty acyl elongation cascade." J Biol Chem **278**(9): 7335-7343.

Mori, K., T. Kawahara, et al. (1996). "Signalling from endoplasmic reticulum to nucleus: transcription factor with a basic-leucine zipper motif is required for the unfolded protein-response pathway." Genes Cells **1**(9): 803-817.

Mueller, P. P. and A. G. Hinnebusch (1986). "Multiple upstream AUG codons mediate translational control of GCN4." Cell **45**(2): 201-207.

Natarajan, K., M. R. Meyer, et al. (2001). "Transcriptional profiling shows that Gcn4p is a master regulator of gene expression during amino acid starvation in yeast." Mol Cell Biol **21**(13): 4347-4368.

Nazar, R. N. (1984). "The ribosomal 5.8S RNA: eukaryotic adaptation or processing variant?" Can J Biochem Cell Biol **62**(6): 311-320.

Noller, H. F. (1991). "Ribosomal RNA and translation." Annu Rev Biochem **60**: 191-227.

Oh, C. S., D. A. Toke, et al. (1997). "ELO2 and ELO3, homologues of the Saccharomyces cerevisiae ELO1 gene, function in fatty acid elongation and are required for sphingolipid formation." J Biol Chem **272**(28): 17376-17384.

Oldfield, S. and C. G. Proud (1992). "Purification, phosphorylation and control of the guanine-nucleotide-exchange factor from rabbit reticulocyte lysates." Eur J Biochem **208**(1): 73-81.

Olsen, D. S., B. Jordan, et al. (1998). "Isolation of the gene encoding the Drosophila melanogaster homolog of the Saccharomyces cerevisiae GCN2 eIF-2alpha kinase." Genetics **149**(3): 1495-1509.

Omura, S. (1976). "The antibiotic cerulenin, a novel tool for biochemistry as an inhibitor of fatty acid synthesis." Bacteriol Rev **40**(3): 681-697.

Orlean, P. (1990). "Dolichol phosphate mannose synthase is required in vivo for glycosyl phosphatidylinositol membrane anchoring, O mannosylation, and N glycosylation of protein in Saccharomyces cerevisiae." Mol Cell Biol **10**(11): 5796-5805.

Orlean, P., C. Albright, et al. (1988). "Cloning and sequencing of the yeast gene for dolichol phosphate mannose synthase, an essential protein." J Biol Chem **263**(33): 17499-17507.

Paddon, C. J., E. M. Hannig, et al. (1989). "Amino acid sequence similarity between GCN3 and GCD2, positive and negative translational regulators of GCN4: evidence for antagonism by competition." Genetics **122**(3): 551-559.

Palade, G. E. (1955). "A small particulate component of the cytoplasm." J Biophys Biochem Cytol **1**(1): 59-68.

Parker, R. and U. Sheth (2007). "P bodies and the control of mRNA translation and degradation." Mol Cell **25**(5): 635-646.

Pavitt, G. D. (2005). "eIF2B, a mediator of general and gene-specific translational control." Biochem Soc Trans **33**(Pt 6): 1487-1492.

Pavitt, G. D. and C. G. Proud (2009). "Protein synthesis and its control in neuronal cells with a focus on vanishing white matter disease." Biochem Soc Trans **37**(Pt 6): 1298-1310.

Pavitt, G. D., K. V. Ramaiah, et al. (1998). "eIF2 independently binds two distinct eIF2B subcomplexes that catalyze and regulate guanine-nucleotide exchange." Genes Dev **12**(4): 514-526.

Pavitt, G. D., W. Yang, et al. (1997). "Homologous segments in three subunits of the guanine nucleotide exchange factor eIF2B mediate translational regulation by phosphorylation of eIF2." Mol Cell Biol **17**(3): 1298-1313.

Pelletier, J. and N. Sonenberg (1988). "Internal initiation of translation of eukaryotic mRNA directed by a sequence derived from poliovirus RNA." Nature **334**(6180): 320-325.

Perrotta, C., C. De Palma, et al. (2005). "Nitric oxide, ceramide and sphingomyelinase-coupled receptors: a tale of enzymes and messengers coordinating cell death, survival and differentiation." Life Sci **77**(14): 1732-1739.

Pestova, T. V., V. G. Kolupaeva, et al. (2001). "Molecular mechanisms of translation initiation in eukaryotes." Proc Natl Acad Sci U S A **98**(13): 7029-7036.

Petry, S., A. Weixlbaumer, et al. (2008). "The termination of translation." Curr Opin Struct Biol **18**(1): 70-77.

Pettus, B. J., C. E. Chalfant, et al. (2004). "Sphingolipids in inflammation: roles and implications." Curr Mol Med **4**(4): 405-418.

Pilz, R. B., I. Huvar, et al. (1997). "A decrease in the intracellular guanosine 5'-triphosphate concentration is necessary for granulocytic differentiation of HL-60 cells, but growth cessation and

differentiation are not associated with a change in the activation state of Ras, the transforming principle of HL-60 cells." Cell Growth Differ **8**(1): 53-59.

Pisarev, A. V., N. E. Shirokikh, et al. (2005). "Translation initiation by factor-independent binding of eukaryotic ribosomes to internal ribosomal entry sites." C R Biol **328**(7): 589-605.

Plourde, M., A. Ferland, et al. (2009). "Analysis of 17beta-hydroxysteroid dehydrogenase types 5, 7, and 12 genetic sequence variants in breast cancer cases from French Canadian Families with high risk of breast and ovarian cancer." J Steroid Biochem Mol Biol **116**(3-5): 134-153.

Poll, G., T. Braun, et al. (2009). "rRNA maturation in yeast cells depleted of large ribosomal subunit proteins." PLoS One **4**(12): e8249.

Powell, D. W., C. M. Weaver, et al. (2004). "Cluster analysis of mass spectrometry data reveals a novel component of SAGA." Mol Cell Biol **24**(16): 7249-7259.

Powell, M. L. (2010). "Translational termination-reinitiation in RNA viruses." Biochem Soc Trans **38**(6): 1558-1564.

Preiss, T. and W. H. M (2003). "Starting the protein synthesis machine: eukaryotic translation initiation." Bioessays **25**(12): 1201-1211.

Preuss, D., J. Mulholland, et al. (1991). "Structure of the yeast endoplasmic reticulum: localization of ER proteins using immunofluorescence and immunoelectron microscopy." Yeast **7**(9): 891-911.

Qiu, H., J. Dong, et al. (2001). "The tRNA-binding moiety in GCN2 contains a dimerization domain that interacts with the kinase domain and is required for tRNA binding and kinase activation." EMBO J **20**(6): 1425-1438.

Reid, P. J., S. S. Mohammad-Qureshi, et al. (2012). "Identification of intersubunit domain interactions within eukaryotic initiation factor (eIF) 2B, the nucleotide exchange factor for translation initiation." J Biol Chem **287**(11): 8275-8285.

Revardel, E., M. Bonneau, et al. (1995). "Characterization of a new gene family developing pleiotropic phenotypes upon mutation in Saccharomyces cerevisiae." Biochim Biophys Acta **1263**(3): 261-265.

Rezanka, T. (1989). "Very-long-chain fatty acids from the animal and plant kingdoms." Prog Lipid Res **28**(3): 147-187.

Richardson, J. P., S. S. Mohammad, et al. (2004). "Mutations causing childhood ataxia with central nervous system hypomyelination reduce eukaryotic initiation factor 2B complex formation and activity." Mol Cell Biol **24**(6): 2352-2363.

Rogers, G. W., Jr., A. A. Komar, et al. (2002). "eIF4A: the godfather of the DEAD box helicases." Prog Nucleic Acid Res Mol Biol **72**: 307-331.

Rose, M. and D. Botstein (1983). "Construction and use of gene fusions to lacZ (beta-galactosidase) that are expressed in yeast." Methods Enzymol **101**: 167-180.

Rossler, H., C. Rieck, et al. (2003). "Functional differentiation and selective inactivation of multiple Saccharomyces cerevisiae genes involved in very-long-chain fatty acid synthesis." Mol Genet Genomics **269**(2): 290-298.

Roth, A. F., J. Wan, et al. (2006). "Global analysis of protein palmitoylation in yeast." Cell **125**(5): 1003-1013.

Rowlands, A. G., R. Panniers, et al. (1988). "The catalytic mechanism of guanine nucleotide exchange factor action and competitive inhibition by phosphorylated eukaryotic initiation factor 2." J Biol Chem **263**(12): 5526-5533.

Sachs, A. B. and G. Varani (2000). "Eukaryotic translation initiation: there are (at least) two sides to every story." Nat Struct Biol **7**(5): 356-361.

Sanders, S. L., J. Jennings, et al. (2002). "Proteomics of the eukaryotic transcription machinery: identification of proteins associated with components of yeast TFIID by multidimensional mass spectrometry." Mol Cell Biol **22**(13): 4723-4738.

Sandhoff, R., R. Geyer, et al. (2005). "Novel class of glycosphingolipids involved in male fertility." J Biol Chem **280**(29): 27310-27318.

Sarre, T. F. (1989). "The phosphorylation of eukaryotic initiation factor 2: a principle of translational control in mammalian cells." Biosystems **22**(4): 311-325.

Sasikumar, A. N., W. B. Perez, et al. (2012). "The many roles of the eukaryotic elongation factor 1 complex." Wiley Interdiscip Rev RNA **3**(4): 543-555.

Schmitt, E., M. Naveau, et al. (2010). "Eukaryotic and archaeal translation initiation factor 2: a heterotrimeric tRNA carrier." FEBS Lett **584**(2): 405-412.

Schneider, C. A., W. S. Rasband, et al. (2012). "NIH Image to ImageJ: 25 years of image analysis." Nat Methods **9**(7): 671-675.

Schneider, R. J. and I. Mohr (2003). "Translation initiation and viral tricks." Trends Biochem Sci **28**(3): 130-136.

Schneiter, R., B. Brugger, et al. (2004). "Identification and biophysical characterization of a very-long-chain-fatty-acid-substituted phosphatidylinositol in yeast subcellular membranes." Biochem J **381**(Pt 3): 941-949.

Schneiter, R., M. Hitomi, et al. (1996). "A yeast acetyl coenzyme A carboxylase mutant links very-long-chain fatty acid synthesis to the structure and function of the nuclear membrane-pore complex." Mol Cell Biol **16**(12): 7161-7172.

Schuldiner, M., S. R. Collins, et al. (2005). "Exploration of the function and organization of the yeast early secretory pathway through an epistatic miniarray profile." Cell **123**(3): 507-519.

Schweizer, E., K. Werkmeister, et al. (1978). "Fatty acid biosynthesis in yeast." Mol Cell Biochem **21**(2): 95-107.

Scolnick, E., R. Tompkins, et al. (1968). "Release factors differing in specificity for terminator codons." Proc Natl Acad Sci U S A **61**(2): 768-774.

Semenkovich, C. F. (1997). "Regulation of fatty acid synthase (FAS)." Prog Lipid Res **36**(1): 43-53.

Shi, Y., K. M. Vattem, et al. (1998). "Identification and characterization of pancreatic eukaryotic initiation factor 2 alpha-subunit kinase, PEK, involved in translational control." Mol Cell Biol **18**(12): 7499-7509.

Silve, S., P. Leplatois, et al. (1996). "The immunosuppressant SR 31747 blocks cell proliferation by inhibiting a steroid isomerase in Saccharomyces cerevisiae." Mol Cell Biol **16**(6): 2719-2727.

Simonetti, A., S. Marzi, et al. (2009). "A structural view of translation initiation in bacteria." Cell Mol Life Sci **66**(3): 423-436.

Simons, K. and E. Ikonen (1997). "Functional rafts in cell membranes." Nature **387**(6633): 569-572.

Sonenberg, N. H., J. Mathews, M (2000). Translational Control of Gene Expression. Cold Spring Harbor, New York, Cold Spring Harbor Laboratory Press.

Song, D., G. Liu, et al. (2006). "Expression of aromatase and 17beta-hydroxysteroid dehydrogenase types 1, 7 and 12 in breast cancer. An immunocytochemical study." J Steroid Biochem Mol Biol **101**(2-3): 136-144.

Sood, R., A. C. Porter, et al. (2000). "A mammalian homologue of GCN2 protein kinase important for translational control by phosphorylation of eukaryotic initiation factor-2alpha." Genetics **154**(2): 787-801.

Spiegel, S. (1993). "Sphingosine and sphingosine 1-phosphate in cellular proliferation: relationship with protein kinase C and phosphatidic acid." J Lipid Mediat **8**(3): 169-175.

Stadtman, E. R. and H. A. Barker (1949). "Fatty acid synthesis by enzyme preparations of Clostridium kluyveri; a consideration of postulated 4-carbon intermediates in butyrate synthesis." J Biol Chem **181**(1): 221-235.

Stadtman, E. R. and H. A. Barker (1949). "Fatty acid synthesis by enzyme preparations of Clostridium kluyveri; preparation of cell-free extracts that catalyze the conversion of ethanol and acetate to butyrate and caproate." J Biol Chem **180**(3): 1085-1093.

Stadtman, E. R. and H. A. Barker (1949). "Fatty acid synthesis by enzyme preparations of Clostridium kluyveri; the activation of molecular hydrogen and the conversion of acetyl phosphate and acetate to butyrate." J Biol Chem **180**(3): 1117-1124.

Stadtman, E. R. and H. A. Barker (1949). "Fatty acid synthesis by enzyme preparations of Clostridium kluyveri; the aerobic oxidation of ethanol and butyrate with the formation of acetyl phosphate." J Biol Chem **180**(3): 1095-1115.

Stadtman, E. R. and H. A. Barker (1949). "Fatty acid synthesis by enzyme preparations of Clostridium kluyveri; the phosphorclastic decomposition of acetoacetate of acetyl phosphate and acetate." J Biol Chem **180**(3): 1169-1186.

Stadtman, E. R. and H. A. Barker (1950). "Fatty acid synthesis by enzyme preparations of Clostridium kluyveri. VI. Reactions of acyl phosphates." J Biol Chem **184**(2): 769-793.

Stoops, J. K. and S. J. Wakil (1978). "The isolation of the two subunits of yeast fatty acid synthetase." Biochem Biophys Res Commun **84**(1): 225-231.

Sud, M., E. Fahy, et al. (2007). "LMSD: LIPID MAPS structure database." Nucleic Acids Res **35**(Database issue): D527-532.

Szajnik, M., M. J. Szczepanski, et al. (2012). "17beta hydroxysteroid dehydrogenase type 12 (HSD17B12) is a marker of poor prognosis in ovarian carcinoma." Gynecol Oncol **127**(3): 587-594.

Taylor, E. J., S. G. Campbell, et al. (2010). "Fusel alcohols regulate translation initiation by inhibiting eIF2B to reduce ternary complex in a mechanism that may involve altering the integrity and dynamics of the eIF2B body." Mol Biol Cell **21**(13): 2202-2216.

Tehlivets, O., K. Scheuringer, et al. (2007). "Fatty acid synthesis and elongation in yeast." Biochim Biophys Acta **1771**(3): 255-270.

Terasaki, M., J. Song, et al. (1984). "Localization of endoplasmic reticulum in living and glutaraldehyde-fixed cells with fluorescent dyes." Cell **38**(1): 101-108.

Thompson, S. R. (2012). "Tricks an IRES uses to enslave ribosomes." Trends Microbiol **20**(11): 558-566.

Tuller, G., B. Prein, et al. (1999). "Deletion of six open reading frames from the left arm of chromosome IV of Saccharomyces cerevisiae." Yeast **15**(12): 1275-1285.

Vallee, B. and H. Riezman (2005). "Lip1p: a novel subunit of acyl-CoA ceramide synthase." EMBO J **24**(4): 730-741.

van der Knaap, M. S., P. G. Barth, et al. (1997). "A new leukoencephalopathy with vanishing white matter." Neurology **48**(4): 845-855.

van der Knaap, M. S., J. C. Pronk, et al. (2006). "Vanishing white matter disease." Lancet Neurol **5**(5): 413-423.

van der Lei, H. D., C. G. van Berkel, et al. (2010). "Genotype-phenotype correlation in vanishing white matter disease." Neurology **75**(17): 1555-1559.

van Kollenburg, B., A. A. Thomas, et al. (2006). "Regulation of protein synthesis in lymphoblasts from vanishing white matter patients." Neurobiol Dis **21**(3): 496-504.

van Meer, G. (1993). "Transport and sorting of membrane lipids." Curr Opin Cell Biol **5**(4): 661-673.

Vattem, K. M. and R. C. Wek (2004). "Reinitiation involving upstream ORFs regulates ATF4 mRNA translation in mammalian cells." Proc Natl Acad Sci U S A **101**(31): 11269-11274.

Vazquez de Aldana, C. R., T. E. Dever, et al. (1993). "Mutations in the alpha subunit of eukaryotic translation initiation factor 2 (eIF-2 alpha) that overcome the inhibitory effect of eIF-2 alpha phosphorylation on translation initiation." Proc Natl Acad Sci U S A **90**(15): 7215-7219.

Veech, R. L., L. V. Eggleston, et al. (1969). "The redox state of free nicotinamide-adenine dinucleotide phosphate in the cytoplasm of rat liver." Biochem J **115**(4): 609-619.

Vries, R. G., A. Flynn, et al. (1997). "Heat shock increases the association of binding protein-1 with initiation factor 4E." J Biol Chem **272**(52): 32779-32784.

Wakil, S. J., J. K. Stoops, et al. (1983). "Fatty acid synthesis and its regulation." Annu Rev Biochem **52**: 537-579.

Wang, X., F. E. Paulin, et al. (2001). "Eukaryotic initiation factor 2B: identification of multiple phosphorylation sites in the epsilon-subunit and their functions in vivo." EMBO J **20**(16): 4349-4359.

Wang, X. and C. G. Proud (2008). "A novel mechanism for the control of translation initiation by amino acids, mediated by phosphorylation of eukaryotic initiation factor 2B." Mol Cell Biol **28**(5): 1429-1442.

Wang, X., N. C. Wortham, et al. (2012). "Identification of residues that underpin interactions within the eukaryotic initiation factor (eIF2) 2B complex." J Biol Chem **287**(11): 8263-8274.

Warner, J. R. (1999). "The economics of ribosome biosynthesis in yeast." Trends Biochem Sci **24**(11): 437-440.

Wei, J., M. Jia, et al. (2010). "Crystal structure of the C-terminal domain of the varepsilon subunit of human translation initiation factor eIF2B." Protein Cell **1**(6): 595-603.

Wek, R. C., M. Ramirez, et al. (1990). "Identification of positive-acting domains in GCN2 protein kinase required for translational activation of GCN4 expression." Mol Cell Biol **10**(6): 2820-2831.

Welch, J. W. and A. L. Burlingame (1973). "Very long-chain fatty acids in yeast." J Bacteriol **115**(1): 464-466.

Welihinda, A. A., W. Tirasophon, et al. (1999). "The cellular response to protein misfolding in the endoplasmic reticulum." Gene Expr **7**(4-6): 293-300.

White, S. W., J. Zheng, et al. (2005). "The structural biology of type II fatty acid biosynthesis." Annu Rev Biochem **74**: 791-831.

Willett, M., M. Brocard, et al. (2011). "Translation initiation factors and active sites of protein synthesis co-localize at the leading edge of migrating fibroblasts." Biochem J **438**(1): 217-227.

Wilson, D. N. and J. H. Doudna Cate (2012). "The structure and function of the eukaryotic ribosome." Cold Spring Harb Perspect Biol **4**(5).

Winzeler, E. A., D. D. Shoemaker, et al. (1999). "Functional characterization of the S. cerevisiae genome by gene deletion and parallel analysis." Science **285**(5429): 901-906.

Wolfner, M., D. Yep, et al. (1975). "Integration of amino acid biosynthesis into the cell cycle of Saccharomyces cerevisiae." J Mol Biol **96**(2): 273-290.

Woods, Y. L., P. Cohen, et al. (2001). "The kinase DYRK phosphorylates protein-synthesis initiation factor eIF2Bepsilon at Ser539 and the microtubule-associated protein tau at Thr212: potential role for DYRK as a glycogen synthase kinase 3-priming kinase." Biochem J **355**(Pt 3): 609-615.

Yang, W. and A. G. Hinnebusch (1996). "Identification of a regulatory subcomplex in the guanine nucleotide exchange factor eIF2B that mediates inhibition by phosphorylated eIF2." Mol Cell Biol **16**(11): 6603-6616.

Zhan, K., J. Narasimhan, et al. (2004). "Differential activation of eIF2 kinases in response to cellular stresses in Schizosaccharomyces pombe." Genetics **168**(4): 1867-1875.

Zhan, K., K. M. Vattem, et al. (2002). "Phosphorylation of eukaryotic initiation factor 2 by heme-regulated inhibitor kinase-related protein kinases in Schizosaccharomyces pombe is important for fesistance to environmental stresses." Mol Cell Biol **22**(20): 7134-7146.

Zhou, F., Y. Xue, et al. (2006). "CSS-Palm: palmitoylation site prediction with a clustering and scoring strategy (CSS)." Bioinformatics **22**(7): 894-896.